Understanding the Role of MiR-16-5p in Prion-induced Neurodegeneration

by

Kristyn Burak

A Thesis submitted to the Faculty of Graduate Studies of

The University of Manitoba

in partial fulfillment of the requirements of the degree of

MASTER OF SCIENCE

Department of Medical Microbiology and Infectious Diseases

University of Manitoba

Winnipeg

Abstract

Neurodegenerative diseases are a diverse group of progressive diseases that include Alzheimer's disease (AD) and prion disease. Although these diseases differ in etiology, they share a number of similarities at the molecular level. For instance, microRNA (miRNA), small RNA molecules that post-translationally regulate gene expression, are often differentially regulated during disease. A previous study identified key miRNA that are dysregulated during prion disease in the hippocampus. Of these miRNA, miR-16-5p is of particular interest, as it has also been found to be dysregulated in AD. The objective of this thesis is to characterize the role of miR-16-5p within hippocampal neurons in order to understand its function during neurodegeneration. It is hypothesized that hippocampal miR-16-5p, given its induction in hippocampal neurons during preclinical disease, plays a role in regulating the dendritic remodeling and synaptic pruning that is the earliest pathological feature of neuronal degeneration in prion disease. To address this hypothesis, primary hippocampal neurons were dissected from embryonic day 18 mice and treated with a lentiviral vector at maturity. This vector either encoded miR-16 or miRZIP-16, causing overexpression or knockdown of miR-16, respectively. Immunoprecipitation of the miRNA-16 enriched RISC complex was then performed, and the co-immunoprecipitated target mRNA was subjected to a whole genome microarray. Analysis of microarray data in Ingenuity Pathway Analysis pinpointed 181 genes involved in neuronal morphology and neurological disease targeted by miR-16. In particular, the MAPK/ERK pathway was targeted at TrkB, MEK1 and c-Raf. This is of interest, as we know that this pathway is disrupted in other neurodegenerative diseases and is directly implicated in neuronal morphology. Subsequent morphological analysis revealed that overexpression of miR-16 in neuronal cells decreased neurite length and branching, consistent with the downregulation of components of the MAPK/ERK pathway. In conclusion, miR-16 targets many mRNA transcripts within the hippocampus that are important members of pathways involved in neuronal development and neurodegeneration, including the MAPK/ERK pathway.

Acknowledgements

I would like to thank my supervisor Dr. Stephanie Booth, Adjunct Professor in the Department of Medical Microbiology and Infectious Diseases, Max Rady College of Medicine, Rady Faculty of Health Sciences at the University of Manitoba and Chief, Molecular PathoBiology, National Microbiology Laboratory, Public Health Agency of Canada for all of her help and support throughout my research project and the writing of this thesis. I would also like to thank my committee members, Dr. Grant McClarty, Professor, Department of Medical Microbiology and Infectious Diseases and Director, Science Technology Cores and Services, National Microbiology Laboratory, Public Health Agency of Canada and Dr. Cynthia Ellison, Associate Professor, Department of Pathology Department of Immunology, both of the Max Rady College of Medicine, Rady Faculty of Health Sciences at the University of Manitoba for their guidance and support throughout this process, and for reviewing my thesis.

I would also like to express my thanks to the Booth lab members, past and present, for welcoming me and continually encouraging and assisting me in my research. Thank you to Dr. Reuben Saba, Dr. Anna Majer, Amrit Boese, Aileen Patterson, Kamilla Kosciuczyk, Sarah Medina, Kathy Frost, Kathy Manguiat, Debra Sorensen, Clark Phillipson, Yulian Niu and Matthew Martin.

Thank you to Research Manitoba (formerly Manitoba Health Research Council) for funding my research both through a University of Manitoba Graduate Fellowship Award and the Research Manitoba Masters Studentship. Thank you to Dr. Stephanie Booth for providing me with funding throughout my research program. Thank you also to the University of Manitoba GETS program for providing me with additional funding. Finally, thank you to the Canadian Institute of Health Research (CIHR) as well as the Public Health Agency of Canada for providing funding for my experiments.

Table of Contents

List of Tables

List of Figures

List of Abbreviations

Aβ - amyloid-beta

AAV - adeno-associated virus

AD – Alzheimer's disease

Ago2 – Argonaute 2 protein

Ago2-IP – Argonaute 2 Immunoprecipitation

ALS – Amyotrophic lateral sclerosis

APP - amyloid precursor protein

AUD - Animal Use Document

BCA - bicinchoninic acid

BDNF - brain-derived neurotrophic factor

BSE - bovine spongiform encephalopathy

CA1 - Cornu Ammonis

CF - cystic fibrosis

CJD - Creutzfeldt-Jacob disease

CLL - chronic lymphocytic leukemia

CWD - chronic wasting disease

DIV - days *in vitro*

DM - dissecting media

DMEM - Dulbecco's Modified Eagle Medium

DPI - days post infection

E18 - embryonic day 18

FBS - fetal bovine serum

FFI - fatal familial insomnia

GFAP - glial fibrillary acidic protein

GFP – green fluorescent protein

GSS - Gerstmann-Sträussler-Scheinker disease

HBSS - Hank's Balanced Salt Solution

HD – Huntington's disease

Hsp70 - heat shock protein 70

IPA - Ingenuity Pathway Analysis

LB - Luria Bertani

LDH - lactate dehydrogenase

MAP - microtubule-associated protein

MAP2 - microtubule-associated protein 2

MDD - major depressive disorder

miRNA – microRNA

MPM - malignant pleural mesothelioma

MS – multiple sclerosis

MSA - multiple system atrophy

NTC - no template control

P-body - processing body

PCIA - phenol:chloroform:isoamyl alcohol

PD – Parkinson's disease

PFA – paraformaldehyde

PrP^{C} – cellular prion protein

PrP^{Sc} – prion protein scrapie

RISC - RNA induced silencing complex

RT - room temperature

SynD - Synapse Detection

sCJD – sporadic Creutzfeldt-Jacob disease

UTR - untranslated region

vCJD – variant Creutzfeldt-Jacob disease

Chapter 1: Introduction

1.1 Neurodegenerative Disease

With much of the population advancing in age, an increasing number of people are at risk for developing age-related illnesses. In particular, neurodegenerative diseases such as Alzheimer's disease (AD) are becoming increasingly common. AD is the most common cause of dementia, representing 60-80% of cases (Alzheimers Association 2015). In total, 65.7 million people worldwide are expected to be afflicted with AD by 2030 (Prince et al. 2013).

Neurodegenerative diseases are invariably fatal illnesses resulting from progressive loss of neuronal function. These diseases are very diverse with AD, Parkinson's disease (PD), Huntington's disease (HD), Multiple sclerosis (MS), Amyotrophic lateral sclerosis (ALS) and prion diseases all belonging to this group. Table 1 summarizes the incidence rates of neurodegenerative diseases throughout Canada.

Pathologies commonly associated with neurodegeneration include synaptic loss, tangles of misfolded proteins and infiltration of glial cells into afflicted regions of the brain. In AD, amyloid-beta (Aβ) aggregates into extracellular senile plaques. Aβ is created by multiple cleavage steps of the amyloid precursor protein (APP) by BACE/β-secretase and γ-secretase (Parsi et al. 2015). Additionally, neurofibrillary tangles composed of hyperphosphorylated tau protein form within neurons (Parsi et al. 2015). Together, these pathologies lead to neuronal death primarily within the hippocampus and cortex, in a mechanism that is not fully understood. Similarly in HD, accumulation of HTT aggregates within neurons causes atrophy in multiple regions of the brain, including the

caudate nucleus, neostriatal nuclei and putamen (Lee et al. 2013). In PD, the second most prevalent neurodegenerative disease, α-synuclein rich Lewy bodies form within degenerating dopaminergic neurons residing in the substantia nigra and striatum (Zhang and Cheng 2014; Dorval et al. 2014). Although a medley of proteins comprise the Lewy body, α-synuclein has been particularly implicated in the neurodegeneration associated with the disease (Zhang and Cheng 2014). In ALS the formation of ubiquitin and SOD1 rich protein aggregates occurs in upper and lower motor neurons followed by their degeneration throughout the cortex, brainstem and the spinal cord (Lin and Beal 2006). The presence of aggregated proteins within each of these diseases suggests that this pathology may be central to the process of neurodegeneration.

Clinical symptoms of neurodegenerative diseases are diverse, dependent on the subclass of neurons that are afflicted, and range from cognitive impairment to motor dysfunction. For instance, AD and HD are both associated with cognitive impairment yet AD typically presents as severe memory loss while HD patients develop psychiatric symptoms (Parsi et al. 2015; Lee et al. 2013; Lin and Beal 2006). HD patients also typically present with chorea (uncoordinated movement) (Lee et al. 2013; Lin and Beal 2006). The key symptoms of PD are tremors, rigidity and slowness of movement along with unstable posture (Dorval et al. 2014). ALS typically presents with muscle weakness, atrophy and spastic movement (Lin and Beal 2006).

The etiology of these diseases is diverse, and much is still unknown. AD typically occurs sporadically with unknown cause but can also be genetically linked to point mutations in genes such as APOE ε4 (Prince et al. 2016; Brodaty et al. 2016). PD and ALS can occur due to inherited mutations in key genes, such as fibroblast growth factor 20 in PD, but

typically occur spontaneously (Lin and Beal 2006; Saugstad 2010). Conversely, HD is highly genetically linked through autosomal dominant transmission. A mutation in the *huntingtin* gene in chromosome 4 results in pathogenic expansion of greater than 40 CAG repeats, resulting in large polyglutamine stretches in the encoded protein (Lee et al. 2013; Lin and Beal 2006). For this reason, family history for HD is a strong indicator of susceptibility, while for other neurodegenerative diseases it is not so clear. Interestingly, certain factors have been proposed to increase the risk of dementia including age, poor education in early life, midlife hypertension, smoking, diabetes, and race (Alzheimers Association 2015; Prince et al. 2016; Brodaty et al. 2016). In addition, strong evidence exists of certain lifestyles reducing dementia risk including lifelong learning and regular physical activity (Alzheimers Association 2015).

Table 1: The Prevalence of Neurodegenerative Diseases within Canada

	CCHS 2010–2011 Project Survey Data[1]		CJD Deaths Reported by CJDSS, 2010-2011[2]	
	Rate per 100,000 population	(95% Confidence Interval)	Total Cases	Rate per 100.000 population **
Alzheimer's Disease & Dementias (age 65+)	2,130	(1,910-2,340)	-	-
Amyotrophic lateral sclerosis	10*	(10-20)	-	-
Huntington's disease	10*	(10-10)	-	-
Multiple sclerosis	290	(260-320)	-	-
Parkinson's disease	170 (All) 1,420 (80+)	(140-200) (All) (1,050-1,790) (80+)	-	-
Creutzfeldt-Jakob disease	-	-	89 (total) 81 Sporadic 0 Iatrogenic 6 Familial 1 GSS 0 FFI 1vCJD	0.259 0.236 Sporadic 0 Iatrogenic 0.017 Familial 0.003 GSS 0 FFI 0.003 vCJD

[1]Canadian Community Health Survey (CCHS) 2010-2011 Project Survey Data: Reflects weighted period prevalence to represent Canadian population and rounded to nearest ten. Age of survey participants was 0+ unless noted otherwise. http://www.phac-aspc.gc.ca/publicat/cd-mc/mc-ec/section-3-eng.php *Coefficient of Variation was between 16.6% and 33.3% in these surveys. [2]Creutzfeldt-Jakob disease Deaths Reported by Creutzfeldt-Jakob disease Surveillance System (CJDSS) between 2010 and 2011. http://www.phac-aspc.gc.ca/hcai-iamss/cjd-mcj/cjdss-ssmcj/stats-eng.php **Based on population of Canada in 2011, 34,342,800 people. http://www.statcan.gc.ca/tables-tableaux/sum-som/l01/cst01/demo02a-eng.htm

1.2 Prion Diseases

A significant problem in neurodegenerative disease research in the past has been the fundamental difficulty in studying sporadic diseases, with no defined singular pathological agent. However, there does exist a family of diseases in this class that fill this requirement; collectively referred to as prion diseases.

Prions are uniquely infectious protein molecules that cause deadly neurodegenerative diseases in humans and animals. These diseases are collectively referred to as transmissible spongiform encephalopathies or prion diseases. Similarly to other neurodegenerative diseases, infection with prions (PrP^{Sc}) results in the aggregation of misfolded human protein (PrP^{C}) into amyloid fibers and massive neuronal degeneration throughout the brain. Prusiner coined the term prion after discovering that the infectious unit of scrapie was nuclease resistant and thus must be a proteinaceous infectious particle (Prusiner 1982). This agent was isolated and fibrils of aggregated protein, soon identified as PrP^{Sc}, were visualized with electron microscopy (Diringer et al. 1983). It was later discovered that PrP^{Sc} is in fact the misfolded form of PrP^{C}, a ubiquitously expressed host-encoded membrane protein. PrP^{C} was long without known function, but is now thought to perform a variety of functions from aiding in synaptic plasticity and cellular differentiation to preventing oxidative stress (Zanetti et al. 2014). Additionally, PrP^{C} has recently been determined to act as a membrane-bound receptor for Aβ, but it is not essential for the synaptic deficits induced by Aβ in hippocampal neurons (Laurén et al. 2009; Kessels et al. 2010). The glycosylphosphatidylinositol (GPI) anchor possessed by

both PrP^{C} and PrP^{Sc} has been shown to be essential for efficient neural spread of PrP^{Sc} (Klingeborn et al. 2011).

Prion diseases of animals include scrapie in sheep, bovine spongiform encephalopathy (BSE) in cattle and chronic wasting disease (CWD) in elk. In humans, prion diseases can be sporadic, heritable or acquired (typically iatrogenic). These include Creutzfeldt-Jacob disease (CJD) (both variant (vCJD) and sporadic (sCJD) forms), Gerstmann-Sträussler-Scheinker disease (GSS), fatal familial insomnia (FFI) and kuru (Wadsworth and Collinge 2011). Prions were first identified in sheep that had scrapie, and subsequently were identified in humans in a cannibalistic tribe in Papua New Guinea in the form of kuru (Gajdusek et al., 1966). Kuru is caused by transmission of prion through cannibalistic ingestion of prion-infected brain matter during ritualistic funeral practices. Its incubation time has been shown to exceed 50 years in some cases (Collinge et al. 2006). Unlike kuru, CJD was identified to be a sporadic form of prion disease (Gibbs et al. 1968). Sporadic CJD represents approximately 85% of human prion diseases (Wadsworth and Collinge 2011).

One of the unifying traits of these diseases is the fact that they are transmissible between hosts (typically through human brain homogenate to laboratory monkeys) (Gibbs et al. 1968; Gajdusek, Gibbs, and Alpers 1966). However, a species barrier does exist that either results in inability of prions to propagate in a new host, or an unusually prolonged period before clinical signs are apparent in that host. This barrier is thought to be due to conformational selection due to steric hindrance of certain conformations of PrP^{Sc} with PrP^{C} (Wadsworth and Collinge 2011). However, stabilization of the prion strain within the new host can occur with serial passaging. Prions have thus been demonstrated to

transmit between unrelated species, overcoming this species barrier (Béringue et al. 2012). For example, variant CJD (vCJD) is the result of cross-species transmission, having originated from the BSE epidemic in the UK. When humans ingested BSE-infected beef, prion replication was able to occur resulting in the development of vCJD (Collinge 1999). Additionally, there is evidence of vCJD transfer between humans through infected blood transfusions (Peden et al. 2004).

Interestingly, these diseases have a range of clinical presentations. The symptoms of prion diseases are dementia, uncoordinated and unintentional movement, hyperreflexia, and seizures (Wadsworth and Collinge 2011). The molecular aspects of these diseases vary to some extent, but are broadly characterized as neuronal vacuolation and death resulting in a spongy phenotype (spongiform) and prolific infiltration of astrocytes and microglia into the affected region of the brain. In addition, there is a marked lack of lymphocytic inflammatory response (Wadsworth and Collinge 2011). Some of the diseases have distinct amyloid plaques of PrP^{Sc}, such as kuru, GSS and vCJD while sCJD, exhibits much more diffuse PrP^{Sc} deposits (Wadsworth and Collinge 2011). These variances are the result of strain-specific differences between the prions that are responsible for these diseases. Different prion strains stem from unique conformations of the same protein structure. Strains can possess drastically different incubation periods, biochemical features as well as unique distribution of PrP^{Sc} throughout the brain (Solforosi et al. 2013).

The uniquely infectious nature of the prion protein is advantageous as it allows for the creation of infected animal models with the true causative agent of disease. This creates an accurate model of disease rather than a model of a pseudo-diseased state like many

other neurodegenerative disease models that rely on the engineering of non-physiological levels of disease-related proteins in rodents. In addition, mice infected with RML-scrapie (a lab-derived mouse form of prion disease) have all of the characteristic signs of prion disease, including cognitive changes unlike other neurodegenerative disease models which frequently display some characteristics of the disease state, but are missing others (Chandler 1961; G. R. Mallucci et al. 2007; Majer et al. 2012; Jucker 2010).

Synaptic loss is one of the earliest pathological features of neurodegeneration, as it occurs long before clinical signs of disease are apparent (Cunningham et al. 2003). In the prion mouse model, the build-up of PrP^{Sc} is first detectable in mice prior to the mid-point of the incubation period. In a murine scrapie model described in detail by Jeffrey et al, PrP^{Sc} accumulation was first seen at 70 days post infection (dpi) within the hippocampus followed by synaptic loss at 84 dpi, axonal degeneration at 98 dpi and neuronal loss at 180 dpi followed by death of the animal around 250 dpi (Jeffrey et al. 2000). Interestingly, this synaptic loss has been shown to be reversible in this model system, with synaptic regeneration occurring in diseased tissues (G. R. Mallucci et al. 2007). This lends support to the idea that studying this stage of the neurodegenerative disease process is important for therapeutic discovery.

In regards to gene regulation during prion disease, it has been found that a core group of 349 genes are consistently dysregulated in prion mouse models of disease (Sorensen et al. 2008). Many of these genes are important for astrocytosis, gliosis, lipid metabolism, protein synthesis and cellular proliferation. Downregulation of many neuronal genes important in cellular pathways such as calcium signaling, synaptic function, long term potentiation and the MAPK/ERK pathway is also apparent (Sorensen et al. 2008).

Additionally, genes that are critical to optimal neuronal function, such as CREB1, were downregulated during disease. In agreement with these findings, another study by Ishikura et al. 2004, showed that genes that were important for inhibiting dendritic growth and maturation were highly expressed during the preclinical incubation period in a mouse model of disease, correlating nicely with increased accumulation of PrP^{Sc} (Ishikura et al. 2005).

Furthermore, prion is a relevant model of neurodegenerative disease because increasing evidence points to proteins involved in other neurodegenerative diseases being more similar to prions than originally thought. While prion diseases are rare, the idea that aggregation of protein causes disease is not unique to this disease. As discussed previously, AD, PD, ALS and HD all involve the aggregation of host-encoded proteins. Recently, many of the aggregating proteins implicated in these diseases have been described to cause similar illnesses when transmitted to neurons *in vitro* or within the brain of a healthy host. These intracellular proteins are prone to seeded aggregation, they are released as "seeds" that have the capacity to penetrate into host cells and promote pathological aggregation of the normal host protein. However, each of these instances demonstrated that the causative proteins were transmissible but not infectious and thus these proteins are termed "prionoids" (Norrby 2011). The crucial difference between these self-aggregating proteins and prions is that they lack microbiologically-defined transmissibility (physical transmission between patients and the ability to be titered) and as such they have not been shown to cause epidemic infectious diseases such as kuru or vCJD (Aguzzi and Rajendran 2009).

One such example of prionoids is in MSA (multiple system atrophy), a neurodegenerative disease caused by formation of α-synuclein rich filaments in glial cells. Inoculation of mice with brain extract from patients with MSA resulted in subsequent neurodegeneration after an incubation time of 120 days (Prusiner et al. 2015). Additionally, α-synuclein has been demonstrated to be transmissible between afflicted neurons from PD-host and healthy donor neurons (Desplats et al. 2009). Intriguingly, Lewy body rich extracts from patients with PD were transmissible to mice, but were not sufficient to cause neurodegeneration (Prusiner et al. 2015). The authors suggested that this was evidence of different strains of α-synuclein, similar to how different strains of PrP^{Sc} exist (Prusiner et al. 2015). Similarly in AD research, mice were infected with sporadic or heritable AD patient brain homogenates, resulting in markedly different deposition patterns of Aβ aggregates within the brain indicating another potentially strain-specific pathology (Watts et al. 2014). In a model of HD, cell to cell transmission of polyglutamine aggregates was demonstrated, with the newly acquired aggregates freely residing in the cytoplasm rather than in endosomes (Ren et al. 2009). This signified that the aggregate was not perceived as a foreign substance by the host cell and thus the cellular mechanisms to break down the aggregate were not engaged. Additionally, extract from brains exhibiting tauopathy (expressing mutant human tau gene) into mice expressing wild-type human tau, resulted in tauopathy in the mice (Clavaguera et al. 2009). Finally, it has been demonstrated that Aβ aggregates could be generated in a APP transgenic mouse model by inoculation of minute amounts of Aβ directly to the brain of mice (Eisele et al. 2009) or via incubation with brain homogenate from human patients afflicted with AD (Meyer-luehmann et al. 2006). Despite the crucial differences in

transmissibility, these studies suggest a similarity of these disease-related proteins to prions that has previously been overlooked.

Unquestionably, neurodegenerative diseases consist of a diverse range of clinical signs, etiologies and pathways of progression. They are not caused by one single variation or mutation, but a variety of different combinations of genetic, environmental and as yet unknown factors. Various cellular processes and pathways have been implicated in disease progression, such as endoplasmic reticulum stress and mitochondrial and oxidative stress in AD, PD, HD, ALS and prion disease (Nolan et al. 2014; Nunomura et al. 2001; Lin and Beal 2006; Guentchev et al. 2000). Currently, the standard care for patients with prion disease, as well as many other neurodegenerative diseases, is to increase quality of life by treating the symptoms. Therapies such as gabaregenic drugs and benzodiazepines are used for this purpose but have no effect on the disease progression.

Due to the lack of knowledge of the mechanisms and molecular pathways that lead to disease it has been difficult to develop treatments. In particular in prion diseases, if we can determine what is occurring in neurons during the long incubation period, we may be able to lengthen this period indefinitely. Therefore, the combination of efficient detection methods and novel therapeutic interventions could make prion diseases treatable. Since the infectious agent in prion disease is so resilient and the cause of many other neurodegenerative disorders stems from our neurons themselves, modifying our own cellular responses is the obvious target for therapeutic design. With this in mind, the more we can understand about what is going on in our cells during early stages of disease the more likely we will be able to prevent the clinical period from occurring. Previously,

efforts to thwart neurodegeneration were always targeted at the abnormally folded host protein involved in the illnesses, this approach has not proved successful in the past, and it is time to move on to other avenues. In particular in prion disease, focusing on inhibiting PrP^{Sc} formation and accumulation, has resulted in development of therapeutic agents with limited success ex) pentosan polysulfate, quinacrine and amphotericin B (Panegyres and Armari 2013).

Recently, a new wave of therapeutic design has centered on targeting the shared pathways that lie downstream of the initial protein-folding event in multiple diseases. Of particular promise in this area are miRNA, small non-coding RNA molecules that are endogenous post-transcriptional regulators of gene expression. Interestingly, little is known about their role in regulating gene expression during prion disease but research has been steadily evolving in this area.

1.3 MiRNA

MicroRNAs (miRNAs) are small, non-coding RNA molecules that function in post-transcriptional gene regulation. MiRNAs were first discovered in *Caenorhabditis elegans* and were thought to function specifically in development (*lin-4* & *let-7*) (He and Hannon 2004). Gene regulation via miRNA can result in mRNA levels significantly or just mildly decreasing (sometimes not to detectable levels) with prominent inhibition of expression at the protein level (Schwanhäusser et al. 2008). To date, 35828 miRNA have been identified in 223 species (Kozomara and Griffiths-Jones 2014).

MiRNAs are originally transcribed as large pri-miRNAs, which can be hundreds to thousands of nucleotides long. These pri-miRNAs are imperfect stem-loop structures that are targeted and cleaved by Drosha and the DGCR8 (DiGeorge critical region 8) protein within the nucleus into approximately 70-nucleotide long hairpin pre-miRNAs (He and Hannon 2004; Winter et al. 2009). The pre-miRNA is then exported out of the nucleus by Exportin-5 (XPO5) and Ran-GTP and cleaved by Dicer into the ~21-25-nucleotide long mature miRNA duplex (Winter et al. 2009). Drosha and Dicer are both dsRNA specific RNase III enzymes (He and Hannon 2004). Following this final cleavage, one strand of the dsRNA duplex is incorporated into the RNA induced Silencing Complex (RISC) while the other strand (commonly referred to as miRNA*) is typically degraded. The abundance of miRNA* strands have been shown to be ~100-fold lower than the incorporated strands, in agreement with this theory (He and Hannon 2004). The RISC complex is primarily composed of an Argonaute-2 (Ago2) protein along with numerous accessory proteins (Friedman et al. 2009).

MiRNA have specific seed regions consisting of nucleotides 2-7 within the 5' end that bind specifically to regions in the 3'-untranslated region (UTR) of mRNA transcripts (Schwanhäusser et al. 2008; Monteys et al. 2014). In association with the RISC complex the miRNA binds these targets resulting either in cleavage by Ago2 when the seed region is perfectly paired, or translational repression if there is a mismatch (Schwanhäusser et al. 2008). Repression occurs due to the interaction of Ago2 with the 7-methylguanosine cap of mRNA, inhibiting the binding of translation initiation factors (Saugstad 2010). This can occur concurrently with sequestration into a processing body (P-body) (Saugstad 2010). Subsequently, when a cellular stress occurs, the RISC-bound miRNA:mRNA complex is released from the P-body and translation can occur (Saugstad 2010). Sequestration into P-bodies commonly occurs at neuronal synapses, as it allows for timely gene expression in response to stimuli in a locale that is spatially distant from the nucleus (Siegel, Saba, and Schratt 2011).

MicroRNAs function to manipulate or 'fine-tune' gene target levels to what is specifically required by the cell at that time. In this way they play a very important role in human health, and consequently in human disease as well. In particular, miRNA have been implicated in cancer by either acting as oncogenes or tumor suppressors (Winter et al. 2009). The importance of miRNA in development is seen with mutations of Dicer and Ago proteins which result in severe developmental defects (Winter et al. 2009; Gurtan and Sharp 2013). They are also switches, turning on or off expression of transcription factors for whole pathways. This quality makes them potentially broad-spectrum therapeutic candidates, with some miRNA replacement therapies already in Phase 2 clinical trials (Dwivedi et al. 2016). MiRNA are endogenous cellular molecules, so they

have low chance of being rejected by the cell, can be produced at biologically relevant levels when virally integrated into the host genome and can be directed to be produced tissue specifically (Parsi et al. 2015). In addition, miRNA are stably present in the plasma without the need for microvessicular transport (Turchinovich et al. 2011). This quality makes them appealing as both therapeutic candidates and biomarkers of disease.

One of the unique aspects of miRNA is their inherent promiscuity. One miRNA may bind to hundreds of different gene targets, allowing regulation of whole signaling cascades or cellular processes (Winter et al. 2009). This typically occurs through mild repression of thousands of proteins (Schwanhäusser et al. 2008; Saugstad 2010). The seed sequence is important for this trait, as an increased number of seed sequences on a transcript results in increased translational repression (Schwanhäusser et al. 2008).

Along the same lines, one mRNA 3'UTR may be targeted by many miRNA, thus allowing tight regulation of gene expression. In this way, miRNA are predicted to play some role in the regulation of more than half of protein-coding genes (Gurtan and Sharp 2013). Genome sequencing has enabled bioinformatic target prediction of miRNA on a global scale. Many programs exist for predicting miRNA targets based sequence alignments which determine the potential for direct Watson-Crick base-pairing between the miRNA seed-sequence and complementary regions within the mRNA (typically in the 3'UTR) (Saugstad 2010). In addition, some programs take into account the accessibility of these binding sites within the mRNA, the location within the 3'UTR and the evolutionary conservation of the site to further ensure the likelihood of it being a true miRNA target (Saugstad 2010). But even with these numerous prediction programs, it is still difficult to accurately predict which targets are biologically relevant as this also

depends on the identities and levels of different miRNA, as well as different target mRNAs, being expressed in different cell types. These may also change with developmental stage and environmental stimuli adding further complexity, disentangling the regulatory potential of miRNAs. In addition many miRNA, do not have a high correlation between expression of the mature miRNA and that of the pri-miRNA (W. X. Wang et al. 2014). This suggests that miRNA are highly regulated post-transcriptionally, perhaps even by other miRNA.

Currently, considerable advancement has occurred in the creation of miRNA-based therapeutics. Often, these therapeutics focus on decreasing miRNA expression, with the use of anti-miRs, small RNA molecules designed to sequester miRNA and inhibit their ability to bind targets. For example, an anti-miR was developed to decrease miR-122 expression in the liver in order to prevent Hepatitis C viral proliferation (Janssen et al. 2013). MiRNA mimics have the opposite effect, and are utilized to increase the expression of the miRNA of interest. Many studies of this nature have proven compelling in animal models. For example, miR-128 overexpression in a mouse model of Parkinson's disease resulted in decreased motor abnormalities (Tan et al. 2013). Similarly, in a mouse model of HD, increased cellular levels of miR-196a were neuroprotective against the disease (Cheng et al. 2013). This was also found to be true in a human-induced pluripotent stem cell study from a patient with HD (HD-iPSCs). Transduction with lentivirus expressing miR-196a resulted in decreased numbers of pathological aggregates and less huntingtin protein accumulation (Cheng et al. 2013). Additionally, miR-196a has been implicated in the reduction of HTT levels in human induced pluripotent stem cells from an individual with HD (Cheng et al. 2013).

Yet, the problem facing development of miRNA-based therapeutics lies in their ability to bind multiple targets, potentially resulting in off-target effects. For this reason, considerable research has gone into identifying tissue specific miRNA, which can be targeted specifically with minimal off-target risk (van Rooij, Purcell, and Levin 2012). For example, numerous miRNAs are specifically expressed in neurons, that are important in neuronal differentiation, development, plasticity and survival (Saugstad 2010). In addition, the use of lentivirus or adeno-associated virus (AAV) for expression of miRNA or anti-miRNA enables constitutive expression, the use of tissue specific promoters and the utilization of natural tropisms that certain viruses possess for different cellular receptors (van Rooij, Purcell, and Levin 2012). Also, in relation to neurodegenerative disease treatment, some diseases primarily effect one particular area of the brain, a trait that can be utilized for targeted administration of therapies (Boese et al. 2013). Furthermore, manipulation of mRNA levels has become more specific, with less off target effects as more research has been done in the area.

1.4 MiRNA in Neurodegeneration

Recently, numerous miRNA have been revealed to be dysregulated during neurodegeneration. MiR-29a has been implicated in multiple neurodegenerative diseases. Expression of miR-29a was significantly increased in brain samples from AD patients, prion disease infected mice and the $SOD1^{G93A}$ mouse model of ALS (Shioya et al. 2010; Nolan et al. 2014; Majer et al. 2012). Interestingly, the miR-29a/b-1 cluster has been found to be decreased in expression in brains of AD patients (Hébert et al. 2008; Saugstad 2010). However, it should be mentioned that miR-29 has been found to be expressed more highly in astrocytes than neurons (Saugstad 2010). This highlights the importance of miRNA as biomarkers of specific stages of disease in specific regions of the tissue, as expression can change drastically as disease progresses and minute changes in one area may be hidden in whole tissue sampling approaches.

Changes in expression of miRNA during AD via comparing hippocampal profiles of patients and controls unveiled that miR-132-3p is significantly downregulated in patients compared to controls (Lau et al. 2013). MiR-106b and miR-107 have both been shown to be downregulated in the brains of AD patients, with decreased miR-107 correlating with rapid disease progression (Saugstad 2010). In addition, miR-9, miR-125b and miR-146a have all been implicated in AD pathogenesis, as their expression increases during disease in AD patient brains (Saugstad 2010). Similarly, increased miR-26b in pathological areas of AD patient brains post-mortem can be seen through all stages of disease (Absalon et al. 2013). MiR-16, miR-34c, miR-107, miR-128a, and miR-146a were all found to be differentially expressed in the hippocampus during AD in patients compared to controls

(Müller et al. 2014). In the hippocampus, miR-16 and miR-146a were upregulated in intermediate stage AD patients compared to late stage patients (Müller et al. 2014). This is interesting, as the expression of miR-16 directly parallels what was seen in the Majer et al. study discussed in section 1.5, with miR-16 upregulated during preclinical disease and downregulated clinically in prion disease mice (Majer et al. 2012). Interestingly, miR-128 was found to be decreased in transgenic HD non-human primates in the frontal cortex and striatum in both pre-symptomatic and symptomatic human patients (Kocerha et al. 2014). MiR-133b is decreased in the brains of PD patients, and was revealed to be important for regulating the maturation and function of dopaminergic neurons (Saugstad 2010). A study looked at changes in miRNA expression during prion infection in mice whole brain samples and ultimately identified 15 miRNA deregulated in disease (Saba et al. 2008). Among the upregulated miRNA were miR-342-3p, miR-320, let-7b, miR-328, miR-128, miR-139-5p and miR-146a, while miR-338-3p and miR-337-3p were downregulated (Saba et al. 2008). Additionally, specifically in the hippocampal neurons of prion infected mice, miR-132-3p, miR-124a-3p, miR-26a-5p, miR-29a-3p, miR-140-5p and miR-16-5p were all upregulated during preclinical prion disease and downregulated at the clinical stage of disease (Majer et al. 2012). A summary of miRNA implicated in neurodegenerative disease as reviewed in this thesis is included in Table 2.

Table 2: Summary of Dysregulated miRNA in Neurodegenerative Disease as Discussed in this Thesis.

Disease	Upregulated	Downregulated
AD*	miR-26b, miR-16, miR-146a, miR-29a, miR-9 & miR-125b	miR-132-3p, miR-29a/b-1, miR-34c, miR-107, miR-106b & miR-128a
AD°	let-7d-5p, let-7g-5p, miR-15b-5p, miR-142-3p, miR-191-5p, miR-301a-3p, miR-545-3p, miR-16, miR-148a, miR-1285-5p, miR-26a-5p, miR-151a-3p, miR-161, let-7d-3p, miR-112 & miR-5010-3p	let7f-5p, miR-107, miR-103a-3p, miR-26b-5p & miR-532-5p
PD°	miR-153, miR-409-3p, miR-10a-5p & let-7g-3p	miR-1 & miR-19b-3p miR-133b*
HD^{x}	-	miR-128 miR-29c
Prion$^{x\ clinical}$	miR-342-3p, miR-320, let-7b, miR-328, miR-128, miR-139-5p & miR-146a	miR-338-3p & miR-337-3p
Prion$^{x\ preclinical}$	miR-26a-5p, miR-29a-3p, miR-16-5p, miR-132-3p, miR-124a-3p & miR-140-5p	
* = patient brain o = patient serum x = model organism brain		

Another avenue in neurodegenerative disease research where miRNAs may have instrumental roles, is as biomarker candidates, in particular to inform diagnosis of disease at early stages when treatment of damaged neurons may still be possible. Such diagnostic methodologies are required to utilize new treatment or neuroprotective strategies that are effective early in disease. For this reason, many researchers have sought to identify unique, disease-specific miRNA expression levels within the serum and CSF of afflicted patients. In AD, numerous potential biomarkers have been described in plasma including let-7d-5p, let-7g-5p, miR-15b-5p, miR-142-3p, miR-191-5p, miR-301a-3p and miR-545-3p (Pavan Kumar et al. 2013). Additionally, miR-16 and miR-148a were found to be higher in abundance within the CSF of AD patients than controls (Müller et al. 2014). Next-generation sequencing has revealed that seven miRNA are particularly abundant in the whole blood of AD patients compared to healthy controls, including miR-1285-5p, miR-26a-5p, miR-151a-3p, miR-161, let-7d-3p, miR-112 and miR-5010-3p. Moreover, the same analysis showed that five miRNA are significantly less abundant in AD patients compared to healthy controls, including let7f-5p, miR-107, miR-103a-3p, miR-26b-5p and miR-532-5p (Leidinger et al. 2013). Another avenue that has been explored is to determine microRNA profile within CSF exosomes in neurodegenerative disease patients. One such study revealed that miR-1 and miR-19b-3p were both reduced in PD CSF exosomes compared to controls, while miR-153, miR-409-3p, miR-10a-5p and let-7g-3p were increased in abundance (Gui et al. 2015). The same study looked at AD patient CSF exosomes as well, and determined that while miR-132-5p and miR-485-5p were upregulated in AD samples compared to controls; miR-29c, miR-136-3p, miR-16-2 and miR-331-5p were all downregulated (Gui et al. 2015). It should be kept in mind that

biomarkers may be helpful in both enabling early detection of disease and assessing the success of therapeutics. In neurodegenerative disease, since these diseases progress slowly, the best course of action may not be therapeutics to treat disease, but rather preventative compounds to preclude the disease from occurring by slowing down the progression to a virtual standstill. This concept relies on finding definitive biomarkers of early disease or disease susceptibility and miRNA may be the perfect candidate due to their ability to survive in CSF and blood better than many other biomolecules (Turchinovich et al. 2011).

1.5 MiRNA Regulation in the Hippocampus During Prion Disease

Within our lab, the research focus is on characterizing the neurodegeneration caused by prions using an RML-CD1 mouse model, with the results potentially being applicable to many neurodegenerative diseases, as well as prion disease. The primary aim is to determine the cellular response to prion infection within the mouse brain by pinpointing changes in gene expression within neurons throughout the course of infection. It is therefore key to study a region of the brain affected early on in the disease process, the hippocampus.

In one previous study by Majer et al. 2012, it was found that not only was there substantial differential regulation of neuronal gene expression within this region throughout prion disease, there was also differential regulation of microRNAs (Majer et al. 2012). Neurons within the Cornu Ammonis (CA1) layer of the hippocampus had significantly reduced dendritic spine numbers at 35-45% of the incubation period and

minimal cell death before 70% of disease progression (Cunningham et al. 2003). PrP^{Sc} was considerably present by 90-110 days within the hippocampus (Majer et al. 2012).

Gene expression analysis of microdissected neurons showed two distinct phases of gene expression in the CA1 region hippocampal neurons during the pre-clinical incubation stage of prion disease in mice (Majer et al. 2012). The first stage was an upregulation of genes involved in the neuronal protective response (positive regulation of transcription and stress activated protein kinase pathways), followed by the second stage which was a downregulation of the same genes, occurring right before clinical signs were apparent (Majer et al. 2012). At the onset of clinical disease, more transcripts were altered, with clear induction of inflammatory gene expression via infiltrating microglia and astrocytes (Majer et al. 2012). Preclinically there was also a downregulation of many genes important for glutamate receptor activity, glutamate metabolism, gamma-aminobutyric acid (GABAa), Ca^{2+} signaling, cytoskeleton organization and synaptic vesicle transport (Majer et al. 2012). In tandem with these changes there was an upregulation of many microRNA followed by the same downregulation seen in mRNA (See Figure 1) (Majer et al. 2012).

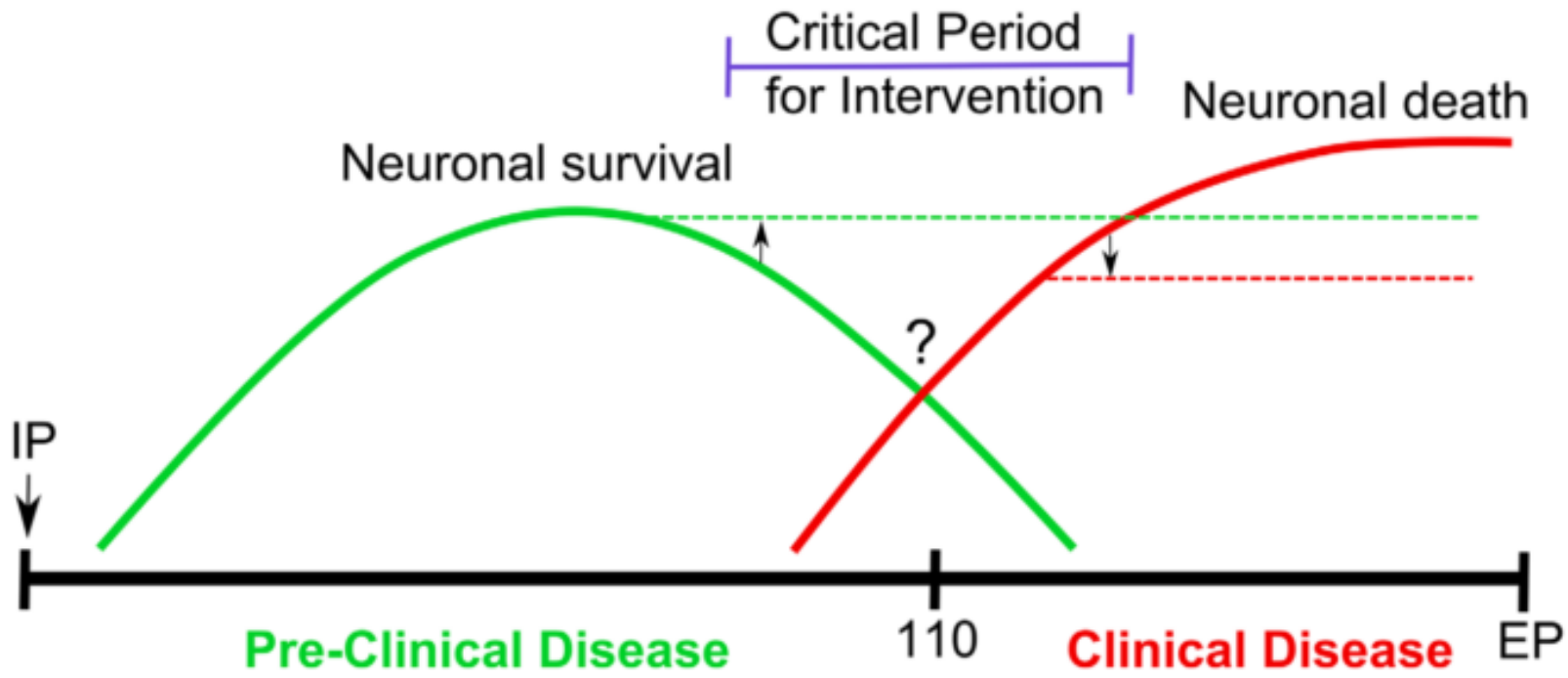
Critical Period
for Intervention
Neuronal death
Neuronal survival
?
IP
Pre-Clinical Disease
110
Clinical Disease
EP

Figure 1: Differential Gene Expression in the CA1 Region of the Murine Hippocampus during Prion Infection (Majer et al. 2012). IP = intraperitonal injection. EP = end-point. The scale bar at the bottom of the figure represents days post infection.

In the study by Majer et al, miRNA expression patterns correlated highly with the mRNA transcriptome with two clear phases of expression evident for miRNA as well. Of particular interest were the miRNA that were upregulated preclinically and declined clinically, as they may be central to staving off disease progression. This group includes miR-132-3p, miR-124a-3p, miR-26a-5p, miR-29a-3p, miR-140-5p and miR-16-5p. MiR-132-3p has previously been shown to be neuroprotective via CREB activation (Wayman et al. 2008). Likewise, miR-124a-3p prevents apoptosis in hippocampal neurons and promotes neurite outgrowth (Sanuki et al. 2011). MiR-29a-3p is important for dendritic spine shaping and development (Lippi et al. 2011). MiR-140-5p, miR-26a-5p and miR-16-5p have been poorly characterized but are known to be expressed in neurons (Majer & Booth 2014).

Interestingly, a similar mRNA expression profile has been identified in the CA1 hippocampal neurons in AD (Ginsberg et al., 2012). However, no studies of miRNA expression within the microdissected CA1 region are currently available to compare to. The sharp downregulation of a group of these molecules occurring at the onset of clinical prion disease suggests that manipulation of their expression may be key to preventing disease onset and consequently an avenue for the development of potential treatments.

1.6 MiR-16

In the prion mouse model, only a handful of miRNA were shown to be upregulated prior to disease onset and downregulated at disease; miR-16-5p, miR-132-3p, miR-124a-3p, miR-29a-3p, miR-26a-5p and miR-140-5p (Majer et al. 2012). These miRNAs are important to take into consideration because they are likely to target genes involved in, or permissive to, neurodegeneration. One miRNA in particular, miRNA-16-5p has never before been investigated in prion disease. MiR-16-5p has been shown to be upregulated from 70 - 110 days post prion infection, returned to baseline levels at 130 days and was downregulated during the clinical stage of disease (Figure 2) (Majer et al. 2012). MiR-16 is a member of the miR-15/107 miRNA family, a group of 10 microRNAs classified as such due to their sharing of the seed sequence 5' AGCAGC (Wang et al. 2014). MiR-16 is highly expressed among all tissues, but in particular is enriched in the human spleen (Wang et al. 2014). It is not one of the most highly expressed miRNA in the brain, but has been shown to be highly upregulated in neuronal development (Wang et al. 2014; Nelson et al. 2006). In addition, studies have shown that compared to other members of it's miRNA family, miR-16 is the highest expressed in cultured glial cells and embryonic neurons (Wang et al. 2014).

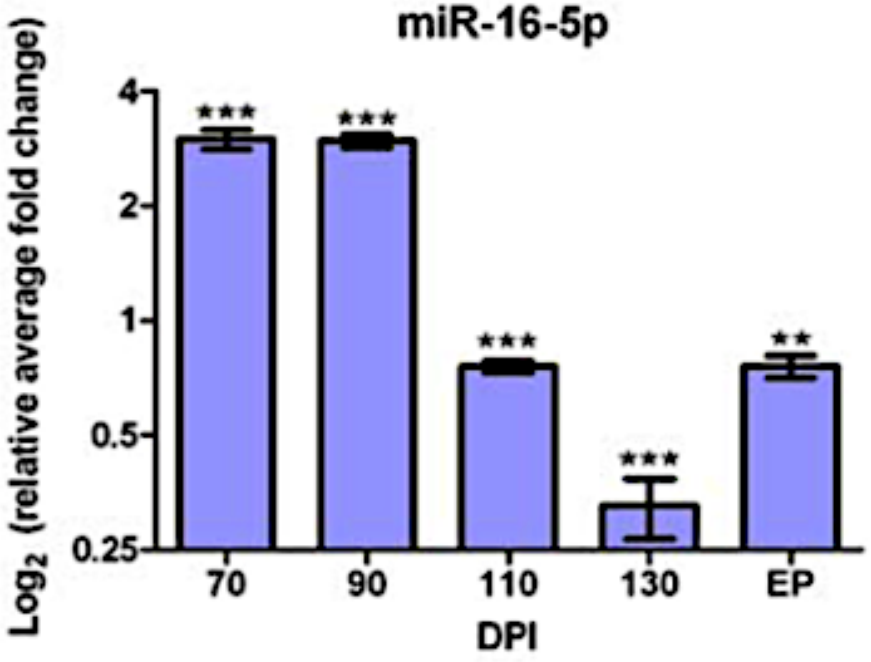
miR-16-5p
Log2 (relative average fold change)
4
2
1
0.5
0.25
***
***
***
***
**
70
90
110
130
EP
DPI

Figure 2: MiR-16-5p Expression is Altered in the CA1 Region of the Hippocampus Throughout Time in an RML-Mouse Model of Prion Disease. Figure from Majer et al. 2012. Expression levels of miR-16-5p were determined at 70, 90, 110, 130 dpi and EP using Real-time PCR.

The sequence of the mature miRNA hsa-miR-16-5p is uagcagcacguaaauauuggcg (22nt long). Hsa- miR-16-1 and hsa-miR-16-2 are genes in different locations in the genome (chromosome 13 and 3, respectively) but lead to identical mature miR-16. However, there are two mature miRNA that are produced from these genes, miR-16-3p and miR-16-5p. These miRNA are produced from opposite arms of the same pre-miRNA and tend to be present in roughly similar amounts. Typically there is a preference for one strand to be loaded into the RISC complex. Based on gene expression analysis, miR-16-5p is the biologically active strand in prion disease (Majer et al. 2012).

Interestingly, miR-16-5p is actually a rather notorious miRNA in the field of cancer research. This particular gene has been implicated in the development of B-cell chronic lymphocytic leukemia (CLL). The region spanning miR-16-1 as well as miR-15a (which is only 0.5kb away from miR-16-1 in Chromosome 13q14) has been shown to be deleted in approximately 68% of the cases of this disease (Calin et al. 2002). MiR-16 binds to many genes that are involved in cell cycle regulation, most importantly BCL-2 an anti-apoptotic gene important for neuronal survival and apoptosis (Bai et al. 2012). CLL is thought to arise via overexpression of BCL-2 in B-cells. There is an inverse correlation between BCL-2 protein expression and miR-16-1 and miR-15a expression in B-cells from CLL patients (Cimmino et al. 2005). Studies have shown that BCL-2 is regulated by miR-15a and miR-16-1 in hematopoietic cancer cells (Cimmino et al. 2005). Additionally in ovarian cancer, BMI1 (B-lymphoma Mo-MLV insertion region 1) is a target of miR-15a and miR-16 as well, with high BMI1 expression implicated with poor prognosis and therapy failure (Dwivedi et al. 2016). For these reasons, miR-16 is considered to be a potent tumor suppressor. In agreement, higher levels of miR-16 and miR-26a correlated

with better survival rate in breast and prostate cancer patients (Lezina et al. 2013). MiR-16 is frequently deleted in cases of CLL, prostate cancer and lung cancer (Calin et al. 2002; Bonci et al. 2008; Bandi et al. 2009). Reduced expression of the miR-15/16 locus in Malignant pleural mesothelioma (MPM) has also been recently determined (Reid et al. 2013). One study showed that introduction of a miR-16 mimic into xenograft-bearing nude mice resulted in inhibition of MPM tumor growth (Reid et al. 2013). A Phase I clinical trial is ongoing in this patient population, with these mimics being coined MesomiR 1 (Kao 2015) (ClinicalTrials.gov NCT02369198). After 8 weeks of weekly treatment, one patient showed a highly reduced glucose uptake within his lungs via fluorodeoxyglucose positron emission tomography (indicative of decreased tumor growth) (Kao 2015). In another instance of miR-16 therapeutic use, in a xenograft mouse model, the miR-16 mimic was successfully targeted to prostate cancer in bone tissue resulting in decreased proliferation of prostate cancer cells (Takeshita et al. 2010).

MiR-16 is implicated in regulation of cell cycle progression, promoting apoptosis and suppressing tumorigenicity (Yan et al. 2013). MiR-16 and miR-26a target two checkpoint kinases of the cell cycle (Chk1 and Wee1) in a synergistic fashion (Lezina et al. 2013). MiR-16 also targets cyclin D1, cyclin D3, cyclin E1 and CDK6 all important in cell cycle progression (inhibits the cell cycle) (Linsley et al. 2007; Q. Liu et al. 2008). Some other studied targets of miR-16 include MAP7 (microtubule-associated protein 7), PRDM4 (PR domain containing 4) and CDS2 (CDP-diacylglycerol synthase 2) in cancer cells (Yan et al. 2013). MiR-16 also has targets in the Wnt signaling pathway (WNT3A) (Bonci et al. 2008).

Multiple studies have identified miR-16 as a key player in the serotonin receptor system, implicating this miRNA in depression. MiR-16 targets the serotonin transporter (SERT) which is important for recapturing serotonin, and is the target of SSRI antidepressants (Baudry et al. 2010). SSRI administration causes a decrease in miR-16 expression in the hippocampus, increasing SERT expression and promoting neurogenesis (Launay et al. 2011). For this reason, miR-16 has been implicated in major depressive disorder (MDD) (Song et al. 2015).

Brain-derived neurotrophic factor (BDNF) is the most abundant neurotrophin in the mammalian central nervous system (Huang & Reichardt 2001). Decreased BDNF in the hippocampus has been implicated in the onset of depression (Bai et al. 2012). MiR-16 targets the mRNA encoding BDNF and decreases its expression (Sun et al. 2013). It has been suggested that stress increases miR-16 expression in the brain, and thus downregulates BDNF levels leading to depression-like symptoms (Bai et al. 2012). In support of this suggestion, mice that experienced maternal deprivation showed lower BDNF mRNA & higher miR-16 than age-matched controls (Bai et al. 2012).

A study by Liu et al. has shown that APP, one of the key proteins in AD, is directly regulated by miR-16 (Liu et al. 2012). They found that miR-16 was downregulated in neurons of SAMP8 mice with early-stage Alzheimer's disease when APP was expressed highly in the hippocampus. Experiments on the effect of overexpression of miR-16 in neuronal cells by this group showed a corresponding decrease in APP expression (Liu et al. 2012). This was in agreement with studies on late-stage AD patient brain samples, which had significantly lower miR-16 within the pre-frontal cortex than control samples (Lau et al. 2013). Thus, the upregulation of miR-16 detected at the pre-clinical period of

prion infection by Majer et al. may be a protective response, functioning in downregulation of genes involved in the progression of the disease, much like APP is in AD. Additionally, miR-16 was identified as a potential biomarker of AD in patient serum. The level of miR-16 in the serum decreased with disease progression and increasing disease severity (Burgos et al. 2014). However, miR-16-2 was downregulated in the CSF exosomes of AD patients vs. controls (Gui et al. 2015).

MiR-16 has previously been implicated in the development of α-synuclein aggregates involved in Parkinson's disease (Zhang and Cheng 2014). MiR-16-1 binds to heat shock protein 70 (Hsp70) which is a negative regulator of α-synuclein aggregation (Zhang and Cheng 2014). Hsp70 is a molecular chaperone that has been highly studied in neurodegeneration, its function is to inhibit misfolding, and accumulation of misfolded proteins yet in PD it fails to perform this function, with α-synuclein and other protein aggregates accumulating within the cell (Zhang and Cheng 2014). Within an α-synuclein-overexpressing human neuroblastoma cell line (SH-SY5Y), one study found that miR-16-1 was binding to Hsp-70 and inhibiting its function to regulate the proper folding of proteins such as α-synuclein (Zhang and Cheng 2014). MiR-16 is increased in expression (the most of any miRNA investigated) in a PD mouse model (Dorval et al. 2014).

Recently, one study looked at changes in protein expression after miR-16 upregulation throughout the brain of wild-type mice (Parsi et al. 2015). They found that miR-16 upregulation resulted in region specific effects on protein level, with APP downregulated in the cortex, brainstem and striatum but not the hippocampus. Similarly, BACE1 was reduced in the hippocampus, brainstem and striatum. Total tau expression was decreased in the hippocampus, brainstem and striatum and there was less phosphorylated Tau in the

hippocampus and striatum. They also showed that protein levels of ERK1 were decreased in the hippocampus and cortex. MiR-16 is a putative regulator of the ERK1/MAPK3 (also ERK2/MAPK1) pathway, which has been implicated in regulation of neuronal tau phosphorylation (Hébert et al., 2012). MiR-16 is found prevalently in the distal axons of neurons and interestingly so is tau (Natera-Naranjo et al. 2010). A proteomic study of the miR-16 overexpressing mouse brain found that few proteins were dysregulated by the addition of miR-16, only 16 in the hippocampus and 103 in the brainstem (Parsi et al. 2015). This was interesting to note, as it suggests that miR-16 overexpression, particularly in the hippocampus, would have little off-target effect.

As is the nature of miRNAs, information about miRNA function in one tissue type is not necessarily true for other types. For instance, as discussed above, miR-16 appears to be inhibitory in the development of AD while it may assist in the development of PD. In addition, one study therapeutically targeted the miR-16 family in cardiac myocytes post myocardial infarction, resulting in decreased infarct size and rescued cardiac function (Hullinger et al. 2012). At the same time, miR-16 has been used as a therapy for cystic fibrosis (CF). A miR-16 mimic has been added to CF lung cells and rescues the function of the F508del-CFTR protein that is dysfunctional in CF (Kumar et al. 2015). The numerous functions of miR-16 are summarized in Figure 3. For these reasons, any treatment with miR-16 would be not without caveats. Yet, some of these diseases are far more treatable than neurodegenerative disease, and for many patients this may be a small price to pay for treatment of a previously incurable disease.

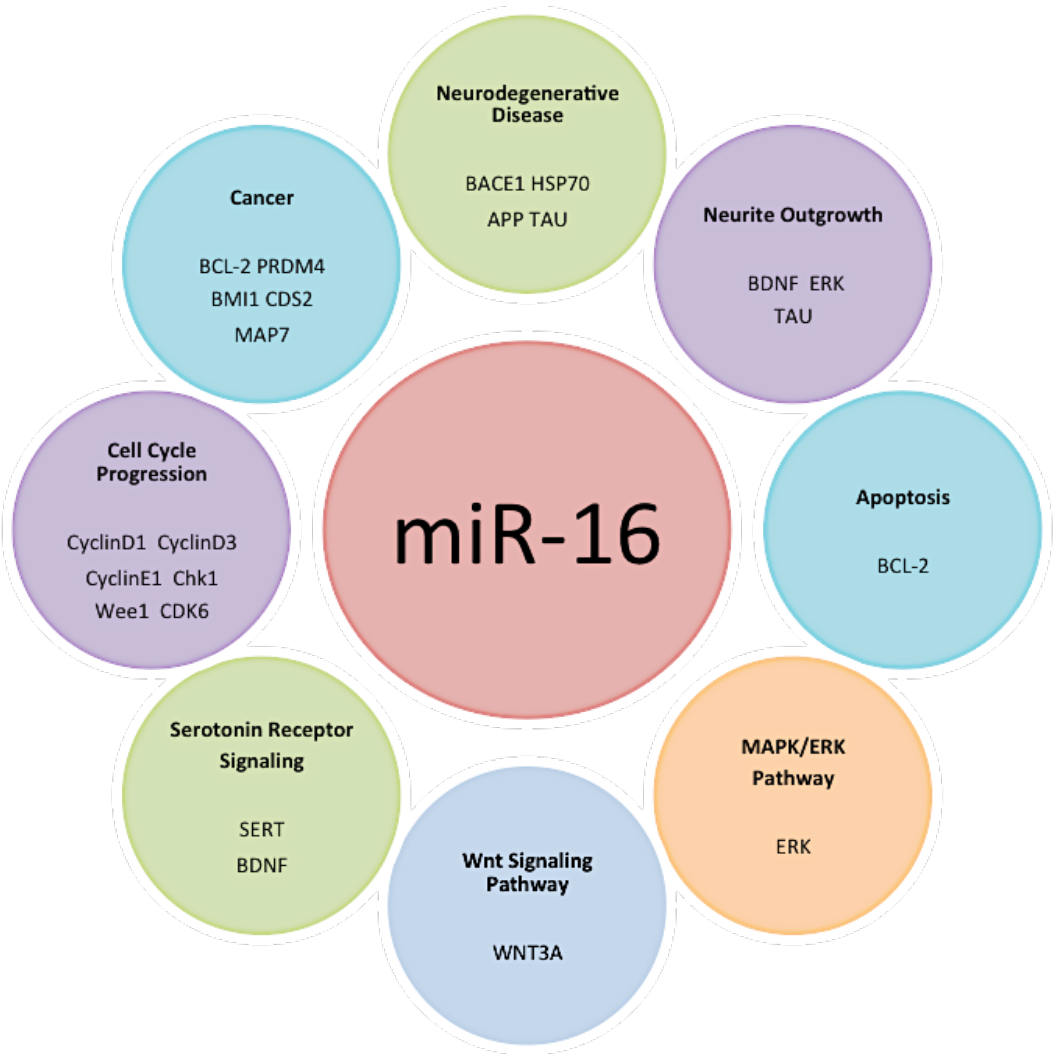
miR-16
Neurodegenerative Disease
BACE1 HSP70
APP TAU
Neurite Outgrowth
BDNF ERK
TAU
Apoptosis
BCL-2
MAPK/ERK Pathway
ERK
Wnt Signaling Pathway
WNT3A
Serotonin Receptor Signaling
SERT
BDNF
Cell Cycle Progression
CyclinD1 CyclinD3
CyclinE1 Chk1
Wee1 CDK6
Cancer
BCL-2 PRDM4
BMI1 CDS2
MAP7

Figure 3: MiR-16 Targets Genes Involved in Many Different Cellular Processes. The circles surrounding miR-16 contain the cellular processes miR-16 that is involved in, with the genes within the pathway that are directly targeted by miR-16 listed beneath.

1.7 Dendritic Remodeling

Localized dendritic translation is integral to dendritic remodeling, a process that is disrupted early in neurodegenerative diseases (Kim et al. 2004). The extension of neurites is due to reassembly of cytoskeletal components, in a dynamic process that is often spatially regulated, with neurite structure depending immensely on extracellular environment of that particular neurite, which can vary drastically (Langhammer et al. 2010). Many miRNA have been implicated in regulating dendritic development (Saugstad 2010). One study identified 86 miRNAs expressed in neurons that co-fractionate with polyribosomes indicating their involvement in active translation (Kim et al. 2004). This type of miRNA localization is highly advantageous for neurons, as miRNA can bind and sequester target mRNA into P-bodies located at neuronal synapses (Huang et al. 2012), as there are more than 400 mRNAs identified to localize to dendrites along with translational machinery (Eberwine et al. 2001) many of which encode synaptic receptors and kinases (important for synaptic changes) (Kim et al. 2004; Eberwine et al. 2001). This is important so that when a stimulus occurs highly regulated protein translation occurs directly at the synapse without the lag time that would be associated with completely new mRNA synthesis (Schacher and Wu 2002; Kaplan et al. 2009). In support of this possibility, inactivation of Dicer in developing mouse hippocampus resulted in decreased branching (Davis et al. 2008). Also at different stages of primary neuron growth in culture, there are distinct changes in groups of miRNAs (48 miRNAs total) that presumably regulate these changes (van Spronsen et al. 2013).

Branching is important for neural function, information processing and communication (Vetter et al. 2001; Schaefer et al. 2003; Langhammer et al. 2010). Abnormal branching

has been attributed to pathogenesis of neurological and neurodegenerative disorders such as AD (Arendt et al.1986; Lewis et al. 2003). As neurites increase in length, there is increased potential for synaptic connections to be made along these appendages (Arendt, Zvegintseva, and Leontovich 1986). Each synaptic connection is important for neuronal health and communication between neurons. Synaptic maintenance is lost early in neurodegenerative diseases, with the complete loss of synapses occurring not long after. During prion disease, decreased numbers of synapses and dendritic spine densities are found in the cortex and hippocampal neurons during preclinical disease suggesting that since such rapid changes in protein abundance occur, they are likely regulated close by, via miRNAs located at the synapse (Boese et al. 2016). There have also been accounts of decreased neurite length, branches and synapses in PD brain samples (Dubey et al. 2015).

Decreased cell body area has been identified in neurons within hippocampi of AD and vascular dementia patients (Arendt, Zvegintseva, and Leontovich 1986; Gemmell et al. 2012). It has been suggested that this decrease in cell body area is related to a decreased neuritic function, as somal volume has been shown to be proportional to dendritic and axonal structure (Gemmell et al. 2012; Lewis et al. 2003). Intriguingly, both degenerative and regenerative changes have been found in the brains of AD patients (Arendt, Zvegintseva, and Leontovich 1986). The degenerative changes comprised dendritic fragmentation and cell death, while the regenerative changes encompassed increased soma size, dendritic arborization and increased dendritic length (Arendt et al. 1986). These regenerative changes were likely compensatory for the neuronal function lost to degenerative changes. The exact mechanism for this is unknown, but it is thought to be a combination of factors including dysfunction of microtubule dynamics.

Microtubules are essential for transporting cellular components from the cell body along the length of dendrites. Microtubules are composed of heterodimers of α- and β-tubulin constantly assembling and disassembling to maintain dynamic cellular functions (Dubey et al. 2015; Götz et al. 2006). The most highly abundant microtubule-associated proteins (MAPs) within neurons are MAP2 (in the somatodendritic domain) and tau (in axons) (Götz et al. 2006). MAPs provide structural support to microtubules and assist in axonal transport.

Axonal transport (due to the length of some neurites and their inability to regenerate) is implicated in cellular dysfunction during neurodegenerative disorders (Götz et al. 2006). Molecular transport and protein trafficking has been shown to be highly regulated in neurons of prion disease mouse model (Sorensen et al. 2008). Axonal transport has been shown to be disrupted in AD (Götz et al. 2006). Compromised axonal transport is one potential cause for impaired synaptic plasticity, a common manifestation in neurodegeneration. Synaptic plasticity is important for information processing (Thomas and Huganir 2004). This is particularly interesting in prion-infected neurons, as a connection between cell death in neurodegenerative diseases and excitotoxicity (overstimulation of neuronal synapses resulting in cell death) has been proposed (Choi 1988; von Engelhardt et al. 2007). In agreement, one of the first physical signs of prion disease progression in the brain is the loss of synapses (Jeffrey et al. 2000; Cunningham et al. 2003) followed closely by the degeneration of axon termini, with clinical disease symptoms occurring well after (Jeffrey et al. 2000).

Chapter 2: Gaps in Knowledge/Hypothesis/Objectives

As research progresses in this field it is becoming clear that although the symptoms and etiologies of neurodegenerative diseases vary, the molecular underpinnings are remarkably similar with each involving the aggregation of a misfolded host protein resulting in neuronal abnormalities and dysfunction. In many cases these pathologies can be seen long before the clinical stage of disease, with evidence of AD present in the brain more than 20 years before symptoms occur (Alzheimers Association 2015). For this reason, developing therapeutics derived from these similarities could be extremely beneficial in staving off disease progression. With this in mind, understanding neurodegenerative disease and the process of neurodegeneration is paramount to success.

The dysregulation of miR-16 in a number of neurodegenerative diseases suggests that it may be directly involved in key disease-related processes. Of most importance to this project, miR-16-5p has been determined to be upregulated preclinically in the hippocampus and downregulated clinically in a RML mouse model of prion disease (Majer et al. 2012). It has also been found to target and inhibit the expression of APP and BACE1, two important molecules in AD, as well as to inhibit phosphorylation of tau (Parsi et al. 2015). Of large interest to this study, is the fact that miR-16 upregulation resulted in a decrease in gene expression of Prnp (major prion protein) with significance (p-value <0.05) although there was no predicted target site in the coding region or the 3'UTR, indicating that it is likely an off-target effect (Parsi et al. 2015). With the increasing evidence for a role of miR-16 in neurodegeneration, the aim of this thesis is to elucidate the function of miR-16 within neurons, and specifically to tie this information

into the function of this miRNA within neurodegeneration. In order to understand miR-16's role in neurodegeneration, we must first understand its role in healthy cells, and how that role may be altered during disease.

2.1 Hypothesis

The hypothesis of this thesis is that hippocampal miR-16-5p, given its induction in hippocampal neurons during preclinical disease, plays a role in regulating the dendritic remodeling that is a characteristic early pathological feature of neuronal degeneration in prion disease.

2.2 Objectives

To address this hypothesis there are two main objectives.

1) To determine the target genes and pathways on which miR-16-5p acts in hippocampal neurons.
2) To examine whether regulation of these pathways affects neuronal phenotype in a way that may be relevant to prion disease pathogenesis.

A primary hippocampal neuronal culture system along with lentiviral vectors to manipulate expression of miR-16-5p within the cells will be used to meet these objectives. To address the first objective, the effect of miR-16-5p upregulation and downregulation on the target mRNA and protein expression profiles of neurons will be examined with microarray profiling and western blot analysis. To address the second objective, the effect of miR-16-5p manipulation on neuronal phenotype will be determined by measuring neurite length, branching patterns and soma area.

Overall, the results of these studies will enable better understanding of the role of miR-16-5p in hippocampal neurodegeneration by assessing the phenotypic and genotypic

effects of changes in cellular miR-16-5p level on hippocampal neurons. These experiments are important in order to understand whether the upregulation of miR-16-5p during preclinical prion disease is beneficial to delaying disease progression.

Chapter 3: Materials and Methods

3.1 Animal Use Document

All animals were cared for as outlined in the Animal Use Document (AUD) H15-032. Timed pregnant CD1 female mice were first anaesthetized and then cervically dislocated. The uterus was collected and the embryos removed and decapitated. Pregnancy was timed to ensure that collections were performed at approximately embryonic day 18. Veterinary Services staff within the Public Health Agency of Canada Biosafety Level 2 Laboratory performed these procedures.

3.2 Primary Hippocampal Culture

Hippocampal dissection was performed within an hour of collection using a Leica KL300 LED microscope. Embryonic mouse heads were kept chilled in 1X Dissecting Media (DM) (10.15g of 100mM MgCl2 x $6H_20$, 0.946g of 10mM Kynurenic acid (Sigma), 11.92g of 100mM HEPES in 500mL HBSS (1X) Hank's Balanced Salt Solution (-Calcium Chloride)(-Magnesium Chloride)(-Magnesium Sulfate) (Life Technologies) brought to pH 7.2 with 1N NaOH) on cold blocks throughout the dissection. Dissections were performed in 60mm x 15mm Polysterene Petri Dishes (Fisherbrand) with Fine Science Tools by DUMONT. The procedure began by cutting the skin caudal to rostral, holding the skull steady at the eye-sockets. Next, three incisions were made through the skull, the first along the superior sagittal sinus and the remaining along the symmetrical transverse sinuses. The skull was removed, exposing the brain, which was then detached from the olfactory lobes and lifted from the skull cavity. The brain was placed into a fresh dish of 1X DM and the left and right cerebral hemispheres were removed. Each hemisphere carefully had the meninges detached with forceps. The hippocampus was

dissected out from the interior of each hemisphere by making a careful incision along the corpus callosum, which resides directly above the hippocampus.

Hippocampi were incubated in a 37ºC water-bath with papain (100µL Papain Suspension (Worthington Biochemical Corporation (44.8 mgP/mL)) in 5mL 1X DM, 25µL of 10mg/mL Deoxyribonuclease I from bovine pancrease (DNAse I) (Sigma-Aldrich) and filter sterilized (Sterile Syringe Filter with 0.2µm Cellulose Acetate Membrane (VWR)) for 4 minutes. Papain was then removed and hippocampi were washed/incubated in 5mL of Trypsin Inhibitor (0.15g Trypsin Inhibitor from Chicken Egg White (Sigma) in 15mL 1X DM, with NaOH added until pH 8.5, and 75µL 10 mg/mL DNAse I, filter sterilized (0.2µm filter)) three times at 3-minute intervals. Following the washes, hippocampi were incubated in 5mL NBActiv4 media (Brain Bits) (Sterile Neurobasal/B27/Dipeptide L-Alanyl-L-Glutamine (Invitrogen)/Creatine/Estrogen) with 1% Penicillin Streptomycin Glutamine (Life Technologies) (10,000 Units/mL Pen. 10,000 µg/mL Strep. 29.2 mg/mL L-Glutamine) for 3 minutes. Upon removal of media, another 1 mL of media was added to the cells, which were then triturated with a P1000 pipette (set to 700µL to avoid creation of bubbles) until a homogeneous suspension was achieved. Cells were counted with a Bright-Line Hemacytometer (Hausser Scientific) using 10µL of cell suspension and 10µL of trypan blue (2X dilution). The method employed to count the cells kept consistent between preps, with the top two rows and bottom two rows counted, and the middle row excluded from calculations. This method results in 20 squares measuring 0.02cm x 0.02cm x 0.01cm.

Cells/mL = cell count/20 (x 2 (dilution factor))(1mL/(0.02mLx0.02mLx0.01mL))

Cells were then diluted in NBActiv4 and plated at 50,000 cells/well on a 24-well plate pre-treated with PDL. Enzymes and 1X DM were always prepared fresh the day of the procedure. Cells were fed with 1mL of NBActiv4 four days post-plating. At eight days post-plating, and every four days after that, half of the media was removed and an equivalent amount of fresh media was added to maintain cell viability.

3.3 Fixing and Staining Primary Hippocampal Neurons

Coverslips (High Precision Microscope Cover Glasses – Deckgläser 13mm Marienfeld-Superior (Zeiss)) were prepared by acid wash (1M HCL) then autoclaved. Coverslips were sprayed with 70% ethanol, buffed with a Kimwipe (Kimberly-Clark) to remove any lasting residue from washes and carefully placed into 24-well plates with forceps. 1mg/mL Poly-D-Lysine (BD Biosciences) dissolved in borate buffer (4.76g Boric acid (EM Science), 2.54g sodium borate (Sigma), 1L ddH_2O, pH to 8.4 with 5M NaOH and sterile filtered) at 0.02mg/mL was then added to wells at 500µL per well, to give a final quantity of 10µg of PDL/well. Plates were incubated at 37ºC for 24 hours. After 24 hours, PDL was removed and wells were washed with 500µL sterile milliQ water twice, before replacing with NBactiv4 media for a final volume (with cells included) of 500µL.

After cells were grown for the required amount of time (usually 12 days) they were fixed in 4% paraformaldehyde (PFA) with 4% sucrose. This was prepared by mixing 4g sucrose (Fisher Chemical) with 4g PFA (Fisher Chemical) and 100µL of 10M NaOH (Fisher Chemical) in 100mL of 1X DEPC-PBS (made in house). The mixture was warmed to 60ºC in a fume hood, and cooled to room temperature once all components were dissolved. In total, 65µL of 37% HCL (Fisher Chemical) was used to adjust the pH to 7.5. The liquid PFA was then aliquoted in 12.5mL aliquots and stored at -80ºC.

Powder PFA was handled with double gloves, lab coat, N100 respirator (3M) and protective eyewear.

On the day that the cells were to be fixed, PFA was thawed in a 37ºC bead bath. After at least 30 minutes of heating, the PFA was taken to the fume-hood to fix the cells. The PFA must be used immediately to maintain optimal temperature for ideal performance. Media was removed from cells and 500µL of PFA added to each well of a 6-well plate. After 12 minutes of incubation in PFA, it was removed and the cells were rinsed 3 times in 1X PBS (Life Technologies). The fixed coverslips were stored in 500µL of 1X PBS at 4ºC until immunostaining was performed.

A variety of antibodies were used for immunostaining depending on the experimental design. Astrocytes were immunostained with an antibody to detect glial fibrillary acidic protein (GFAP) (1:500 dilution)(Dako; Z0334) with a 1:200 dilution of a goat anti-rabbit secondary antibody conjugated to Cy3 (Abcam; ab6939) or Cy5 (Abcam; ab97077). Neurons were detected with antibody to microtubule-associated protein 2 (MAP2) (1:1000)(Abcam; ab5392) with a 1:200 dilution of a goat anti-chicken secondary antibody conjugated to Alexa Fluor 555 (Abcam; ab150174). All antibodies were diluted in 1X PBS pH 7.4 (Life Technologies). Cells were first permeabilized with 0.5% Triton X-100 (Sigma-Aldrich) for ten minutes, followed by incubation with primary antibodies (as described above) for 1 hour at room temperature (RT). Subsequently, coverslips were washed once with 0.1% Triton X-100 and then twice with 1X PBS. Following this, coverslips were incubated with secondary antibody (as described above) for 1 hour at RT in the dark. The washes were repeated as described and then the coverslips were mounted

on slides (Thermo Scientific) using ProLong Gold Mounting Media containing DAPI (Life Technologies).

Slides were scanned for image acquisition using the MIRAX MIDI scanner (Zeiss). Pannoramic Viewer (3DHISTECH) was employed to view images and to take pictures at different magnifications for subsequent analysis. The brightness and contrast of the filtered images were optimized and the 'tracking' function was turned on to ensure that cells were not captured in photos more than once.

3.4 Analysis of Culture Purity with Immunostaining for Neurons and Astrocytes

Primary hippocampal neurons plated on coverslips were fixed at days *in vitro* (DIV) 5, 7, 11 and 14. Coverslips were immunostained as outlined in Section 3.3, with antibodies to detect MAP2 and GFAP. Immunostained coverslips were then visualized with the MIRAX MIDI scanner. Pannoramic Viewer was used to visualize the scans. In total, twenty photos were taken per slide, this ensured that the vast majority of the slide was captured which enabled counting of the cells with reduced selection bias. Images were saved as tiff files at 10X magnification for cell counting, as well as both 5X and 20X magnification for representative images of cell health.

The ImageJ Cell Counter plug-in was employed to count the number of MAP2 positive cells (indicating neurons) and the number of GFAP positive cells (indicating glia). The average number of each of these cell types throughout the twenty images was used to determine the percentage of neurons in the culture.

3.5 RNA Analysis (Endogenous miR-16 Expression)

In order to isolate RNA from tissue culture samples the Total RNA Purification Micro Kit (Norgen Biotek Corp.) was used. The protocol entitled "Cell Lysate Preparation from Cells Growing in a Monolayer" was utilized with slight modifications. In a BSC, media was removed and 350µL of Buffer RL was added to each well, of either a 24-well or 6-well plate. A 24-well plate contained 50,000 primary hippocampal cells per well while a 6-well plate contained 250,000 cells per well. No PBS wash was performed to prevent unnecessary cell loss. Cells were lysed via scraping with either a cell scraper or a pipette tip. Lysates were placed in 1.5mL tubes and transferred to the benchtop for the remainder of the procedure. Upon addition of 200µL of anhydrous ethyl alcohol (Commercial Alcohols) the lysate was vortexed and transferred to a micro spin-column. The column was centrifuged for 1 minute at 3500 x g (Eppendorf Centrifuge 5417C) and flow-through discarded. The column was then washed three times with 400µL of Wash Solution A (containing anhydrous ethyl alcohol) and centrifuged for 1 minute at 14,000 x g with every wash, followed by a 2 minute spin at the same speed to dry the resin. The column was placed into a new RNase-free tube and the RNA was eluted from the resin with 20µL of Elution Solution A via centrifugation at 200 x g for 2 minutes, followed by 14,000 x g for 1 minute. The RNA was stored at -80ºC until used.

Immediately upon thawing, RNA was quantified with a NanoDrop. RNA quality and quantity was analyzed using a BioAnalyzer. Six samples were analyzed in duplicate via a Eukaryote Total RNA NanoChip. RIN numbers were all between 5 and 10. On two samples the RNA was too little to conclude RIN but the gel clearly depicted 18S and 28S peaks. As all of my samples are from the same cell culture conditions and the

concentrations determined by Bioanalyzer were very similar to those determined by Nanodrop, I made the assumption that the RNA used in this Bioanalyzer run was indicative of all of my sample RNA and therefore I used the Nanodrop from this point on to assess RNA quality (Data is included in Appendix 1.1).

Reverse Transcription was performed using the TaqMan MicroRNA Reverse Transcriptase Kit (Cat# 4366596; Life Technologies) (10ng of total RNA was used per 15µL reaction). Master mix was created by mixing: 0.15µL 100mM dNTPs (with dTTP), 1µL MultiScribe Reverse Transcriptase, 50 U/µL, 1.5µL 10X Reverse Transcription Buffer, 0.19µL RNase Inhibitor, 20 U/µL and 4.16µL Nuclease-free water totaling 7µL per 15µL reaction. The master mix was added to 3µL of 5X RT Primer (gene of choice or housekeeping gene (usually U6 (Cat #4427975; Life Technologies)) and 5µL of RNA sample containing 10ng of total RNA. These were gently mixed together, and centrifuged before placing in a thermal cycler. The following reverse transcription reaction was performed: 30 minutes at 16ºC, 30 minutes at 42ºC, 5 minutes at 85ºC followed by a hold at 4ºC. This was performed on a MJ Research PTC-200 Peltier Thermal Cycler with a heated lid. The cDNA product was stored at -20ºC or used for Real-time PCR immediately.

TaqMan Small RNA Assays (Applied Biosystems by Life Technologies) were used to determine target transcript levels in the cDNA product via Realtime PCR. No template controls (NTCs) were used for each probe. Endogenous control assays were used for comparison. Each reaction was 20µL in volume, containing 1µL of TaqMan Small RNA Assay (20X), 1.33µL of cDNA, 10µL of TaqMan Universal PCR Master Mix II (2X), no UNG and 7.67µL of Nuclease-free water. Each reaction was performed in duplicate, and

the 96-well 0.1mL plates were sealed with MicroAmp Optical Adhesive Film (Applied Biosystems), vortexed and centrifuged at 1000rpm for 2 minutes at 4ºC (Thermo Electron Corporation- Sorvall Legend RT Centrifuge). The ViiA7 (Applied Biosystems) thermal cycling conditions were as follows: 10 minutes at 95ºC for enzyme activation, followed by 40 cycles of 15 seconds at 95ºC for denaturation and 60 seconds at 60ºC for annealing and extension. The resulting data was analyzed using the ΔΔCt method in Microsoft Excel. Technical replicates had low standard deviation in Ct values, averaging <0.05.

3.6 Manipulation of miR-16 Expression with Lentivirus

3.6.1 Production of miRNA Containing Plasmids

Plasmids containing miR-16, miR-Scr, miRZIP-16 or miRZIP-Scr were ordered from System Biosciences (Lentivector-based MicroRNA Precursor Constructs (Cat.# PMIRHxxxPA-1)). Each vector contained a pUC origin of replication that enabled high copy replication in *E.coli* cells, and an ampicillin resistance gene for colony selection. Other important elements included in the vectors are highlighted in Figure 4. *E.coli* stock plates were received and incubated overnight at 37ºC and single colonies were streaked onto Luria Bertani (LB) +Carbenicillin (50μg/mL) plates. Single colonies were then used to inoculate 3mL LB+Carbenicillin (50μg/mL) broth, which was grown for 8 hours at 37ºC with shaking.

This broth (200μL) was used to inoculate a 500mL flask containing 100mL of the same media, which was left for 16 hours at 37ºC shaking. The broth was then centrifuged at 6000 x g for 15 minutes at 4ºC and the bacterial pellet was used for an endotoxin free Maxi prep using the established high-copy plasmid protocol from the QIAGEN EndoFree

Plasmid Maxi Kit. The pellet was resuspended in 10mL of Buffer P1 for cell lysis followed by addition of 10mL of Buffer P2, inversion and incubation at RT for 5 minutes. Subsequently, 10mL of chilled Buffer P3 was added followed by another inversion to precipitate genomic DNA, protein and cell debris. The lysate was added to a QIAfilter Maxi Cartridge and incubated for 10 minutes at RT before filtering into a 50mL tube. Buffer ER was added to the filtrate, inverted and left on ice for 30 minutes. The lysate was then added to an equilibrated QIAGEN-tip 500 and allowed to empty via gravity flow. The QIAGEN-tip was next washed twice with 30mL of Buffer QC to remove contaminants and finally, the DNA eluted with 15mL of Buffer QN. The DNA was precipitated with 10.5mL of RT isopropanol, mixed and centrifuged at 5,000 x g for 60 minutes at 4ºC. The supernatant was then decanted and the pellet washed with 5mL endotoxin-free RT 70% ethanol and centrifuged again at 5,000 x g for 60 minutes at 4ºC. The supernatant was decanted again, and the pellet left to air-dry for 10 minutes, before resuspending it in endotoxin-free Buffer TE. The final plasmid product was quantified with a Nanodrop at 260nm. All samples yielded approximately 1000ng/µL of plasmid product.

Plasmids were sequenced to verify specific miRNA presence. Sanger Sequencing was performed at the NML DNA Core Facility. Plasmids were supplied to core facility as 150ng/µL stocks (5µL per reaction) and primers were supplied as 1µM stocks (5µL per reaction). The miR-ZIP clones were sequenced using the Fwd GNH Primer – TGCATGTCGCTATGTGTTCTGGGA and the miRNA clones using the EF1 rev Primer- 5`- GCACCCGTTCAATTGCCG-3`. Sequences were analyzed using DNASTAR Lasergene 13 SeqMan Pro and SeqBuilder (DNASTAR Madison, WI). Blast

Nucleotide analyses were performed using NCBI Nucleotide Blast and miRBase hairpin directed Blast (Kozomara and Griffiths-Jones 2014).

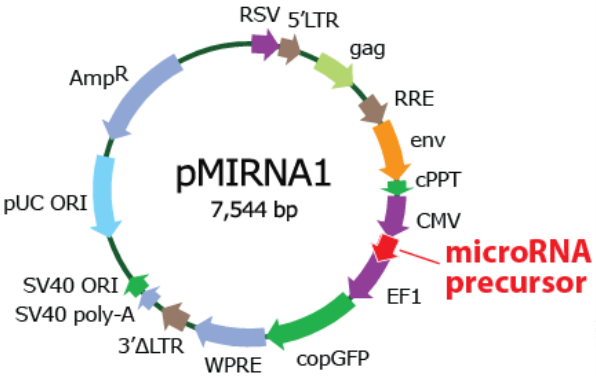

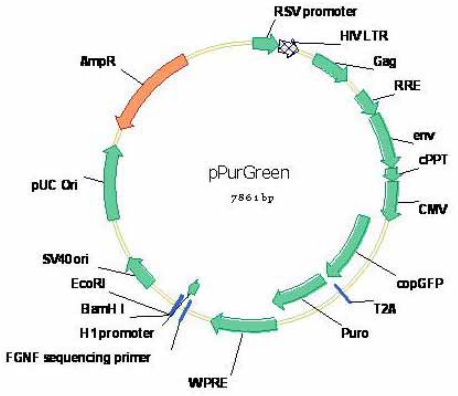

Feature	Location*	Function
RSV/5'LTR	7-414	Hybrid RSV promoter-R/U5 long terminal repeat; required for viral packaging and transcription
gag	567-919	Packaging signal
RRE	1076-1309	Rev response element binds gag and involved in packaging of viral transcripts
cPPT	1798-1916	Central polypurine tract (includes DNA Flap region) involved in nuclear translocation and integration of transduced viral genome
CMV promoter	1922-2271	Human cytomegalovirus (CMV)--constitutive promoter for transcription of cloned cDNA insert
EF1	2315-2860	Elongation factor 1α promoter--constitutive promoter for transcription of Reporter gene (Puromycin resistance or copGFP)
copGFP	2874-3629	Copepod green fluorescent protein (similar to regular EGFP, but with brighter color) as a reporter for the transfected/transduced cells
WPRE	3639-4229	Woodchuck hepatitis virus posttranscriptional regulatory element--enhances the stability of the viral transcripts
3' ΔLTR (ΔU3)	4301-4534	Required for viral reverse transcription; self-inactivating 3' LTR with deletion in U3 region prevents formation of replication-competent viral particles after integration into genomic DNA
SV40 Poly-A	4606-4737	Transcription termination and polyadenylation
SV40 Ori	4746-4892	Allows for episomal replication of plasmid in eukaryotic cells
pUC Ori	5262-5935 (C)	Allows for high-copy replication in *E. coli*
AmpR	6080-6940 (C)	Ampicillin resistant gene for selection of the plasmid in *E. coli*

* The notation (C) refers to the complementary strand.

Feature	Location*	Function
RSV/5'LTR	7-413	Hybrid RSV promoter-R/U5 long terminal repeat; required for viral packaging and transcription
gag	566-920	Packaging signal
RRE	1076-1309	Rev response element binds gag and involved in packaging of viral transcripts
cPPT	1806-1923	Central polypurine tract (includes DNA Flap region) involved in nuclear translocation and integration of transduced viral genome
CMV promoter	1929-2278	Human cytomegalovirus (CMV)--constitutive promoter for transcription of copGFP-T2A-puro
copGFP	2293-3048	Copepod green fluorescent protein (similar to regular EGFP, but with brighter color) as a reporter for the transfected/transduced cells
T2A	3049-3102	*Thosea asigna* virus 2A translational cleavage site containing 18 amino acid residues. Cleavage occurs via a co-translational ribosome skipping mechanism between the C-terminal Glycin and Prolin residues, leaving 17 residues attached to the end of copGFP and 1 residue to the start of the puromycin resistance marker
Puro	3103-3702	Puromycin-resistant marker for selection of the ransfected/transduced cells
WPRE	3703-4291	Woodchuck hepatitis virus posttranscriptional regulatory element--enhances the stability of the viral transcripts
3' ΔLTR(ΔU3)	4631-4813	Required for viral reverse transcription; self- inactivating 3' LTR with deletion in U3 region prevents formation of replication-competent viral particles after integration into genomic DNA
H1 RNA promoter	4526-4616	RNA polymerase III promoter for expression of anti-microRNA insert
SV40 Poly-A	4911-5219	Transcription termination and polyadenylation
SV40 Ori	4911-5219	Allows for episomal replication of plasmid in eukaryotic cells
pUC Ori	5584-6252	Allows for high-copy replication in *E. coli*
AmpR	6397-7257 (C)	Ampicillin resistant gene for selection of the plasmid in *E. coli*

Figure 4: Maps of the HIV-1 Derived Plasmid Vectors used to Manipulate miR-16 Expression (Systems BioSciences) pMIRNA1 encodes miR-16 and miR-Scr. pPurGreen encodes miRZIP-16 and miRZIP-Scr. Tables below each plasmid outline the important components for both plasmid and miRNA propagation.

3.6.2 Lentiviral Packaging of miRNA Containing Plasmids

HEK293T cells were grown up in (1X) Dulbecco's Modified Eagle Medium (DMEM)(+4.5g/L D-glucose)(+L-Glutamine)(-Sodium Pyruvate) with 10% Fetal Bovine Serum (FBS) (Life Technologies) and 1% Penicillin Streptomycin Glutamine (Life Technologies) (10,000 Units/mL Penicillin 10,000 µg/mL Streptomycin 29.2 mg/mL L-Glutamine). HEK293T cells were used as they stably express the SV40 large T antigen, which is useful for producing large quantities of virus. The Lentivector Expression Systems: Guide to Packaging and Transduction of Target Cells protocol was used to package the plasmids.

Cells were plated at 7.0 x 10^6 cells per 150cm^2 cell culture plate in 20mL of antibiotic free media until ~70% confluent. 1mL of DMEM (serum free) was added to a sample tube along with 45µL pPACKH1 and 4.5µg of the lentivector with the mixture of these plasmids totaling 0.5µg/mL each. The pPACK Lentivector Packaging System (pPACKH1-XL HIV Lentivector Packaging Kit (LV510A-1) (System Biosciences)) includes all viral genes (env, gag, pol, rev and vsv-g) encoding proteins necessary to produce pseudoviral particles (envelope protein, structural protein, polymerase, reverse transcriptase and vesicular stomatitis virus glycoprotein G to aid in viral entry, respectively). These genes are encoded on separate plasmids, which are not incorporated into the viral product, ensuring that they are replication incompetent viruses.

To the plasmid mixture, 55µL of Lipofectamine 2000 (Invitrogen) was added with vortexing 10 seconds. This mixture was incubated RT for 15 minutes before evenly adding it to the culture dish. After 24 hours the media was changed. At 48 hours the media was collected (containing the pseudoviral particles) and centrifuged at 3000 x g for

15 minutes at RT to pellet the cell debris. Supernatant was then transferred to a new conical tube and 1 volume of cold PEG-it Virus Precipitation Solution (5X) (Cat# LV810A-1; System Biosciences) was added to every 4 volumes of supernatant. The mixture was refrigerated for 24 hours and subsequently centrifuged at 1500 x g for 30 minutes at 4ºC. The supernatant was then transferred to a fresh tube (saving the pellet) and the spin was repeated. The combined pellets were resuspended in 1/10 of original volume in cold sterile 1X PBS and aliquoted at -80ºC.

The pseudoviral particles were subsequently used to transduce primary hippocampal cells. Upon entering the primary cells, the expression constructs were reverse transcribed and integrated into the neuronal genome. The miR-16 and miR-Scr constructs were transcribed, using host machinery, via the constitutive CMV promoter. In this system GFP was transcribed from an elongation factor 1a (EF1) promoter. Alternatively, the miRZIP-16 and miRZIP-Scr constructs were transcribed, using host machinery, from the constitutive H1 promoter, an RNA polymerase III promoter. In this system GFP was transcribed from the constitutive CMV promoter. All experiments were performed 72-96 hours after pseudoviral administration, as optimal expression occurs at this time point. In addition, pseudovirus was only used after the first thaw as the titer drops ~30% with each freeze-thaw.

3.6.3 Titering of Pseudovirus

Primary hippocampal cells were plated at 50,000 cells/well in 24-well plates containing coverslips. They were then treated with 2-10µL of virus at DIV 8. At DIV 12, primary hippocampal cells were viewed on the Fluorescent Microscope OLYMPUS 1X70 with X-Cite 120PC to confirm GFP expression. The cells were subsequently fixed and

immunostained with antibodies directed at MAP2 as described in section 3.3. The coverslips were then viewed on the MIRAX MIDI scanner and 15 images per coverslip were taken at 10X magnification. The number of MAP2 positive cells were noted for each image as well as the number of MAP2 positive, GFP positive cells using the ImageJ Cell Counter plugin. The proportion of MAP2 positive cells that were also GFP positive was determined to represent the titer of the virus. Two biological replicates were used for tittering. The average of each biological replicate was plotted with the SEM between the two replicate sets.

3.7 Checking for Cytotoxic Effect of Lentivirus on Hippocampal Primary Cells

Promega CytoTox 96 Non-Radioactive Cytotoxicity Assay was used to assess the cytotoxic effect of lentivirus expressing miRNA or miRZIP. This protocol uses excreted Lactate Dehydrogenase (LDH), a stable cytosolic enzyme, as a quantitative measure of cell death. This works by coupling two enzymatic reactions (featured below), which result in the reduction of tetrazolium salt to a red formalin compound. The production of this compound, as assessed by absorbance at 490nm, is proportional to the number of cells lysed.

$$\mathbf{NAD^+ + lactate \text{ –(LDH)} \rightarrow pyruvate + NADH}$$

$$\mathbf{NADH + INT\text{—(diaphorase)} \rightarrow NAD^+ + foramazan\ (red)}$$

Hippocampal primary cells were isolated and plated 50,000 cells/well on a 24-well plate in 500μL NBActiv4 media without antibiotic. At day 8 in culture, the cells are treated with pseudovirus of predetermined amount (ex. 4μL per well). Control wells included cells that weren't treated with virus, media alone and media + virus. After incubation at

37ºC for 4 days (day 12 in culture), 200µL of supernatant was removed from wells and put into a 96-well cell culture to measure the excreted LDH (a marker of cell death). The cells were then ruptured via freeze-thaw by incubating the plate at -80ºC for 30 min followed by thawing at 37ºC for 15 min. This step allowed quantitation of total cytoplasmic LDH. The 96-well plates containing supernatant and cell lysate were centrifuged at 250 x g for 5 minutes (at 4ºC). Next, reconstituted Substrate Mix was added at 50µL/well and incubated for 30 minutes at RT in the dark followed by equivalent addition of stop solution. Absorbance was then measured at 450nm. An LDH Positive Control was used (bovine heart LDH) included in the kit. This was vortexed and 2µL was added to 10mL of PBS + 1% BSA, prepared fresh for each assay. All samples were prepared in triplicate. Two biological replicates were performed. The calculations were performed by first subtracting the media alone absorbance from the absorbance of the sample. This was done for both supernatant and total cell lysate wells to normalize the absorbance. The normalized absorbance of a particular treatment supernatant (representing cell death) was then divided by the average normalized absorbance of that treatments total cell lysate (representing total cell death) yielding the percentage cytotoxicity in that well. The normalized absorbance as well as the percentage cytotoxicity of all samples was then plotted with the SEM.

3.8 Optimizing Viral Amount by Checking with Fluorescent Microscope and RNA Analysis with Realtime PCR

Transduced primary hippocampal cells at 12 DIV were viewed on a fluorescent microscope in order to visualize viral transduction via GFP expression. The optimal

amount of virus to use for further experiments was determined by selecting a quantity of virus that infected approximately 60% of cells.

RNA was isolated from transduced primary hippocampal cells at 12 DIV as previously described in section 3.5. RNA was quantified via Nanodrop and subsequent cDNA synthesis and Realtime PCR were performed as previously described. U6 was used as a housekeeping gene. Results were analyzed using the ΔΔCt method in Microsoft Excel.

3.9 Argonaute Immunoprecipitation in Hippocampal Primary Cells Overexpressing miR-16

Primary hippocampal cells were plated at 250,000 cells per well in three 6-well plates, totaling 4.5 million cells. The cells were plated in 2.5mL of NBActiv4 on plates coated with PDL. The cells were either treated with lentivirus expressing miR-16 or miR-Scr at 8 DIV. At 12 DIV the cells were used to perform the immunoprecipitation procedure described for the microRNA Isolation Kit, Mouse Ago2 (Wako). One slight modification to the procedure was the final product, as we were collecting mRNA targeted and thus bound by miR-16 rather than aiming to isolate cellular miRNA alone. This did not require a true change to the protocol, as no step is present to degrade the cellular mRNA in the miRNA end-goal procedure. First, 1mL of the 2.5mL media was removed from the cells, cells were scraped within the media and collected into a 50 mL conical tube, pooling all wells together. Cell suspension was centrifuged at 1000 rpm for 5 minutes at 4ºC, the supernatant removed and the cells were washed in 1mL RT 1X PBS. The suspension was then centrifuged and resuspended twice more, with the final resuspension being in 1mL of Cell Lysis Solution. This suspension was then moved to a 1.5mL sample tube and incubated on ice for 10 minutes. The lysate was centrifuged at 4ºC for 20

minutes at 20,000 x g. During this time Anti Mouse Ago2 Antibody Beads were prewashed, by adding 50µL of Anti Mouse Ago2 Antibody Beads Solution to a 1.5mL sample tube and centrifuging at 3000 x g for 30 seconds at 4ºC, followed by washing with 1mL of cell lysis solution twice, centrifuging and removing the supernatant each time. The cell lysate post-centrifugation was added to the tube of prewashed beads, vortexed and rotated at 4ºC for 2 hours. Following this incubation, the mixture was centrifuged at 3000 x g for 30 seconds at 4ºC and the supernatant removed. The antigen-antibody-bead complexes were washed twice with 1mL of Cell Lysis Solution, vortexed and centrifuged at 3000 x g for 30 seconds at 4ºC. Next, 50µL of Elution solution was added to the complexes in order to elute the antibody-Ago2 complexes from the beads. This was vortexed, and then centrifuged at 3000 x g at 4ºC for 30 seconds. The supernatant was kept and the beads discarded. The supernatant was taken for Western Blotting, and was acetone precipitated. For sample preparation for microarrays the following steps were taken to isolate Ago2 bound RNA. First, 350µL of sterile distilled water was added to the supernatant, followed by 400µL of phenol:chloroform:isoamyl alcohol (PCIA) which was then vortexed and centrifuged at 20,000 x g for 10 minutes at RT. The supernatant was kept and 400µL of chloroform was added with vortexing and centrifugation was repeated. The supernatant was again removed, and 3µL of Ethachinmate, 40µL of 3mol/L Sodium Acetate Solution and 1mL of 99.5% Ethanol were added with vortexing and centrifugation at 20,000 x g for 15 minutes at 4ºC to precipitate the RNA. The supernatant was removed from the pellet, and 1mL of 70% Ethanol was added, vortexed and centrifuged at 20,000 x g for 10 minutes at 4ºC. The

supernatant was again removed, and the pellet was dried before dissolving in 10μL of dH_20.

A BioAnalyzer run was performed in order to see if the RNA yield could be determined. A Eukaryote Total RNA PicoChip was utilized, but no yield could be determined. Run data is included in Appendix 1.3. In order to ensure that miR-16 was highly present within the immunoprecipitated RNA, Realtime PCR was performed before microarray analysis was completed. The housekeeping genes in this run were U6 and let-7c and miR-132 was also used as a positive control.

3.10 Microarray

Reverse transcription, second-strand synthesis, cRNA synthesis, aaUTP modification and purification were all performed using the protocols provided with the Amino Allyl MessageAmp II aRNA Amplification Kit (Life Techologies).

In order to preserve sample, 4μL of the AgoIP RNA was used in the Reverse transcription step (of each AgoIP-miR16 and AgoIP-miRScr). The 1st round of the Invitro Transcription to Synthesize Amino Allyl-Modified aRNA was performed via the unmodified protocol. Approximately 500ng of aRNA was subjected to 2nd round amplification. Nanodrop determined that the 260/280 ratio was 1.90 or greater for all samples. Dye coupling was performed with Alexa Fluor 555 and Alexa Fluor 647. In total, 745ng of dye-coupled sample for each treatment (miR-16 and miR-Scr) was mixed together (with opposing dyes) for hybridization. Dye switching was utilized, with a repeat hybridization reaction using the Two-Color Microarray-Based Gene Expression Analysis – Low Input Quick Amp Labeling Protocol (Agilent Technologies, Edition 6.6). The

repeat hybridization reaction was performed using the Agilent Gene Expression Hybridization kit. Fragmentation mix was made up as stated for a 4x44K microarray for each array. As follows: 845ng of both Cyanine 3-labeled and Cyanine 5-labeled, linearly amplified cRNA, 11µL of 10X Blocking agent, 2.2µL of 25X Fragmentation Buffer and Nuclease-free water were added together for a final volume of 55µL. A dye swap was performed, meaning that miR-16 and miR-Scr were each labeled with Cy-3 and Cy-5 and oppositely labeled miR-16 and miR-Scr were added to each of the two fragmentation tubes. They were then allowed to fragment for 30 minutes at 60°C. The reactions were stopped with 2X Hybridization Buffer of equivalent volume (55µL) and mixed carefully followed by centrifuging at 13,000rpm for 1 minute at RT. Samples were then incubated on ice until loaded onto an Agilent Whole Mouse Genome (4X44K) Oligo Microarray. Carefully, 100µL of the prepared hybridization sample was then added to the gasket slide of the microarray and an array slide was placed on top and clamped into a chamber. The slide was left to rotate at 65ºC for 17 hours. The array was then removed from the chamber, and the gasket removed while submerged in Gene Expression Wash Buffer 1. The slide was washed in this buffer for 1 minute, followed by washing in pre-warmed Gene Expression Wash Buffer 2 for 1 minute. The slide was immediately scanned using the Agilent Technologies DNA Microarray Scanner With Surescan High-Resolution Technology. Feature Extraction Software version 12 (Agilent) was used to extract the genetic information from the array.

3.11 Analysis of Data from Microarray with Ingenuity Pathway Analysis

Information extracted from the array was log2-transformed and cross-referenced to miR-16 putative target information from TargetScanMouse Release 7.1 using Excel. Data was

then uploaded into Ingenuity Pathway Analysis (IPA) (Build Version: 366632M; Content Version: 26127183) and a Core Analysis was performed. Ingenuity Knowledge Base (Genes Only) was used as a reference set with both direct and indirect relationships taken into account.

3.12 Stimulation of Hippocampal Cells to Elicit Changes in Target Expression at Protein Level

6-well dishes containing primary hippocampal cells were treated with pseudovirus at 8 DIV and at 12 DIV they were stimulated. Brain-derived neurotrophic factor human (BDNF) (B3795 Sigma) was used to stimulate the primary hippocampal cell cultures. BDNF was first diluted in H_20 from powder stock and then 1X PBS (1:100) before adding to cells at 25ng/mL and 50ng/mL. Protein and RNA were collected at 24 hours after BDNF addition.

3.13 Protein Extraction and Western Blots to Validate Targets at Protein Level

Protein was extracted from hippocampal neurons using N-PER Neuronal Protein Extraction Reagent (Thermo Scientific). First, the media was removed and 100µL of N-PER was added per well of a 6-well plate, with 1µL Halt Protease and Phosphatase Inhibitor Cocktail, EDTA-Free (100X) (Thermo Scientific) and left on ice for 5 minutes. Plates were scraped and lysate was collected and frozen at -80ºC.

For the Argonaute immunoprecipitation western blot and blots of dilute samples, an acetone precipitation was performed using the Thermo-Scientific protocol. Protein was thawed, cold (-20ºC) acetone amounting to 4X the volume of protein sample was added to the protein, vortexed and incubated for 1 hour at -20ºC. It was then centrifuged for 10

minutes at 13,000 x g, decanted and the acetone was evaporated on the benchtop for 30 minutes at RT. The sample was finally dissolved in Cell Disruption Buffer (PARIS Kit) (Ambion).

Pierce BCA Protein Assay Kit (Thermo Scientific) was used to determine protein amount within each sample. This kit works based on the knowledge that Cu^{2+} is reduced to Cu^{1+} by protein within an alkaline environment and bicinchoninic acid (BCA) chelates Cu^{1+} resulting in development of a purple colour strongly absorbed at 562nm. Using a standard curve, this property is used to determine protein quantity within a sample. Bovine serum albumin (BSA) is used as the standard protein to create a standard curve of known concentration (from 0-2000µg/mL). The standard was diluted in the same N-PER/HALT mixture that the samples were in. The microplate procedure was used to allow a small concentration of protein to be used. In total, 25µL of standard was added to a 96-well plate in duplicate. Next, 4µL of sample was added in duplicate as well, diluted in 21µL of buffer. Finally, 200µL of Working reagent (50 parts BCA Reagent A and 1 part BCA Reagent B) was added to each well and mixed by pipetting. The plate was placed at 37ºC for 30 minutes and the absorbance was measured at 562nm. Calculations were performed in Excel to determine the amount of protein in each sample using the BSA standard curve.

Between 50 and 100µg of sample was aliquoted for each well of a 10% NuPAGE Bis-Tris Mini Gel (Invitrogen) or ExpressPlus PAGE 4-12% Gel (GenScript). To these samples, 5µL of NuPAGE LDS Sample Buffer (4x) (Life technologies), 2µL of NuPAGE Sample Reducing Agent (10X) (Life technologies) and 3µL of dH_20 were added to make a total loading volume of 20µL. The samples were then heated at 70ºC for 10 minutes,

vortexed again and centrifuged. The samples were added to the gels along with one lane containing two ladders: 5μL of MagicMark XP Western Protein Standard (Invitrogen) and 3μL of Novex Sharp Pre-Stained Protein Standard (Invitrogen). Electrophoresis was performed in an Xcell SureLock chamber (Invitrogen) with Novex MOPS SDS Running Buffer (20X) (Life technologies) diluted to 1X in dH_20. NuPAGE Antioxidant (Thermo Fisher) was added to the running buffer to keep proteins in a reduced state throughout electrophoresis. Electrophoresis was performed at 200 Volts for 55 minutes. The protein was then transferred to a nitrocellulose membrane using the Novex iBlot Gel Transfer Stacks Nitrocellulose (Life Technologies) using the iBlot (Invitrogen). The membrane was next blocked at RT for 1 hour in 5% Skim Milk in 1X TBST shaking. It was washed three times in TBST (1X Tris Buffered Saline, pH 8.0 (1X TBS) (SIGMA), 0.1%Tween20 (Thermo Fisher)) for 5 minutes shaking, at RT. Blots were left at 4ºC overnight, or alternatively at RT 1 hour, shaking in primary antibody. Primary antibodies were diluted in 5% w/v Bovine Serum Albumin (BSA) (Fisher Bioreagents) in 1X TBST. Blots were then washed as previously described and incubated for 1 hour shaking at room temperature in secondary antibody. Secondary antibodies were diluted in 5% Skim Milk in 1X TBST. Blots were washed twice in TBST for 5 minutes at room temperature, shaking, followed by a single wash in TBS under the same conditions. For detection, blots were incubated for 5 minutes in SuperSignal West Pico Chemiluminescent Substrate (Thermo Scientific) before developing using the Bio-Rad Versa Doc Imaging System. Alternatively, blots were developed using an X-ray film developer (Konica Minolta SRX-201A). Densitometry analysis was performed using the Quantity One Software (Bio-Rad) or alternatively using ImageJ.

The antibodies used for western blotting were as follows: Anti-APP Rabbit Antibody (SIGMA A8717) (recognizes APP_{695} APP_{751} and APP_{770} (95-100kDa)); Anti-BCL-2 Mouse Antibody (SIGMA B9804) (recognizes an epitope between amino acids 61 and 76 of the BCL-2 protein (doublet 26kDa and band at 30kDa)); Anti-Ago2 Mouse Monoclonal Antibody (Wako 014-22023) (recognizes Ago2 protein at 100kDa and is identical to the antibody used in the Ago-IP kit); MEK1/2 (47E6) Rabbit mAb (Cell Signaling Technology; 9126) (MW 45kDa); TrkB (80E3) Rabbit mAb. (Cell Signaling Technology; 4603) (MW 90, 140kDa); P44/42 MAPK (Erk1/2) (137F5) Rabbit mAb (Cell Signaling Technology; 4695) (MW 42, 44kDa); c-Raf (D4B3J) Rabbit mAb (Cell Signaling Technology; 53745) (MW 75kDa); β-Actin Antibody Rabbit (Cell Signaling Technology; 4967) (MW 45kDa); Phospho-c-Raf (Ser338) (56A6) Rabbit mAb (Cell Signaling Technology; 9427) (MW 74kDa); Phospho-MEK1/2 (Ser217/221) (41G9) Rabbit mAb (Cell Signaling Technology; 9154) (MW 45kDa); Phospho-p44/42 MAPK (Thr202/Tyr204) (D13.14.4E) XP Rabbit mAb (Cell Signaling Technology; 4370) (MW 42, 44kDa); Phospho-p90RSK (Ser380) (D3H11) Rabbit mAb (Cell Signaling Technology; 11989) (MW 90kDa); Phospho-MSK1 (Thr581) Antibody (Cell Signaling Technology; 9595) (MW 90kDa) and Anti-rabbit IgG, HRP-linked Antibody (Cell Signaling Technology; 7074).

3.14 Looking at Morphological Changes in Hippocampal Cultures after miR-16 Overexpression via Immunostaining

Primary hippocampal cells were plated on coverslips, treated with pseudovirus, fixed and immunostained as described in section 3.3. MAP2 primary antibody was used to detect neurons, in addition to the GFP expressed by the transduced cells.

3.15 Analysis of Morphological Changes via SynD Program

The images were collected as described in section 3.3. Neurite length, soma area and Sholl analysis were performed using Synapse Detection (SynD) (Schmitz et al. 2011) (www.cncr.nl/resources). Upon running the SynD_extract program in MATLAB R2016a, a tiff image was uploaded, the soma and neurites detected and the results exported. The soma was detected using an erosion radius of 2, and threshold of 130 to remove neurites from contention. The soma mask was manually edited to ensure the entire soma was detected. Neurite masks were created by automated addition of pixels at a cost to the system lower than 0.9 with a steerable filter set to 0.5μm (matched to neurite diameter in images). The neurite mask was then manually edited to ensure all masked regions represented neurites stemming from the masked soma. The results of each SynD analysis were then exported to a mat file. SynD_aggregate, another application within the SynD program, was used to compile mat files from images from the same coverslip into xml files. The data was then sorted within Excel and GraphPad Prism 7 was utilized to present the information graphically and to perform statistical analysis.

Chapter 4: Results

4.1 Establishing and Analyzing Hippocampal Primary Cell Culture

Decreased number of synapses and decreased number of dendritic spines are both signs of prion disease, which are seen highly in the stratum radiatum of region 1 of the CA1 region of the hippocampus in mouse prion disease. This includes both pre- and post-synaptic degeneration (Majer and Booth 2014). In human prion infection as well, synaptic loss is not uniform throughout the brain with hippocampal and cortical regions showing the most consistent synapse loss (Clinton et al. 1993; Šišková et al. 2009). Of additional interest, is the homogeneous cellular composition of the CA1 region of the hippocampus. In healthy brains, astrocytes, microglia and oligodendrocytes largely outnumber neurons. However, the CA1 region of the hippocampus is almost exclusively composed of neurons (Klausberger and Somogyi 2008). For these reasons, the hippocampus, particularly the CA1 region, is of interest because looking at brain tissues as a whole can be a vast mixture of cell types, which can mask what is really going on at the transcriptional level (low abundance transcripts) or significant hippocampal neuron specific changes (Majer and Booth 2014).

In order to create an *in vitro* model of the hippocampus, a region of the brain that undergoes significant neurodegeneration during prion disease (Cunningham et al. 2003), primary hippocampal cells were dissected from embryonic day 18 (E18) mice.

Collection of primary embryonic cells is a lengthy process involving coordinating breeding, embryo collection and dissections. These cells are very sensitive to perturbation and environmental stressors and are not kept more than four weeks. However, primary

cells are used rather than a neuronal derived cell line, as cell lines often lack traditional neuronal morphology and the ability to make synaptic connections (Beaudoin et al. 2012). In addition, embryonic cell cultures were chosen over postnatal cultures due to their superior ability to withstand stress incurred during culture preparation, as well as the higher proportion of neurons within the culture due to less integration of glial cells and the meningeal structure (Beaudoin et al. 2012). In addition, the synaptic loss and dendritic changes that occur early in prion disease cannot be modeled in cell lines, however those cellular processes can be evaluated using primary neuronal cultures.

Despite the maintenance required, primary embryonic cell cultures have become well established as a tool in neuroscience, and the steps necessary to produce them have been well characterized. In order to cultivate a primarily neuronal cell population, serum-free Neurobasal/B27 media is used (Brewer et al. 2008). As well, NbActiv4 is a complex version of Neurobasal/B27 medium with supplemented estrogen, creatine and cholesterol which substantially increases the strength and number of synapses within the culture, an established marker of neuronal health (Brewer et al. 2008).

4.1.1 Analysis of Culture Purity via Immunostaining

In order to assess the characteristics of the culture, as well as the health and maturation of neuronal cells over time, cells were fixed every few days for 14 days. This time period was chosen to reflect the average length of time that cells would be used in experiments. These cultures were then immunostained with antibodies to microtubule-associated protein 2 (MAP2), a dendrite-specific neuronal marker, glial fibrillary acidic protein (GFAP) a glial cell marker, as well as DAPI, a DNA-specific stain. The use of GFAP allowed visual confirmation that the cultures were predominantly neuronal, with a low number of astrocytes.

Analysis of these cultures revealed that they were a true representation of a primary hippocampal culture, indicated by visibly increased neurite outgrowth and branching over time (Figure 5). The first stage of pyramidal neuronal development in culture is the extension of lamellopodia into neurites (as visualized at 4 and 7 DIV; Figure 5) (Beaudoin et al. 2012). This is closely followed by the extension of axons and dendrites beginning at 8 DIV (as visualized at 11 DIV; Figure 5) and the ability to tell the two apart, with the dendrites being thick and branching and the axon thin and spineless (Beaudoin et al. 2012; van Spronsen et al. 2013). The first synapses also are apparent at this stage (van Spronsen et al. 2013). The final stage of neuronal development begins at 12 DIV with the formation of defined dendritic spines, and the maturation of synapses into a complex network (which likely could be visualized at a higher magnification at 14 DIV; Figure 5) (Beaudoin et al. 2012; van Spronsen et al. 2013).

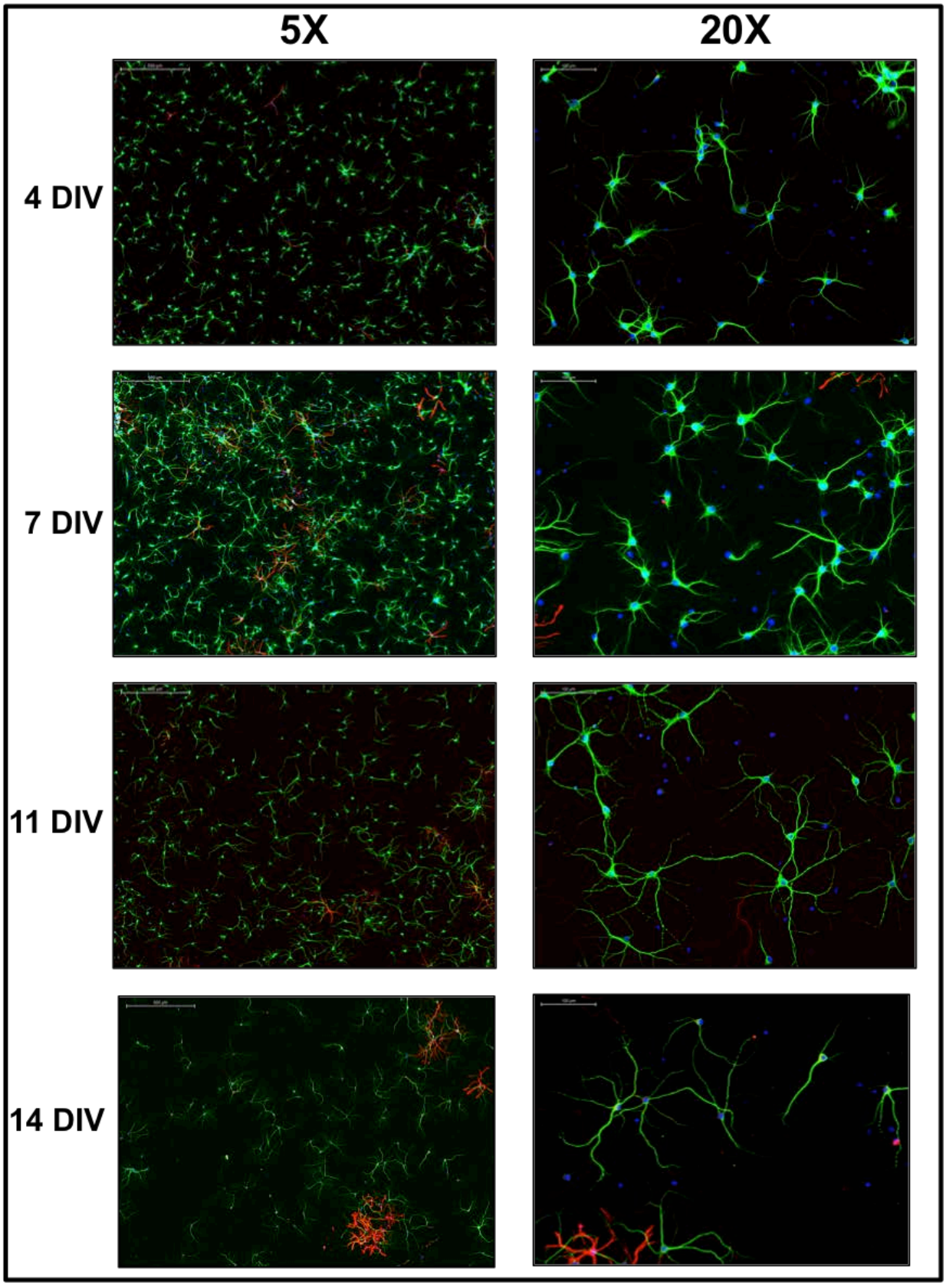
5X
20X
4 DIV
7 DIV
11 DIV
14 DIV

Figure 5: Immunohistochemistry Highlights the Development of Primary Hippocampal Neurons Over Time in Culture. Cells are pictured from the top at 4, 7, 11 and 14 DIV in both 5X (left) and 20X (right) magnification. Green: MAP2. Red: GFAP. Blue: DAPI.

In order to determine the distinct proportions of cell types within the cultures, cells were counted using the ImageJ Cell Counter plugin. Figure 6 illustrates both the percentage of neurons in culture as well as the total cell population over time. There was an overall decline in the percentage of neurons in culture over time. In order to determine if this was due to increased glial presence, or merely from normal culture death over time the total cell population was characterized further. As seen in Figure 6, there was a steady number of neuronal cells (approx. 100 per image) up until day 15 where the number dropped down to about 50 cells per image. This was likely due to the death of neuronal cells within the culture, a normal feature of primary neuronal cultures. Additionally, no relative rise in glial cell number within the culture over time was apparent. This was confirmation that the lower percentage of neurons at day 15 was due to cell death rather than the expansion of the glial cell population. Taken together, the data show that these cultures are more than 70% neuronal, even at day 15, reflecting that this is a relatively pure neuronal culture, and thus a good model of the hippocampus, which is primarily neuronal in cell structure (Mattson and Kater 1989). As well, a small number of astrocytes persist within the culture at all time points, which is desirable as they have been shown to be important for promoting neuronal health and maturation (Haber et al. 2006).

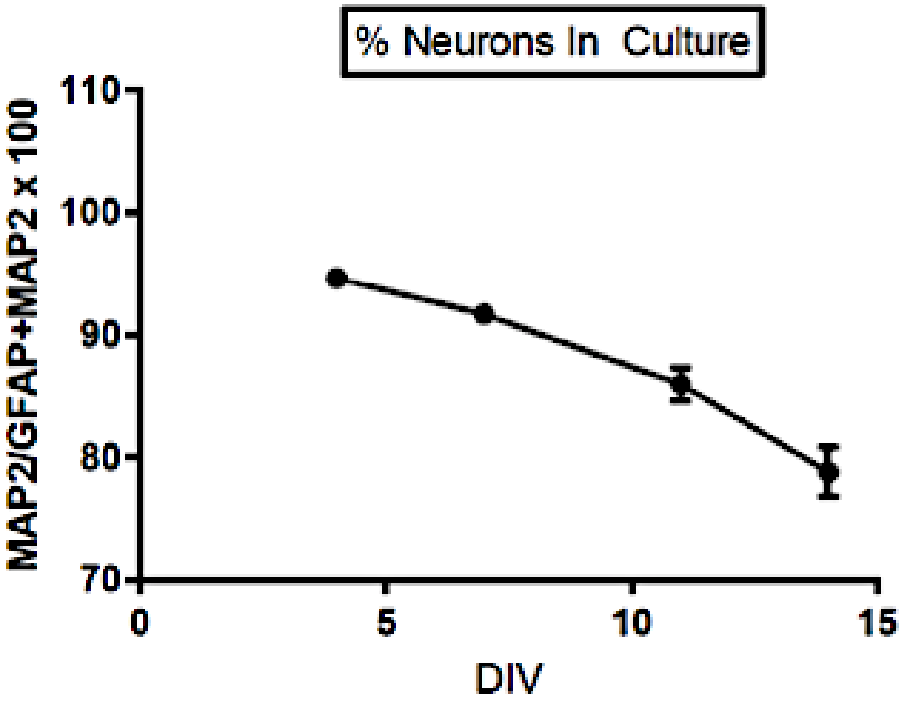
% Neurons In Culture
MAP2/GFAP+MAP2 x 100
110
100
90
80
70
0
5
10
15
DIV

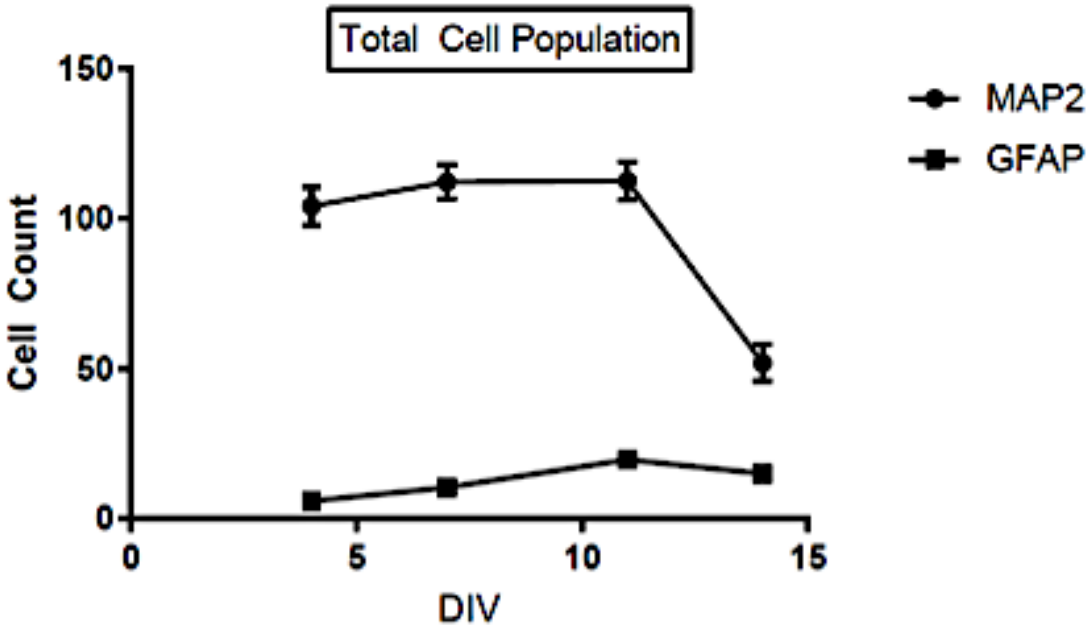
Total Cell Population
Cell Count
150
100
50
0
0
5
10
15
DIV
MAP2
GFAP

Figure 6: The Proportion of Neurons in Culture Over Time Relative to Astrocytes. On the top, the percentage of neurons in culture from 4 to 14 DIV is shown. On the bottom, the total cell population is plotted; comprising the total number of neurons and the total number of astrocytes from 4 to 14 DIV. Error bars represent SEM of triplicate counts. MAP2: Neuronal Marker. GFAP: Astrocyte Marker.

4.1.2 Endogenous miR-16 Expression Within Neuronal Primary Cultures

Primary cultures were utilized in order to analyze the endogenous levels of miR-16-5p present over time in culture, with RNA collected every few days from 4 to 12 DIV. Between 3 and 5 biological replicates (and triplicate technical replicates) were collected for each time point. 4 DIV was used as a starting point because before that the cells are under a great deal of stress following the dissection procedure. GraphPad Prism was used to perform multiple t-tests using the Holm-Sidak method, with $\alpha = 0.05$. This indicated that there was a statistically significant difference between U6 and miR-16 at all time points. There was a significant increase in miR-16 expression between 8 and 9 DIV, with P-value=0.00018 (Figure 7). There was also a significant difference between 10 & 11 DIV and 11 & 12 DIV with P-values= 0.00154 & 0.00321 respectively, with expression of miR-16 decreasing (Figure 7). However, as there is never more than a 2-fold change in expression it appears that miR-16-5p expression is not highly altered during cellular development.

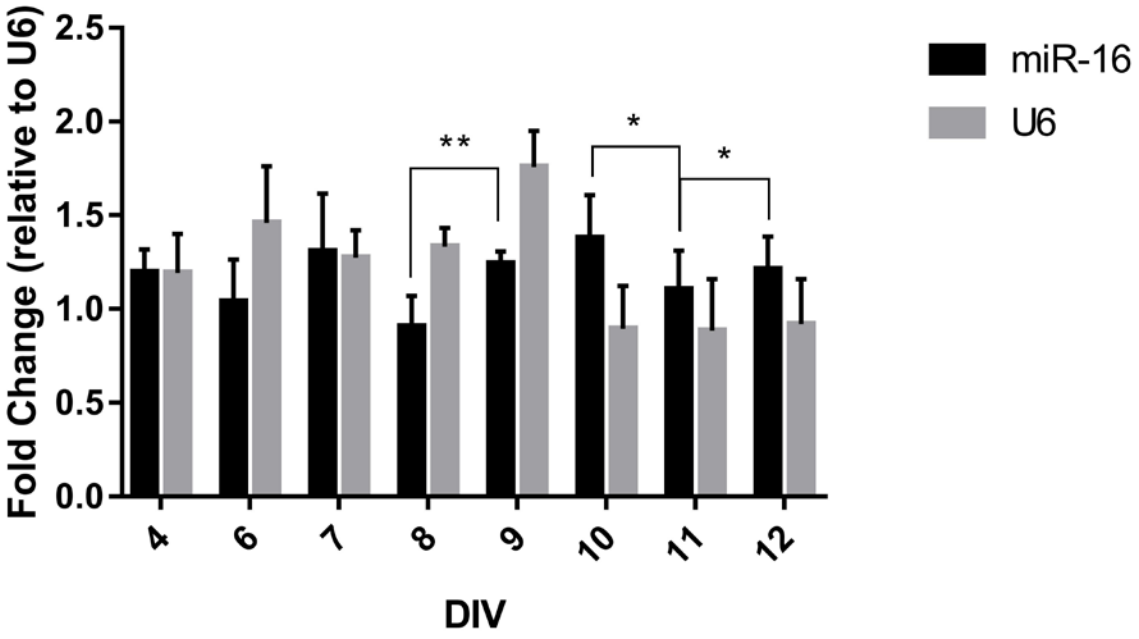
Fold Change (relative to U6)
2.5
2.0
1.5
1.0
0.5
0.0
**
*
*
4
6
7
8
9
10
11
12
DIV
miR-16
U6

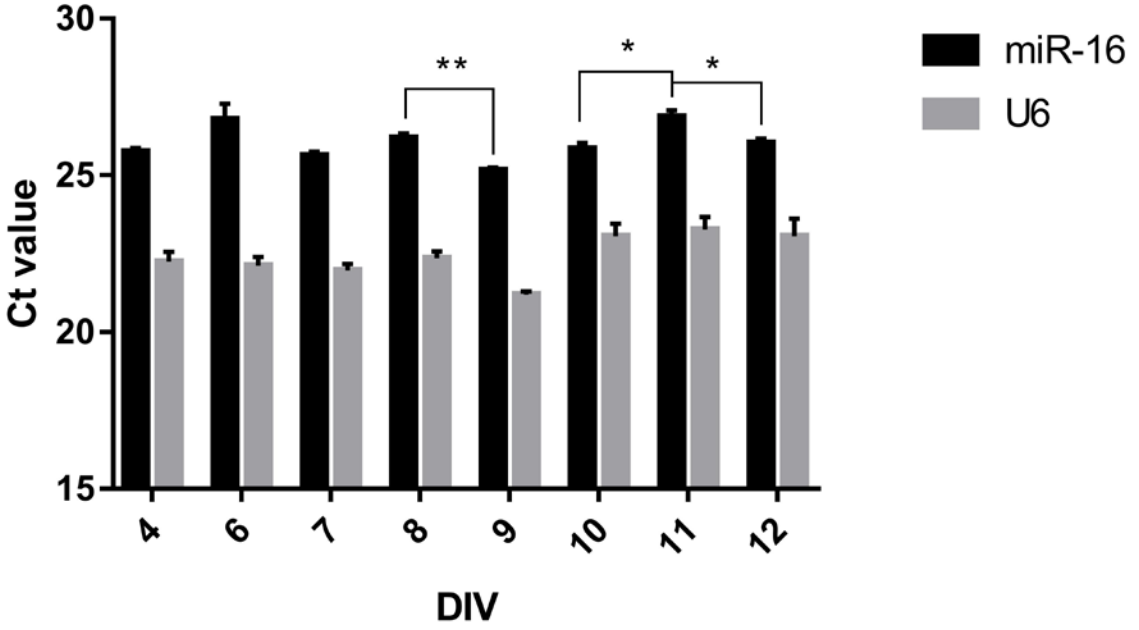
Ct value
30
25
20
15
**
*
*
4
6
7
8
9
10
11
12
DIV
miR-16
U6

Figure 7: Endogenous MiR-16-5p Expression Level in Primary Hippocampal Neurons Over Time in Culture. Top: Fold change of miR-16 expression normalized to U6 snRNA from 4 to 12 DIV. Fold change at all time points was measured relative to 4 DIV. Bottom: Ct values of miR-16 and U6 snRNA from 4 to 12 DIV. Data represents the mean +/- SEM (n=3-5) biological replicates. Multiple t-tests using the Holm-Sidak method determined statistical significance. α=0.005 with * = <0.005 and ** = <0.0005.

4.2 Manipulation of the Levels of Mature miR-16 in Primary Hippocampal Cells

Lentiviral transduction was chosen to manipulate the miR-16 expression in the primary hippocampal cells. Replication incompetent pseudo-lentivirus was used due to its ability to infect non-dividing cells, as well as its applicability for subsequent use in animal models. Most importantly, the ability to integrate into the neuronal genome is useful for stable, long-term expression of the miRNA constructs from constitutive promoters.

The constructs were expressed as single-stranded siRNA sequences that formed hairpin secondary structures, which were recognized by Dicer and processed via the endogenous miRNA processing system within the cell ensuring proper cleavage of the hairpins into mature miRNA. This system allowed normal cellular miRNA to be processed as well, an advantage over other methods of miRNA manipulation that monopolize the miRNA processing machinery, potentially interfering with regulation of many genes and cellular processes that are not directly regulated by the miRNA being manipulated.

Sequencing of the plasmids yielded the following results. An NCBI Nucleotide Blast revealed that the miR-16 containing plasmid aligned to *Mus musculus* miR-16-1 (NR_029734.1) with 96% sequence identity and no gaps (Appendix 1.2.1). In addition, a hairpin Blast search using miRBase revealed that this sequence aligned to mmu-miR-16-1 and mmu-miR-16-2 but the former had a higher alignment score (411 vs. 146) indicating better alignment (Appendix 1.2.1). A miRBase Blast of the miR-Scr containing plasmid revealed alignment to miR-169p in both *Arabidopsis spp.* and *Populus spp.*

(Appendix 1.2.2). A miRBase Blast of the miRZIP-16 containing plasmid revealed alignment to both mmu-miR-16-1 and mmu-miR-16-2 with marginally better alignment to the latter (115 vs 119) (Appendix 1.2.3). A miRBase Blast of the miRZIP-Scr showed strong confidence in alignment to miR-168a from the *Glycine spp.* and miR-1616 & miR-2671c from *Medicago spp.* (Appendix 1.2.4).

As noted in the previous section, endogenous levels of miR-16 are highest within the primary culture at 8 DIV. Therefore, cells were treated with lentiviral vectors containing either miR-16, miR-Scr, miRZIP-16 or miRZIP-Scr at 8 DIV. This allowed the virus to be overexpressed when the endogenous levels are highest, and at the point when the cells will be extending their neurites and developing synaptic connections allowing analysis of miR-16's effect on these processes. MiR-16-5p overexpression supplemented the endogenously expressed miRNA while miRZIP-16 overexpression resulted in a specific knockdown of endogenous miR-16-5p by "zipping up" the miRNA due to complementary binding. Together they represent a model of high miR-16-5p expression (analogous to the preclinical stage of prion infection) and low miR-16-5p expression in hippocampal neurons (analogous to the clinical stage of prion infection). In addition to miR-16-5p, miRZIP-16 or Scramble the lentiviral vectors also constitutively expressed copGFP. This allowed for convenient identification of whether the virus had stably integrated into the cellular genome and successfully undergone gene expression via fluorescent microscopy.

4.2.1 Titering of Virus

Titering infection competent viral particles is complicated with lentivirus as a traditional plaque assay cannot be used as it doesn't replicate in culture. Instead, the proportion of infected cell (MAP2 positive + GFP positive) to uninfected cells (MAP2 positive + GFP negative) was used as a method of titering. Increasing amounts of virus from 2-10μL were added to primary cells at 8 DIV. A one sample t-test of the two treatments showed a significant difference in the percentage of cells transduced with increasing viral addition for both miR-16 and miR-Scr with two-tailed P-values of 0.0007 and <0.0001, respectively (Figure 8).

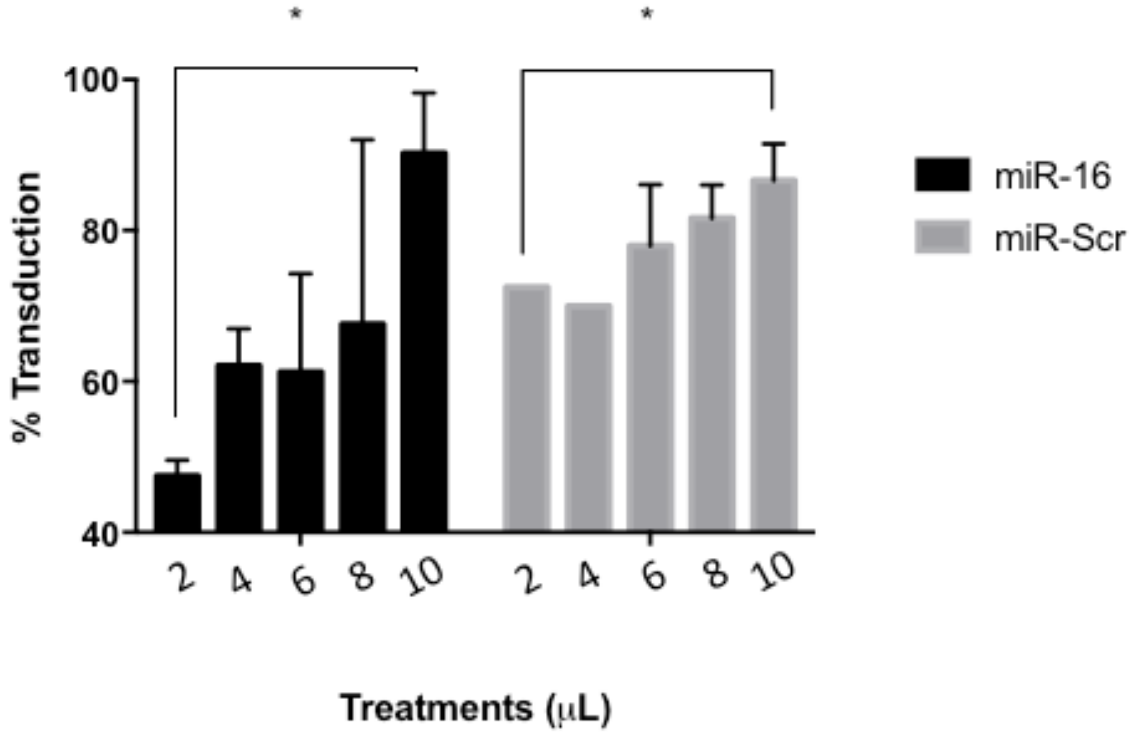
*
*
100
80
60
40
% Transduction
2 4 6 8 10
2 4 6 8 10
Treatments (μL)
miR-16
miR-Scr

Figure 8: Titering of Virus. 2μL to 10μL (from left to right) of virus was added to primary hippocampal cells. T-tests of each treatment revealed a significant increase in the percentage of cells transduced with virus with increasing viral addition. $\alpha = 0.05$. * = <0.05.

4.2.2 Results of Cytotoxicity Analysis

Cytotoxicity analysis was used to ensure that any changes in gene expression, or morphology that were found were attributable to the changes in miR-16 expression, and not a result of an increase in cell death due to the pseudoviral infection of the cells. A one-way ANOVA with Holm-Sidak's multiple comparisons test was used for significant differences between primary cell spontaneous or untreated samples and treatments. The mean of each treatment was compared to the mean of the control. Cells were treated with 1 to 10μL of virus for miR-16, miR-Scr, miRZIP-16 and miRZIP-Scr. At no point was the level of cell death in any of the treatments higher than primary cell spontaneous cell death (Figure 9). However, both miR-16 and miRZIP-Scr had significantly less cell death than primary cell spontaneous cell death at certain dosages. Looking at the percentage of cell death with different treatments, again there was no instance when treatments had increased cell death over controls (Figure 9). The percentage of cell death was significantly lower with all treatments of both miRZIP-16 and miRZIP-Scr than untreated cells (Figure 9). Therefore, it can be concluded that none of the lentiviral vectors used in this study had a negative effect on cell viability.

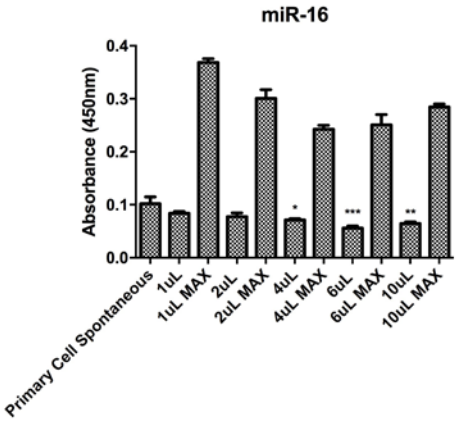
miR-16
Absorbance (450nm)
0.4
0.3
0.2
0.1
0.0
*
***
**
Primary Cell Spontaneous
1uL
1uL MAX
2uL
2uL MAX
4uL
4uL MAX
6uL
6uL MAX
10uL
10uL MAX

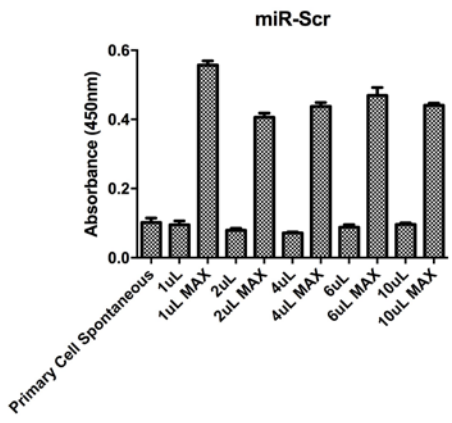
miR-Scr
Absorbance (450nm)
0.6
0.4
0.2
0.0
Primary Cell Spontaneous
1uL
1uL MAX
2uL
2uL MAX
4uL
4uL MAX
6uL
6uL MAX
10uL
10uL MAX

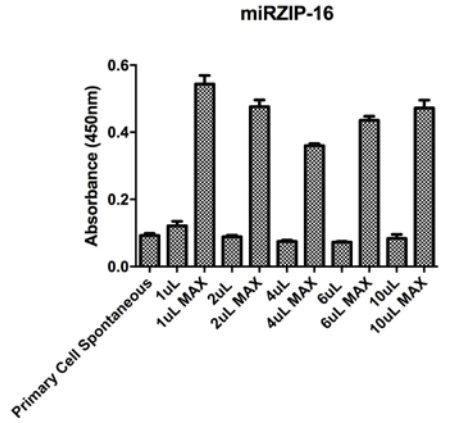
miRZIP-16
Absorbance (450nm)
0.6
0.4
0.2
0.0
Primary Cell Spontaneous
1uL
1uL MAX
2uL
2uL MAX
4uL
4uL MAX
6uL
6uL MAX
10uL
10uL MAX

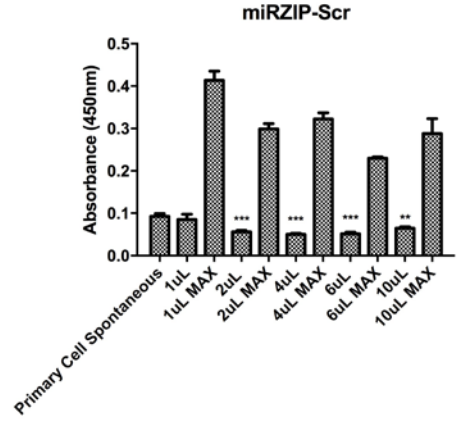
miRZIP-Scr
Absorbance (450nm)
0.5
0.4
0.3
0.2
0.1
0.0
***
***
***
**
Primary Cell Spontaneous
1uL
1uL MAX
2uL
2uL MAX
4uL
4uL MAX
6uL
6uL MAX
10uL
10uL MAX

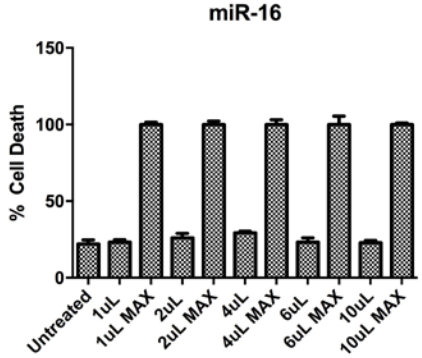
miR-16
% Cell Death
150
100
50
0
Untreated
1uL
1uL MAX
2uL
2uL MAX
4uL
4uL MAX
6uL
6uL MAX
10uL
10uL MAX

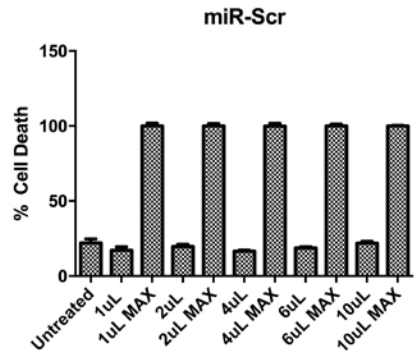
miR-Scr
% Cell Death
150
100
50
0
Untreated
1uL
1uL MAX
2uL
2uL MAX
4uL
4uL MAX
6uL
6uL MAX
10uL
10uL MAX

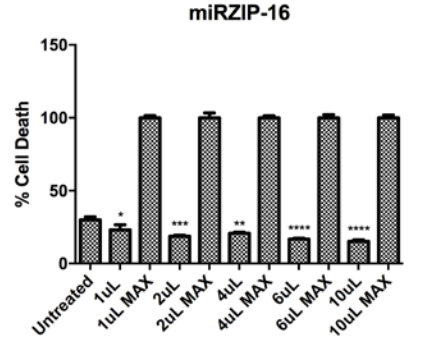
miRZIP-16
% Cell Death
150
100
50
0
*
***
**
****
****
Untreated
1uL
1uL MAX
2uL
2uL MAX
4uL
4uL MAX
6uL
6uL MAX
10uL
10uL MAX

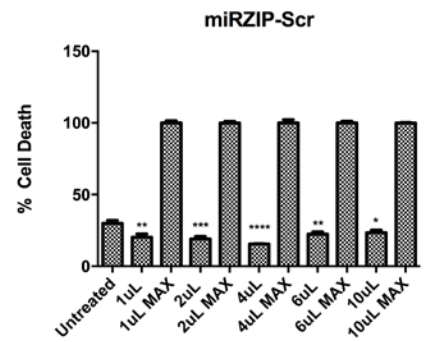
miRZIP-Scr
% Cell Death
150
100
50
0
**
***
****
**
*
Untreated
1uL
1uL MAX
2uL
2uL MAX
4uL
4uL MAX
6uL
6uL MAX
10uL
10uL MAX

Figure 9: Cytotoxicity Assay to Determine the Percentage of Cell Death in Hippocampal Cultures After Lentiviral Treatment. The top four graphs show the cell death with each viral addition (supernatant absorbance) compared to the maximal cell death (lysed cell absorbance). The bottom four graphs show the percentage of cell death induced by the viral addition compared to the maximal cell death. One-way ANOVA with Holm-Sidak's multiple comparisons was employed to test for significant differences between treatments and untreated control cells. α =0.05. * = <0.05, ** = <0.005, *** = <0.0005 and **** = <0.0001. MAX absorbance or % cell death is defined as the respective level reached in each treatment when cells were lysed via freeze thaw.

4.2.3 Fluorescent Microscopy and Realtime Analysis

The optimal amount of virus to add to cultures was determined by selecting a quantity of virus that didn't infect every single cell, as it was desirable for GFP expressing cells to be separated enough to do efficient single cell analysis. As well, it was important to choose an amount of virus that was efficient in upregulating miR-16 expression, or downregulating its expression, depending on treatment. First, the vector expression was visually verified after cells had been exposed to varying amounts of virus by detecting GFP with the confocal microscope (Figure 10).

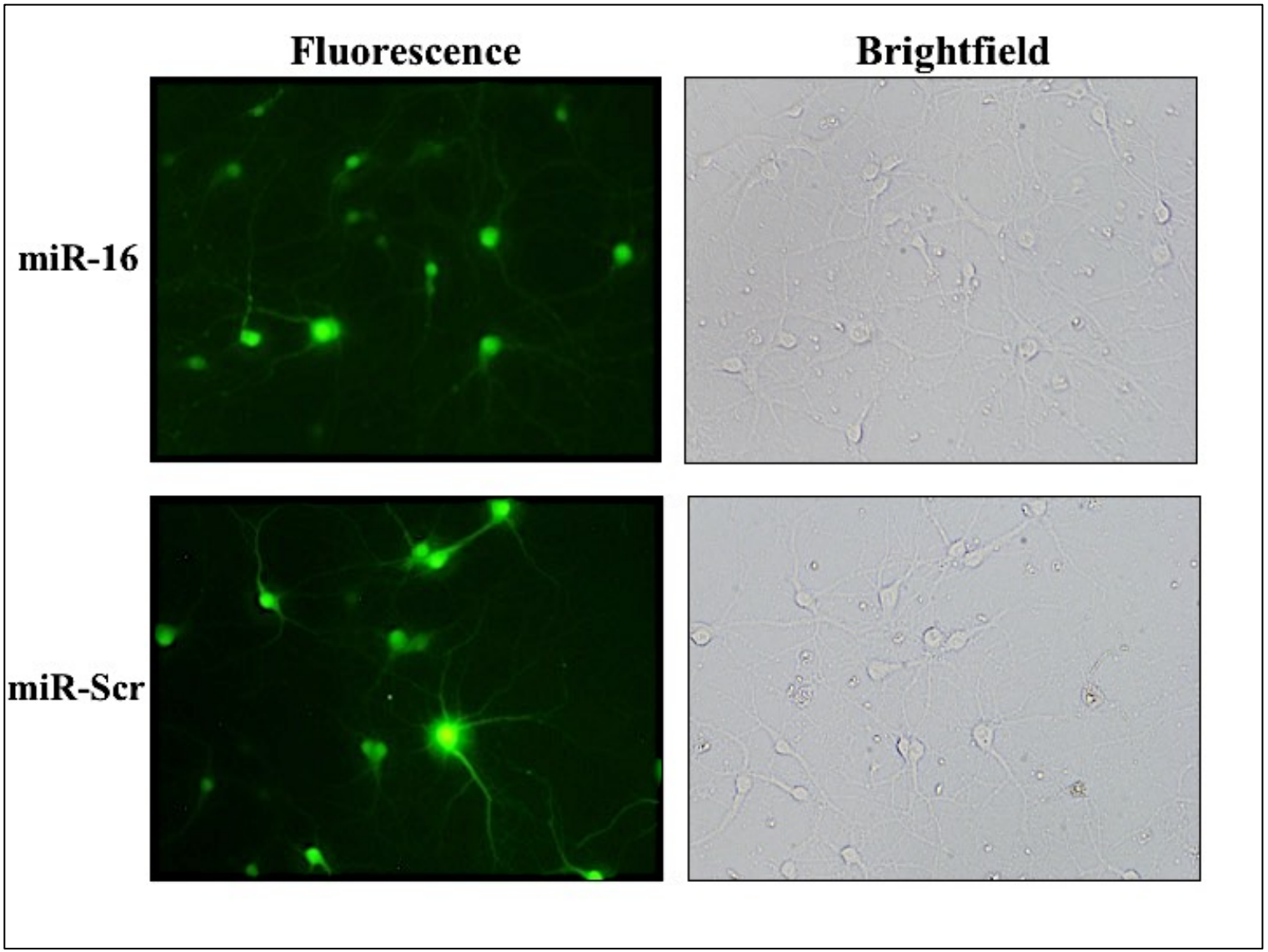
Fluorescence
Brightfield
miR-16
miR-Scr

Figure 10: Fluorescent Microscopy of Hippocampal Primary Cells Transduced with Pseudovirus. Both miR-16 and miR-Scr were added at 20µL/well in a 6-well plate. Cells were viewed on the fluorescent microscope after 4 days with the 20X objective.

Next, the optimal amount of virus necessary for adequate manipulation of miR-16 levels was determined. Overexpression of miR-16 and miR-Scr in primary hippocampal cells was visualized in Figure 11A. In Figure 11C, the overexpression of miR-16 was verified by Realtime PCR. The miR-16 was over expressed in comparison to miR-Scr treated cells after transduction with both 2 and 4µL of virus in this experiment. For the remainder of experiments, 4µL of miR-16 and miR-Scr expressing pseudo-lentiviruses were used for addition to cells. Figure 11B contains images of miRZIP-16 and miRZIP-Scr treated cells to visually verify pseudoviral expression. Realtime results indicated that miRZIP-16 treated cells had decreased miR-16 expression relative to miRZIP-Scr at both 2 and 4µL treatments (Figure 11D). For all further experiments, 4µL of all viruses was added to cells (or the equivalent addition to a 6-well plate, 20µL) because as we could see in Figure 8, this amount of virus gave roughly equivalent titers of both miR-16 and miR-Scr.

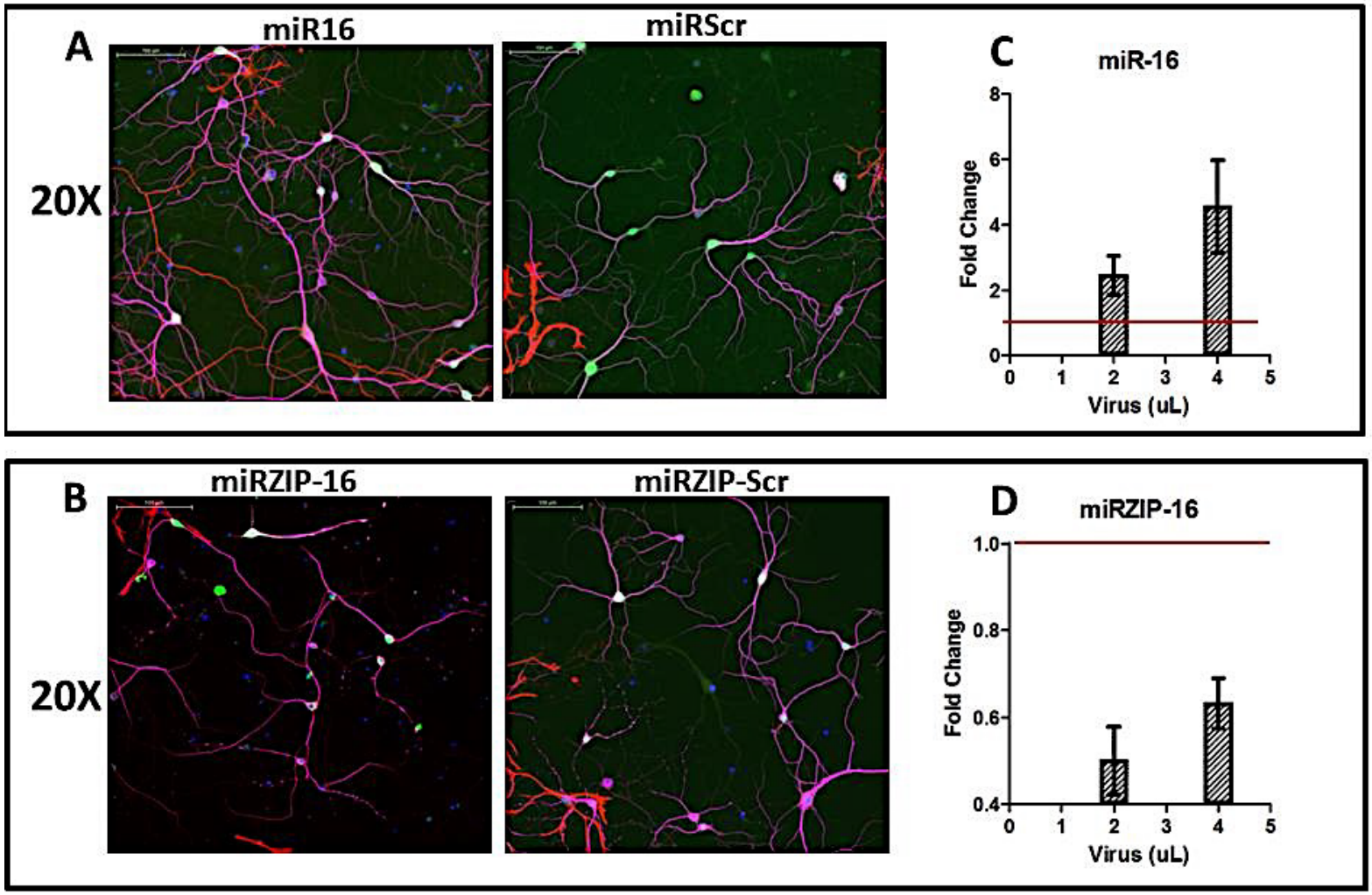
A
miR16
miRScr
20X
C
miR-16
Fold Change
Virus (uL)
B
miRZIP-16
miRZIP-Scr
20X
D
miRZIP-16
Fold Change
Virus (uL)

Figure 11: Manipulation of MiR-16 Expression in Primary Hippocampal Neurons Verified by Immunohistochemistry and Realtime PCR. A&B) Pink: MAP2 (neurons), Green: GFP (lentiviral expressing cells), Red: GFAP (astrocytes) and Blue: DAPI. C&D) Realtime PCR results relative to miR-Scr and miR-ZIPScr respectively. Realtime was performed in triplicate, with 3 biological replicates. The line in each graph denotes the baseline U6 Expression that miR-16 is measured relative to.

4.2.4 Verification of model

Previous studies have shown that miR-16 binds to mRNA encoding APP and BCL-2 and decreases the expression of these proteins (Liu et al. 2012; Cimmino et al. 2005). Both of these genes are expressed in hippocampal neurons and so it was important to validate that upregulation of miR-16 in experimental primary hippocampal cells was capable of effectively downregulating the expression of these proteins.

Six-well plates were treated with increasing amounts of miR-16 and miR-Scr and protein was extracted after 4 days. A western blot was performed with primary antibodies to APP and Bcl-2 (Figure 12). Visually, the miR-16 treated wells had lower levels of both of these proteins relative to miR-Scr treated wells (Figure 12B). This was verified with densitometry, with both APP and Bcl-2 having on average lower protein levels in miR-16 treated wells relative to miR-Scr treated wells (Figure 12A). However, increasing viral addition appears to increase the protein level of APP (although miR-16 still downregulates it compared to miR-Scr treated cells). This occurrence is likely due to the cellular response to lentiviral infection, which would be of interest to investigate in further studies. Regardless, these findings support the use of the miR-16 overexpression system in primary hippocampal cells as a model of functional miR-16 overexpression as they agree with literature findings.

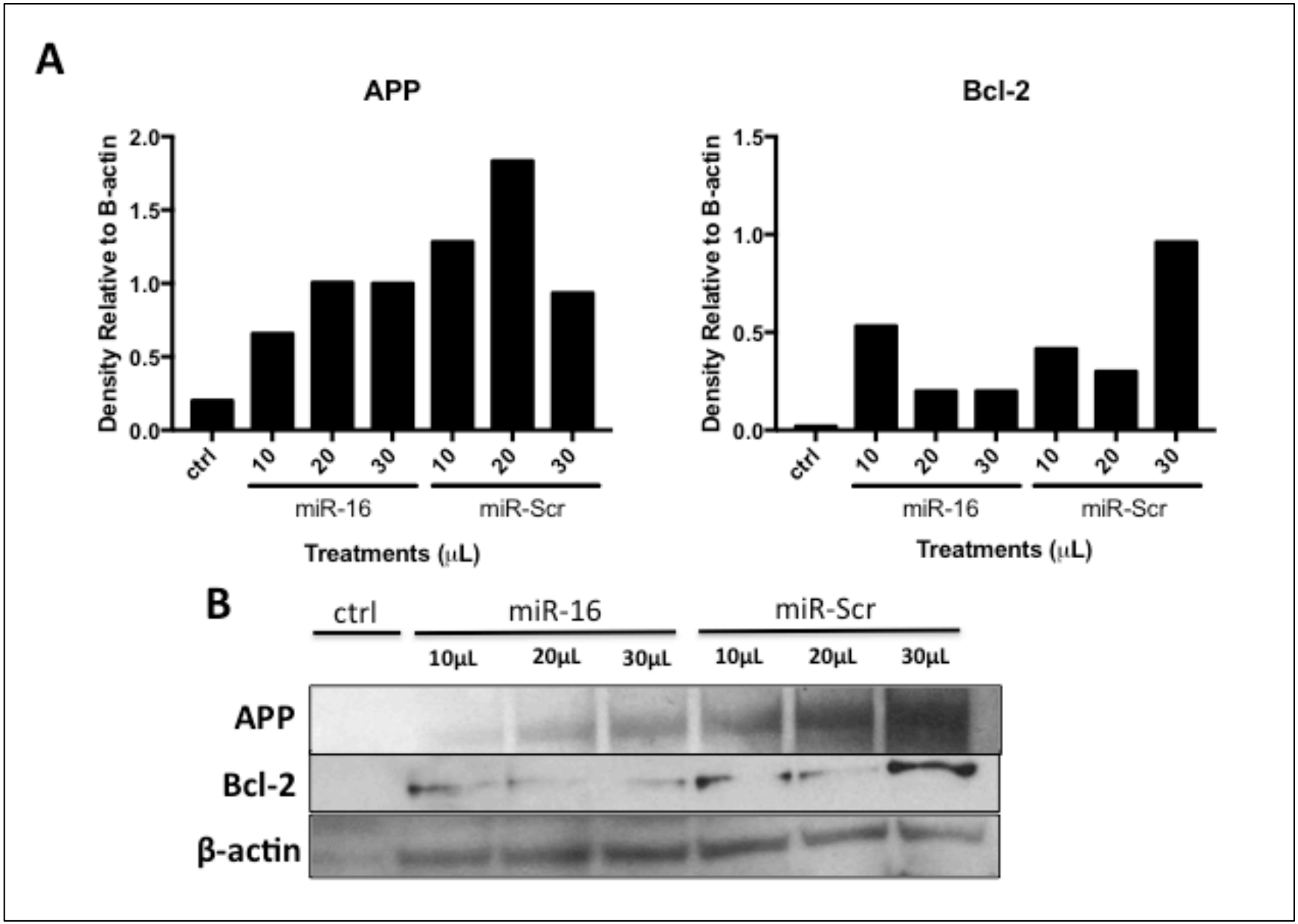
A
APP
Density Relative to B-actin
2.0
1.5
1.0
0.5
0.0
ctrl
10
20
30
10
20
30
miR-16
miR-Scr
Treatments (μL)
Bcl-2
Density Relative to B-actin
1.5
1.0
0.5
0.0
ctrl
10
20
30
10
20
30
miR-16
miR-Scr
Treatments (μL)
B
ctrl
miR-16
miR-Scr
10μL
20μL
30μL
10μL
20μL
30μL
APP
Bcl-2
β-actin

Figure 12: Western blots to verify experimental model. A) APP and Bcl-2 protein levels were lower in miR-16 treated cells than miR-Scr treated cells. All protein levels were normalized to B-actin levels in the same well. B) Western blots of APP, Bcl-2 and B-actin. Ctrl = untreated cells.

4.3 Argonaute Immunoprecipitation for Target Detection via Microarray

In order to understand which mRNA transcripts miR-16 is directly targeting, immunoprecipitation of Argonaute 2 complexes (Ago2-IP) was performed. Using the knowledge that miRNA associates with the RISC complex to knock down targets, Ago2-IP allows specific immunoprecipitation of Ago2, a protein in the RISC complex, thereby co-precipitating all RNA bound to the complex. In addition, miRNA are highly stable in complex with Ago2 (Turchinovich et al. 2011) and in this system of miR-16 overexpression, the RISC complexes are primarily associated with miR-16, allowing specific precipitation of miR-16 mRNA targets.

Ago2-IP is a very powerful methodology to use for miRNA target analyses. In this study, Ago2-IP was utilized in combination with a microarray for gene expression analysis. This methodology is often used to screen for miRNA that are associated with the RISC complex or to profile miRNA targets (Goff et al. 2009; Parsi et al. 2015). However, when Ago2-IP is used to determine miRNA targets it is typically in easy-to-culture cell lines and rarely, if ever, in neuronal populations (Fan et al. 2013). This method represents a biologically relevant assessment of mRNA targets of miRNA within hippocampal neuronal primary cells.

TargetScan or other computational programs are typically used to make miRNA target predictions, with validation of those targets further explored in cell culture (Shioya et al. 2010). That approach can be useful, but the platforms are deficient in their ability to identify tissue-specific targets, an area that Ago2-IP gene expression analysis excels in. Additionally, unlike overexpressing a particular miRNA and determining potential targets

based on transcriptomic changes of the culture system, selecting for Ago-2 bound mRNA has the benefit of including all miRNA bound by the RISC complex, even those that are destined for degradation. This is important to note, as miRNA do not always exhibit a detectable effect on expression changes at the transcriptional level regardless of their effect at the protein level (Schwanhäusser et al. 2008). Therefore, using the Ago2-IP technique allows selection for all miRNA bound to Ago2, whether they will subsequently be degraded or not.

To perform Ago2-IP, primary hippocampal neurons were treated with lentiviral vectors at 8 DIV and incubated for four days (Figure 13). Ago2-IP was then performed using antibodies specific to Ago2. The mRNA collected in this way was then converted to cDNA, amplified and subsequently applied to a Whole Genome Mouse microarray for mRNA identification. In order to precipitate enough mRNA for further analysis, large numbers of cells were plated (approx. 5 million per lentiviral treatment). This procedure was optimized for use with hippocampal cells, as it is difficult to culture high number of cells at once. Completion of the Ago2-IP procedure yielded a visible pellet of RNA. RNA was resuspended but the yield was below the threshold for an accurate quantitative analysis of yield and quality using the Agilent BioAnalyzer. However, the results of this analysis are included in the appendix as the presence of RNA is evident despite the low yield (Appendix 1.3).

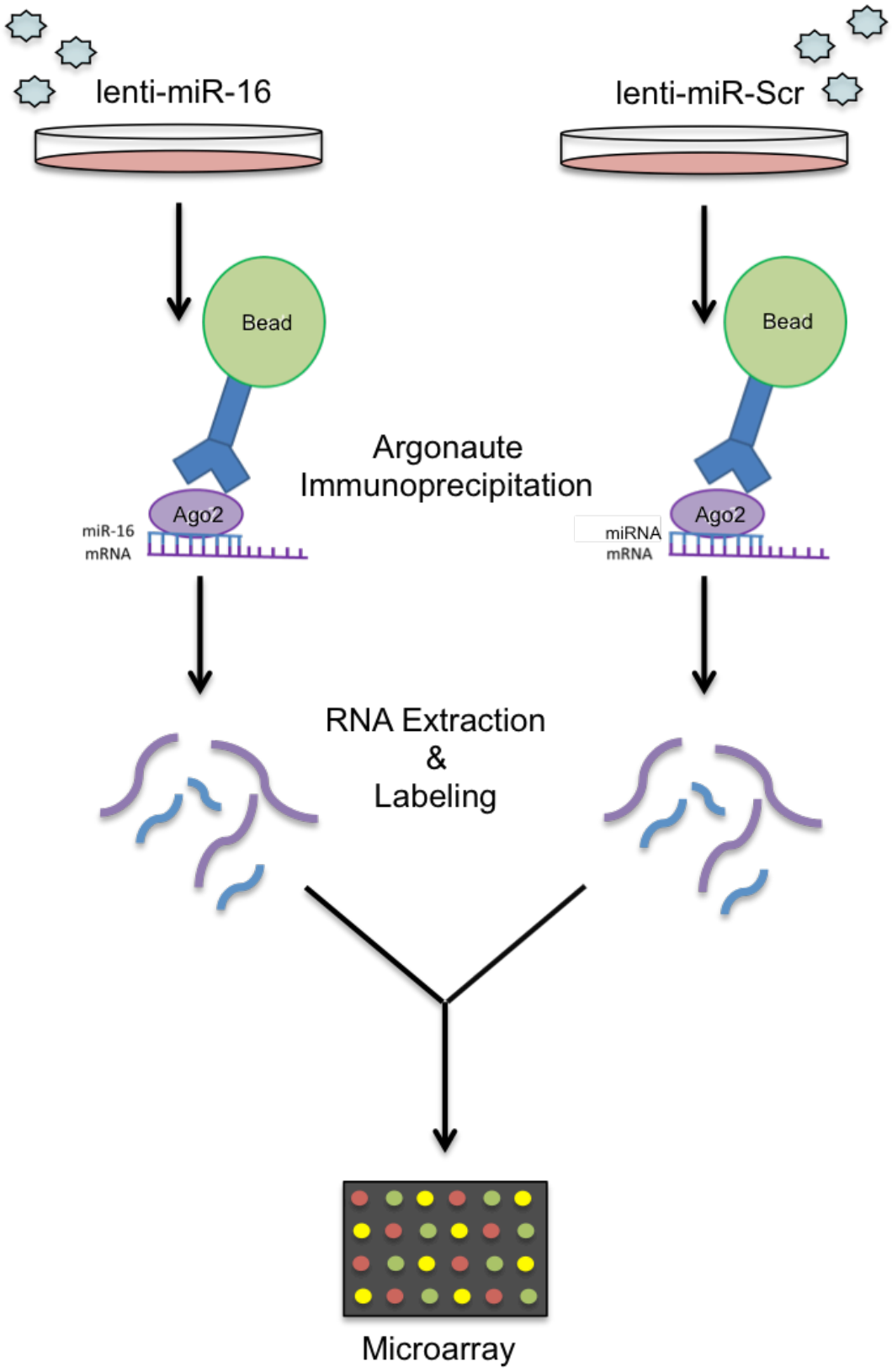
lenti-miR-16
lenti-miR-Scr
Bead
Bead
Argonaute
Immunoprecipitation
Ago2
Ago2
miR-16
mRNA
miRNA
mRNA
RNA Extraction
&
Labeling
Microarray

Figure 13: Ago2-IP Procedure. On the left, the miR-16 treated cells were incubated with anti-Ago2 antibody conjugated to beads. Immunoprecipitation was performed and miRNA (mainly miR-16) and target mRNA were eluted. This RNA was then labeled and applied to a microarray. On the right, the same procedure is illustrated with miR-Scr treated cells. Instead of primarily miR-16 being pulled down, it was a variety of endogenous miRNA and their targets.

For additional validation of the experimental procedure, it was important to determine that the Ago2 protein was successfully immunoprecipitated. Therefore a western blot was performed on the immunoprecipitate (Figure 14). Although the amount of protein was low, a faint band in the miR-16 and miR-Scr Ago2-IP fractions at approximately 100kDa was apparent. This corresponds to the expected molecular weight of Ago2. Furthermore, there are clear bands corresponding to both the heavy and light chain of the anti-Ago2 antibody on the blot, indicating that all of the proteins did elute from the beads. Additionally, it should be mentioned that there are bands corresponding to the antibody heavy and light chain in the control (non-immunoprecipitated protein) lane as well, likely due to contamination with miR-Scr protein sample during loading. However, there is a clear non-specific band at approximately 35 kDa (due to presence of many proteins in the cell lysate) that is not present in the other two lanes. Additionally there is no Ago2 band present in this lane, supporting our successful precipitation of the Ago2 protein.

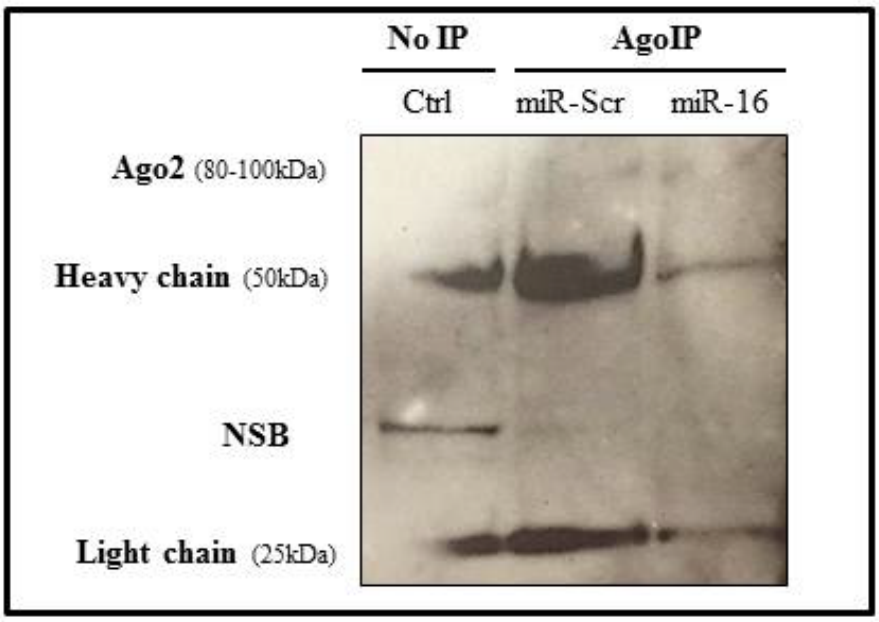
No IP
AgoIP
Ctrl
miR-Scr
miR-16
Ago2 (80-100kDa)
Heavy chain (50kDa)
NSB
Light chain (25kDa)

Figure 14: Western Blot to Confirm the Immunoprecipitation of the Argonaute 2 Protein. Heavy chain and Light chain represent the respective chains of the Ago2 antibody used to perform the immunoprecipitation. Ago2 represents the Argonaute 2 protein that is co-immunoprecipitated with the miRNA:mRNA complexes. NSB: non-specific band.

4.3.1 Validation of MiR-16 Presence in Immunoprecipitated RNA

In order to ensure that miR-16 was highly present within the immunoprecipitated RNA, Realtime PCR was performed before microarray analysis was completed. MiR-16 has previously been shown to associate with Ago2 (Turchinovich et al. 2011), thus it was expected to co-immunoprecipitate with anti-Ago2. The snoRNA U6 has not been shown to associate with Ago2, and thus it was used as a non-target control RNA for non-immunoprecipitated RNA. Let-7c on the other hand, has been shown to be highly prevalent in combination with Ago2 and thus served as an endogenous control (Krell et al. 2016). To ensure the relevancy to neuronal tissue, the level of miR-132 within the RNA sample was also determined, as it is known to be highly prevalent in neurons (Sempere et al. 2004). The level of miR-16 in the miR-16 treated Ago2-IP sample was approximately 10-fold higher than that of let-7c, and miR-132 was approximately 2-fold higher than let-7c (Figure 15). In the miR-Scr treated Ago2-IP sample, the miR-16 level was very similar to that of let-7c and the miR-132 level was approximately 2-fold higher than let-7c (Figure 15). The results of this analysis indicate that miR-16 was indeed overrepresented in the miR-16 treated Ago2-IP sample.

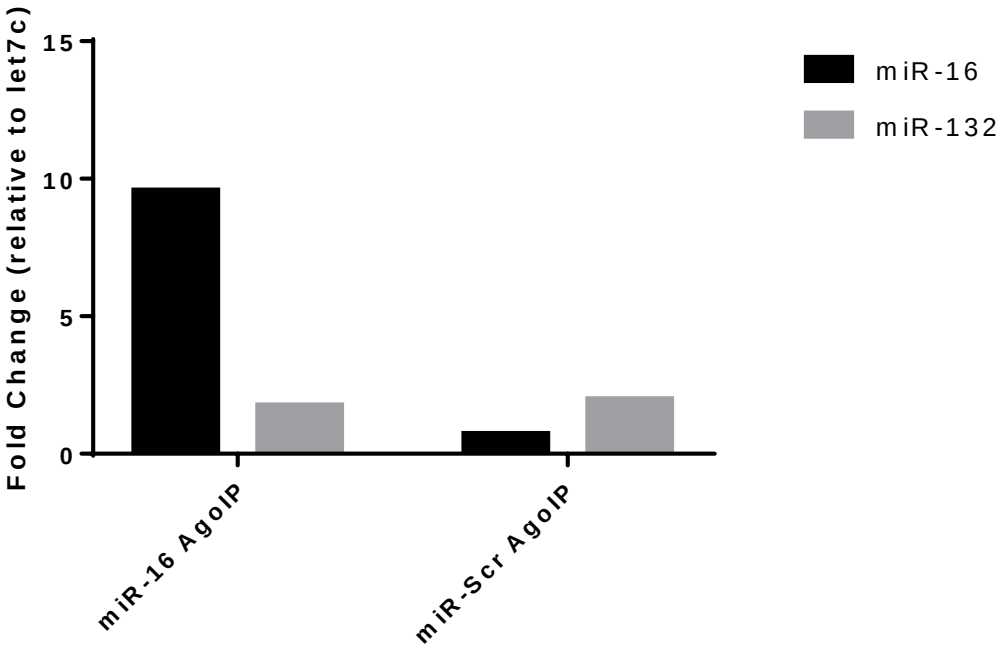
Fold Change (relative to let7c)
15
10
5
0
miR-16 AgoIP
miR-Scr AgoIP
miR-16
miR-132

Figure 15: Relative Abundance of MiR-16 in RNA Extracted from Ago-IP Samples. Relative Abundance was determined via Realtime PCR with probes for miR-16, miR-132 and let-7c in the same RNA samples from both miR-16 treated AgoIP and miR-Scr treated AgoIP. Let-7c was used as a normalizing control. Statistical analyses/additional replicates were not performed due to limited sample quantity.

4.3.2 Identification of Immunoprecipitated mRNA via microarray

The identities of immunoprecipitated mRNA targets were assessed using a Whole Genome Mouse microarray. Microarrays are useful due to their ability to detect gene expression changes on a whole genome scale. The array was used to compare genes pulled down with Ago2 in miR-16 treated vs. miR-Scr treated hippocampal cells. Feature Extraction was utilized to extract the data from the array. The Quality Control report is included in the Appendix 1.4.

4.3.3 Cross Reference with TargetScan

In order to exclude any genes pulled down during the Argonaute immunoprecipitation in combination with miRNAs other than miR-16, the microarray data was cross-referenced with data generated from a miR-16 target search generated in TargetScanMouse Release 7.1. TargetScan is a web-based tool that allows target determination by searching databases of mRNA transcripts for sequences that would facilitate binding by the 7-nucleotide binding site (seed sequence) present on miR-16-5p. TargetScan was used, rather than another of the many prediction programs available, because it is a seed sequence based algorithm and those have been proven to be the most accurate (Schwanhäusser et al. 2008). TargetScan presented 4443 genes as putative targets of miR-16-5p, while the immunoprecipitation yielded 2059 genes. Cross-referencing the two data sets revealed 690 genes that were predicted targets of miR-16-5p within the Argonaute immunoprecipitated RNA (Figure 16).

This data set was uploaded into Ingenuity Pathway Analysis (IPA). IPA then analyzed the data, specifically looking only at relationships where confidence was equivalent to experimental observations. The Exp. Fold Change Cutoff was 4.0 with a range from -1.9253E4 to 8098.07 with a focus on the transcripts that were increased in relative abundance within miR-16 bound RISC complex. In this way, 673 genes were identified as putative targets of miR-16-5p in hippocampal primary cultures with high confidence.

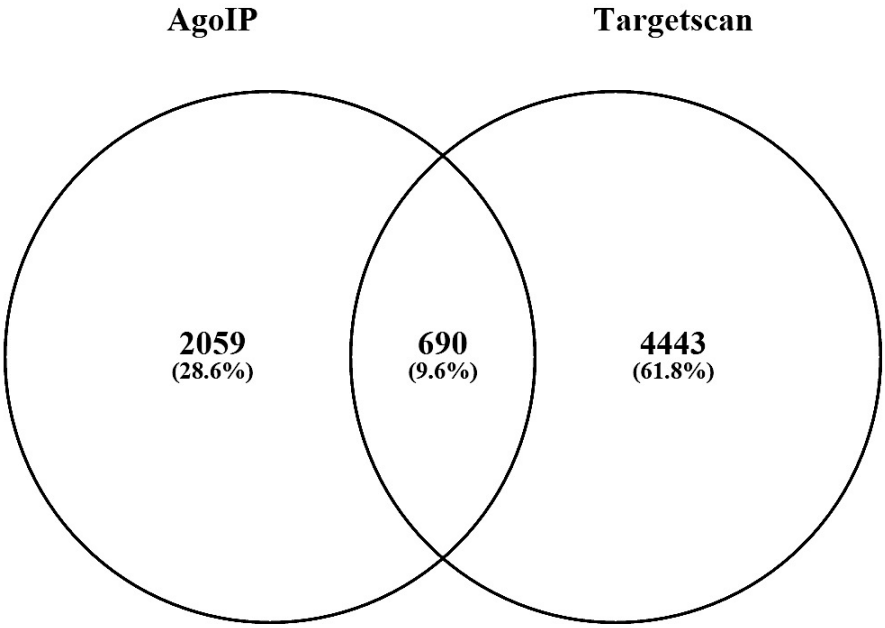
AgoIP
Targetscan
2059
(28.6%)
690
(9.6%)
4443
(61.8%)

Figure 16: Venn Diagram Highlighting the Overlap Between Genes Identified as Targets via Microarray of AgoIP Samples and TargetScan Prediction. Produced using Venny version 2.1. (http://bioinfogp.cnb.csic.es/tools/venny/).

4.4 Functional Analysis of Microarray Results

A core analysis was performed on IPA analysis, with both direct and indirect relationships taken into account. It should be kept in mind that throughout the analysis of the results, transcripts that are present at high amounts indicate genes that are targeted by miR-16 and thus would be presumably be downregulated in a system of high miR-16 expression, such as the “pre-clinical” stage of prion disease in the CA1 region of the mouse hippocampus.

4.4.1 Top Canonical Pathways

The top canonical pathways that were highly represented in the array were as depicted in Table 3. The p-values indicate a strongly significant relationship between miR-16 and these pathways. Of greatest interest is mitochondrial dysfunction, with the highest significance, because while the others are mostly implicated in cancer, mitochondrial dysfunction has been highly implicated in the pathogenesis of Alzheimer's disease (Nunomura et al. 2001). This spurred taking a closer look at the pathway, as shown in Figure 17. As seen in Figure 17, many genes involved in mitochondrial dysfunction are directly related to AD such as α-synuclein, Aβ, and APP. This is also a good indicator of the success of the immunoprecipitation, as previously described targets of miR-16-5p like APP, BACE2 and BCL2 are all present in this pathway (Figure 17).

Table 3: Pathways Identified as Highly Targeted by MiR-16 via IPA.

Pathway	p-value	Overlap with Pathway Components
Mitochondrial Dysfunction	1.21E-05	9.9% (17/171)
Pancreatic Adenocarcinoma Signaling	6.50E-05	11.3% (12/106)
Molecular Mechanisms of Cancer	8.42E-05	6.8% (25/365)
Gq Signaling	1.11E-04	9.5% (14/147)
Docosahexaenoic Acid (DHA) Signaling	1.23E-04	17.9% (7/39)

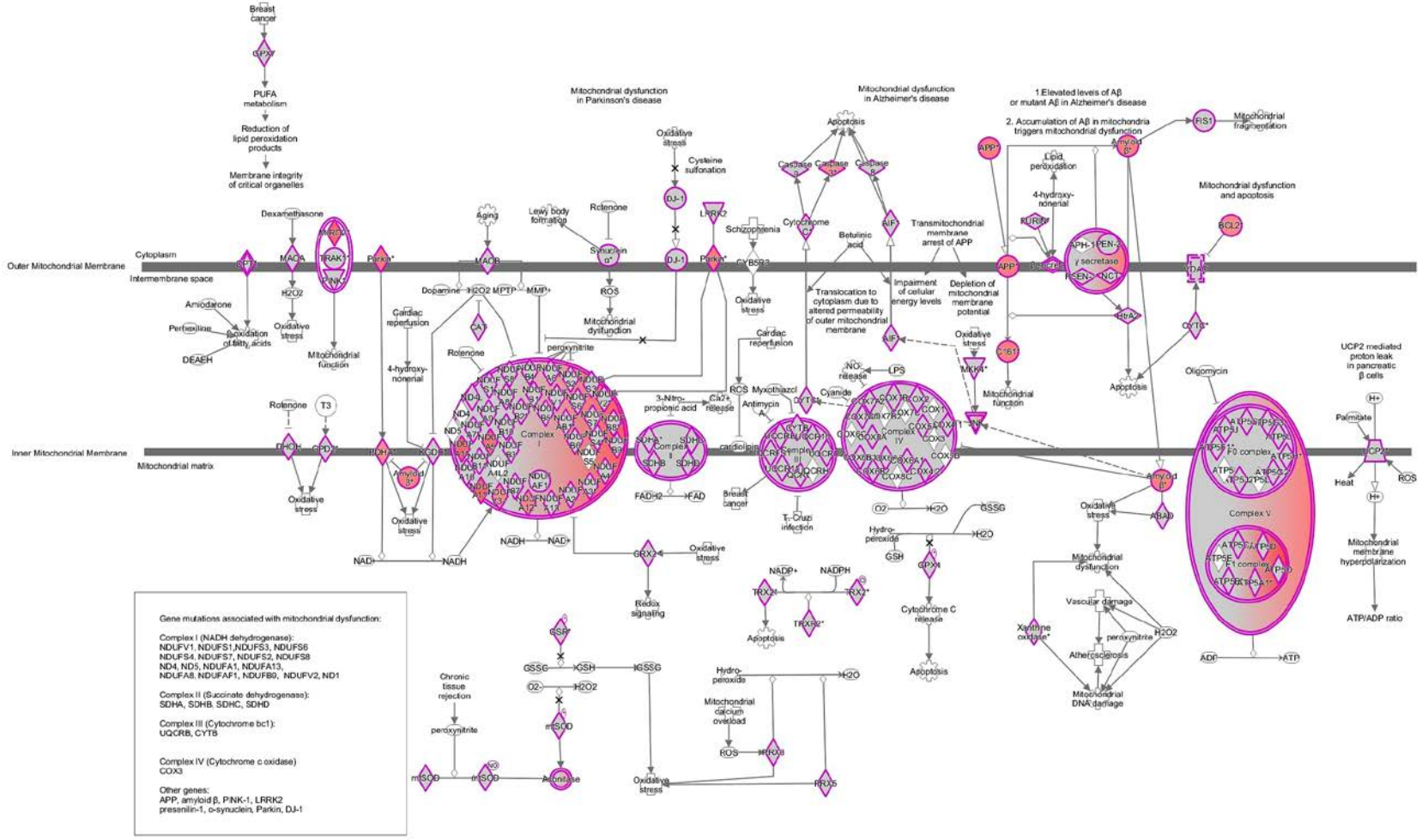
Breast cancer
GPX7
PUFA metabolism
Reduction of lipid peroxidation products
Membrane integrity of critical organelles
Mitochondrial dysfunction in Parkinson's disease
Mitochondrial dysfunction in Alzheimer's disease
1.Elevated levels of Aβ or mutant Aβ in Alzheimer's disease
2. Accumulation of Aβ in mitochondria triggers mitochondrial dysfunction
Mitochondrial fragmentation
Mitochondrial dysfunction and apoptosis
Dexamethasone
Cytoplasm
Outer Mitochondrial Membrane
Intermembrane space
Inner Mitochondrial Membrane
Mitochondrial matrix
Aging
Lewy body formation
Rotenone
Schizophrenia
Betulinic acid
Transmitochondrial membrane arrest of APP
Impairment of cellular energy levels
Depletion of mitochondrial membrane potential
Translocation to cytoplasm due to altered permeability of outer mitochondrial membrane
Amiodarone
Perhexiline
DEAEH
Cardiac reperfusion
Dopamine
MPTP
MPP+
Oxidative stress
Mitochondrial dysfunction
peroxynitrite
4-hydroxy-nonenal
Lipid peroxidation
Mitochondrial function
Apoptosis
Oligomycin
UCP2 mediated proton leak in pancreatic β cells
Palmitate
Heat
ROS
Mitochondrial membrane hyperpolarization
ATP/ADP ratio
Complex I
Complex II
Complex III
Complex IV
Complex V
Rotenone
T3
3-Nitro-propionic acid
Myxothiazol
Antimycin A
Cyanide
LPS
NO release
cardiolipin
Breast cancer
T. Cruzi infection
Hydro-peroxides
GSH
GSSG
Cytochrome C release
Vascular damage
Atherosclerosis
Xanthine oxidase
Mitochondrial DNA damage
Chronic tissue rejection
Mitochondrial calcium overload
Redox signaling
Gene mutations associated with mitochondrial dysfunction:
Complex I (NADH dehydrogenase):
NDUFV1, NDUFS1,NDUFS3, NDUFS6
NDUFS4, NDUFS7, NDUFS2, NDUFS8
ND4, ND5, NDUFA1, NDUFA13,
NDUFA8, NDUFAF1, NDUFB0, NDUFV2, ND1
Complex II (Succinate dehydrogenase):
SDHA, SDHB, SDHC, SDHD
Complex III (Cytochrome bc1):
UQCRB, CYTB
Complex IV (Cytochrome c oxidase)
COX3
Other genes:
APP, amyloid β, PINK-1, LRRK2
presenilin-1, α-synuclein, Parkin, DJ-1

Figure 17: Mitochondrial Dysfunction Pathway. Genes shown in red were highly present in the microarray data and thus are targeted by miR-16. Figure created in IPA.

In keeping with this theme, some other pathways that are highly enriched in targets found in this analysis include amyloid processing and synaptic long-term potentiation (Figure 18 & 19). Similar molecules are targeted in both mitochondrial dysfunction and amyloid processing, with APP and BACE2 present in both pathways. Both APP and BACE2 were highly represented in the array (5.165 fold and 4.682 fold respectively). Synaptic long-term potentiation included the MAPK/ERK pathway, with MAP2K1 (a key member of the pathway) being highly represented in the array (502.72 fold higher than in AgoScr-IP). This indicates that miR-16-5p is likely to have a strong impact on that pathway and since the MAPK/ERK pathway is a ubiquitous pathway involved in many cellular processes, it is likely that this microRNA has a significant impact on cell function.

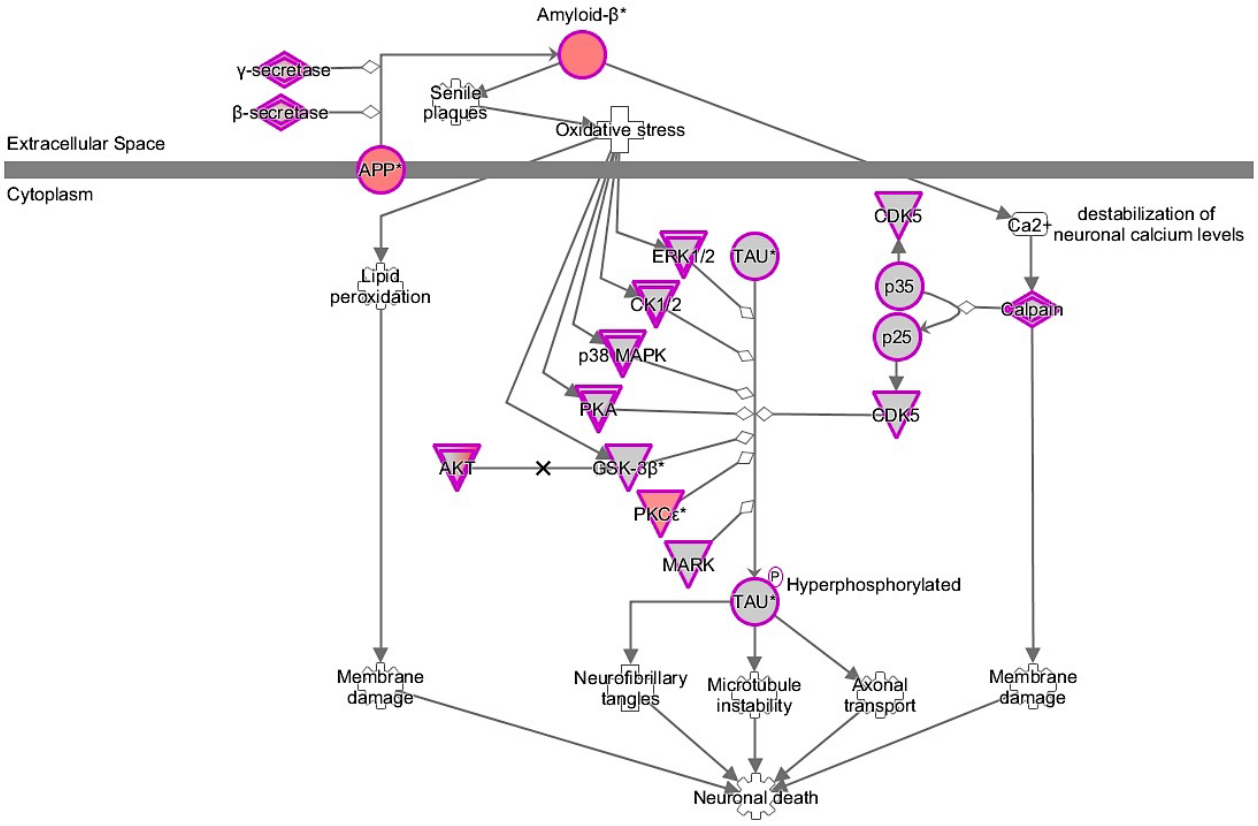
Amyloid-β*
γ-secretase
β-secretase
Senile plaques
Oxidative stress
Extracellular Space
Cytoplasm
APP*
Lipid peroxidation
ERK1/2
TAU*
CK1/2
p38 MAPK
PKA
AKT
GSK-3β*
PKCε*
MARK
CDK5
p35
p25
CDK5
Ca2+
destabilization of neuronal calcium levels
Calpain
P
Hyperphosphorylated
TAU*
Membrane damage
Neurofibrillary tangles
Microtubule instability
Axonal transport
Membrane damage
Neuronal death

Figure 18: Amyloid Processing Pathway. Shapes filled in with red colour are targeted by miR-16 and were upregulated in the microarray. Figure created in IPA.

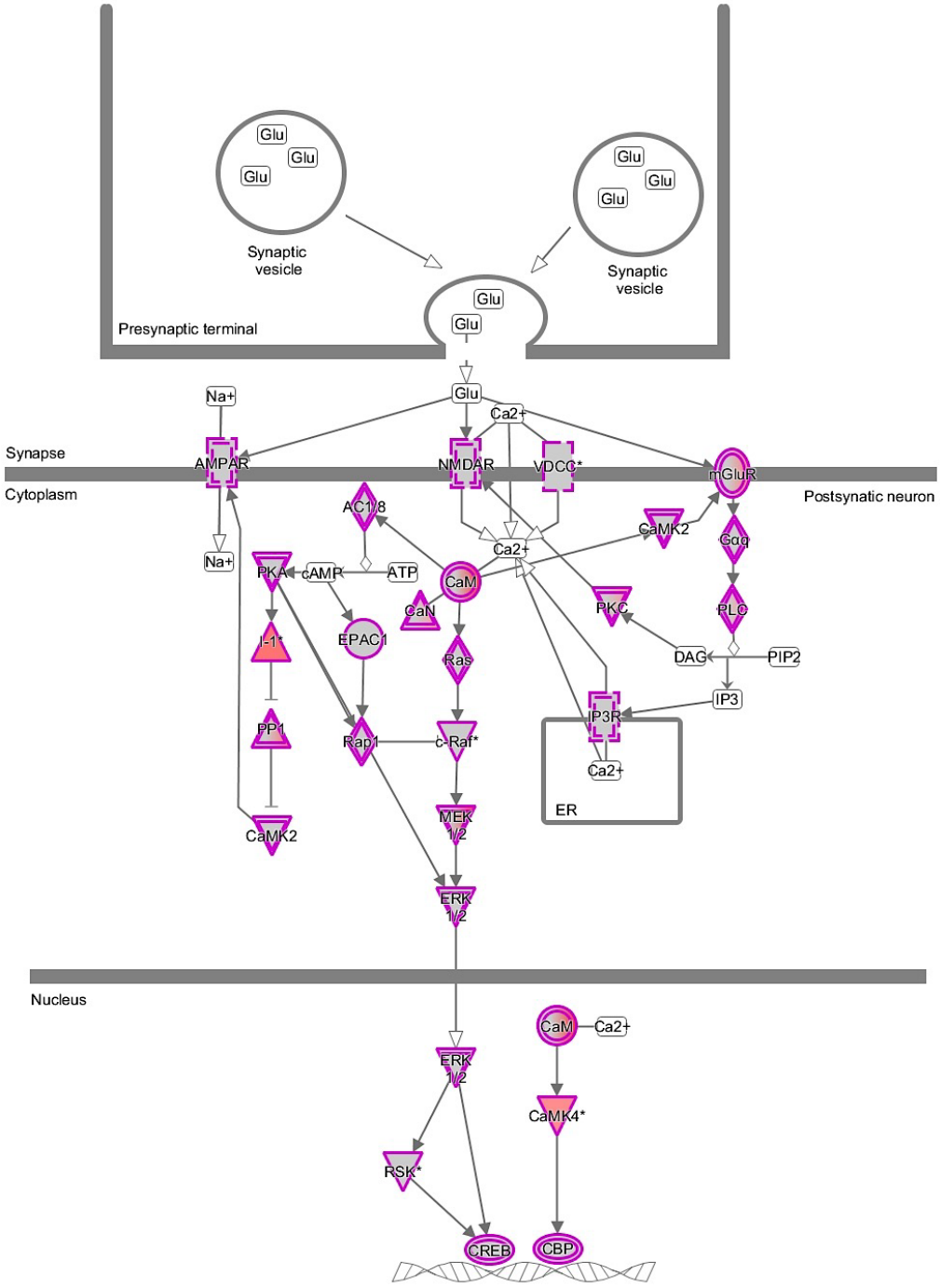
Glu
Glu
Glu
Synaptic vesicle
Glu
Glu
Glu
Synaptic vesicle
Presynaptic terminal
Glu
Glu
Na+
Glu
Ca2+
Synapse
AMPAR
NMDAR
VDCC*
mGluR
Cytoplasm
Postsynatic neuron
AC1/8
CaMK2
Gαq
Na+
Ca2+
PKA
cAMP
ATP
CaM
CaN
PKC
PLC
I-1*
EPAC1
Ras
DAG
PIP2
IP3
IP3R
PP1
Rap1
c-Raf*
Ca2+
ER
CaMK2
MEK 1/2
ERK 1/2
Nucleus
CaM
Ca2+
ERK 1/2
CaMK4*
RSK*
CREB
CBP

Figure 19: Synaptic Long Term Potentiation. Shapes filled in with red colour are targeted by miR-16 and were upregulated in the microarray. Figure created in IPA.

4.4.2 Top Upstream Regulators

L-dopa was identified as the top upstream regulator of the genes represented on the array, with an activation z-score of 1.579 and a p-value of 7.47E-09. The second upstream regulator on the list was CREB1 with a z-score of 0.032 and a p-value of 3.06E-07. Interestingly, CREB1 was found to be present in the array (1.901 fold higher than AgoScr-IP) indicating that it is a potential direct target of miR-16. The rest of the top 10 regulators are summarized in Table 4. BDNF (a neurotrophin) and glutamate (a neurotransmitter) are of significant interest, as the results of this array are not neurospecific (IPA has an inherent bias towards cancer cells and miRNA have many targets in many tissues) yet these are the most prominent upstream regulators along with L-dopa, indicating that miR-16 has important neurospecific effects. This spurred investigation into important pathways that all three regulate potentially clinically relevant targets of miR-16 in neurons. Of particular interest is that all three of these putative upstream regulators stimulate the MAPK/ERK pathway and CREB1 is a direct target of that pathway. The analysis program was not able to make a determination of the predicted activity of L-dopa, CREB1, MYC, L-glutamic acid and CXCR1 on miR-16 due to insufficient data, this does not however, mean that they are not activating or inhibiting miR-16. Furthermore, both MYC and BDNF are relatively decreased in abundance in the miR-16 AgoIP vs the miR-Scr AgoIP, 6.849 and 2.101 fold, respectively. This indicates that they are unlikely to be directly targeted by miR-16.

Table 4: Top Upstream Regulators of miR-16 As Predicted by IPA.

Upstream Regulator	Exp. Fold Change	Molecule Type	Predicted Activity	Activation z-score	p-value of overlap
L-dopa	-	Endogenous mammalian chemical	-	1.579	7.47E-09
CREB1	1.901	Transcription Regulator	-	-0.032	3.06E-07
miR-17-5p (and other miRNAs with seed AAAGUGC)	-	Mature miRNA	Inhibited	-3.276	3.33E-07
MYC	-6.849	Transcription Regulator	-	1.258	3.72E-07
L-glutamic acid	-	Endogenous Mammalian Chemical	-	1.890	4.72E-07
Mitomycin C	-	Chemical Drug	Activated	2.534	4.84E-07
CXCR1	1.127	G-Protein Coupled Receptor	-	1.000	8.50E-07
Prednisolone	-	Chemical Drug	Inhibited	-2.400	1.74E-06
BDNF	-2.101	Growth Factor	Activated	2.966	3.31E-06
Dihydrotestosterone	-	Endogenous Mammalian Chemical	Activated	2.0777	5.03E-06

4.4.3 Top Diseases and Biological Functions

The top diseases and disorders associated with genes targeted by miR-16 are presented in Table 5. Neurological diseases predominate, with psychological disorders also largely prevalent in this group. Altogether, diseases/disorders that are the result of an affliction of neurons, are most highly represented, out of all disorders and diseases in this microarray. This may be simply due to the fact that a neuronal population was sampled, but these are also a concentrated population of targets of miR-16 due to the cross-referencing to TargetScan. Therefore, it can be concluded that miR-16 is targeting molecules with important roles in these diseases and disorders of neurons.

Table 5: Top Diseases and Disorders Involving the Targets of MiR-16 as Predicted by IPA.

Disease/Disorder	p-value	Number of Molecules
Neurological Disease	2.88E-03 → 7.42E-08	181
Psychological Disorders	2.58E-03 → 1.08E-07	95
Hereditary Disorder	2.53E-03 → 3.12E-07	50
Organismal Injury and Abnormalities	3.14E-03 → 3.12E-07	512
Skeletal and Muscular Disorders	2.99E-03 → 3.12E-07	86

In Table 6 the top molecular and cellular functions associated with the genes overrepresented in the microarray are outlined. Cellular Development and Cellular Growth and Proliferation were both significantly present with 182 and 245 molecules representing them each, respectfully. All of the top five molecular and cellular functions

have a lot to do with increased growth and development of cells, in this case neurons. The significant effect on these functions indicates that miR-16 is regulating them at a number of locations within their underlying pathways. In other words, miR-16 is inhibiting cell growth and development.

Table 6: Top Molecular and Cellular Functions Involving the Targets of miR-16 as Predicted by IPA.

Molecular/Cellular Function	p-value	Number of Molecules
Cellular Development	2.99E-03 → 1.63E-09	182
Cellular Growth and Proliferation	2.99E-03 → 1.63E-09	245
Cell Morphology	2.53E-03 → 1.73E-09	170
Cellular Assembly and Organization	2.95E-03 → 1.73E-09	142
Cellular Function and Maintenance	2.95E-03 → 1.73E-09	178

The next aspect of biological functions that investigated in IPA was physiological system development and function, moving from the microscopic to the macroscopic system view of an organism. The results of this analysis are outlined in Table 7. It is clear again that genes involving nervous system function and neurons are the primarily the targets of miR-16 in our primary culture system. As well, miR-16 is targeting and thus inhibiting the expression of genes that further tissue development, in keeping with the previous section on cellular development. Overall, the results of this array predict that miR-16 putatively has an anti-development function. This is all tied together in Figure 20, a heat map exploring the diseases and functions that miR-16 is involved in regulating. The

genes in blue are downregulated genes that are involved in cell death and survival. In addition, neurological diseases are downregulated in this microarray. The genes in orange are upregulated genes involved in differentiation and neuronal growth. This sums up the overall bioinformatics prediction that miR-16 is pro-survival, and anti-neurodegeneration but also consequently anti-growth and differentiation.

Table 7: Top Pathways within Physiological System Development and Function Involving the Predicated Targets of miR-16 Determined using IPA.

Physiological System Development and Function	p-value	Number of Molecules
Nervous System Development and Function	2.97E-03 → 1.63E-09	152
Tissue Development	2.93E-03 → 1.63E-09	164
Behavior	1.20E-03 → 2.97E-07	76
Tissue Morphology	2.53E-03 → 1.07E-05	97
Organismal Development	2.56E-03 → 3.06E-05	135

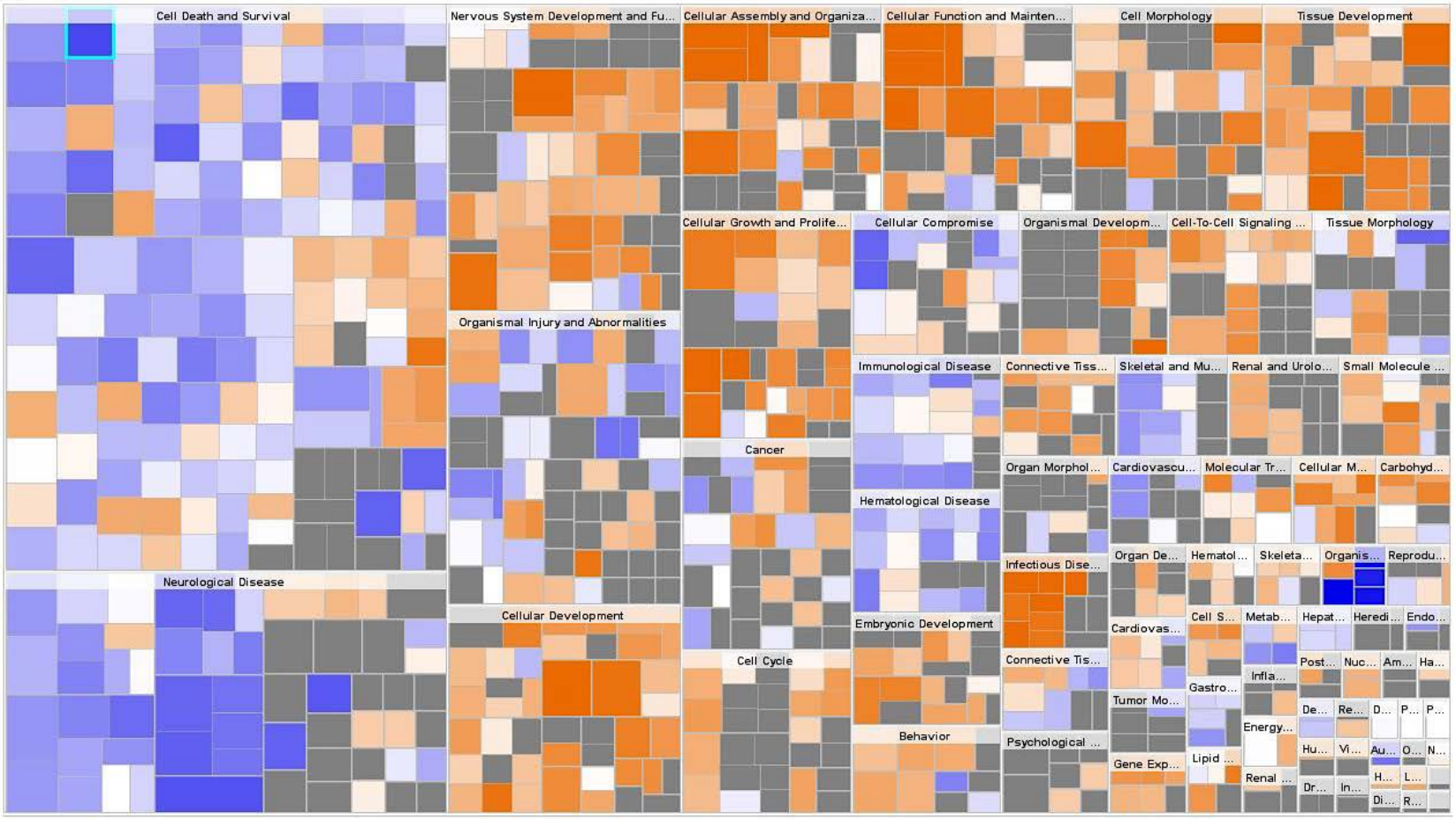
Cell Death and Survival
Nervous System Development and Fu...
Cellular Assembly and Organiza...
Cellular Function and Mainten...
Cell Morphology
Tissue Development
Cellular Growth and Prolife...
Cellular Compromise
Organismal Developm...
Cell-To-Cell Signaling ...
Tissue Morphology
Organismal Injury and Abnormalities
Immunological Disease
Connective Tiss...
Skeletal and Mu...
Renal and Urolo...
Small Molecule ...
Cancer
Organ Morphol...
Cardiovascu...
Molecular Tr...
Cellular M...
Carbohyd...
Hematological Disease
Infectious Dise...
Organ De...
Hematol...
Skeleta...
Organis...
Reprodu...
Neurological Disease
Cellular Development
Embryonic Development
Cardiovas...
Cell S...
Metab...
Hepat...
Heredi...
Endo...
Cell Cycle
Connective Tis...
Post...
Nuc...
Am...
Ha...
Infla...
Tumor Mo...
Gastro...
De...
Re...
D...
P...
P...
Energy...
Behavior
Psychological ...
Hu...
Vi...
Au...
O...
N...
Gene Exp...
Lipid ...
Renal ...
H...
L...
Dr...
In...
Di...
R...

Figure 20: A Heat Map of the Diseases and Functions Involving the Targets of miR-16. This figure was created in IPA.

4.4.4 Closer Evaluation of Nervous System Development and Function

Further evaluating miR-16 targets in the category of Nervous System Development and Function unveils genes involved in neuritogenesis, development of neurons and morphogenesis of neurites are all increased in abundance relative to AgoScr-IP (z-scores are 3.717,4.582 and 2.588 respectively). All three of these pathways are involved in "neuronal growth and differentiation" which is supporting evidence that miR-16 decreases neuronal growth and differentiation. In Figure 21 the vast interconnections between all three of these pathways are visualized. The darker the red colour, the higher the abundance of that gene on the array. It is important to note that again members of the MAPK/ERK pathway (specifically NTRK2 and MAP2K1) are involved in all three pathways.

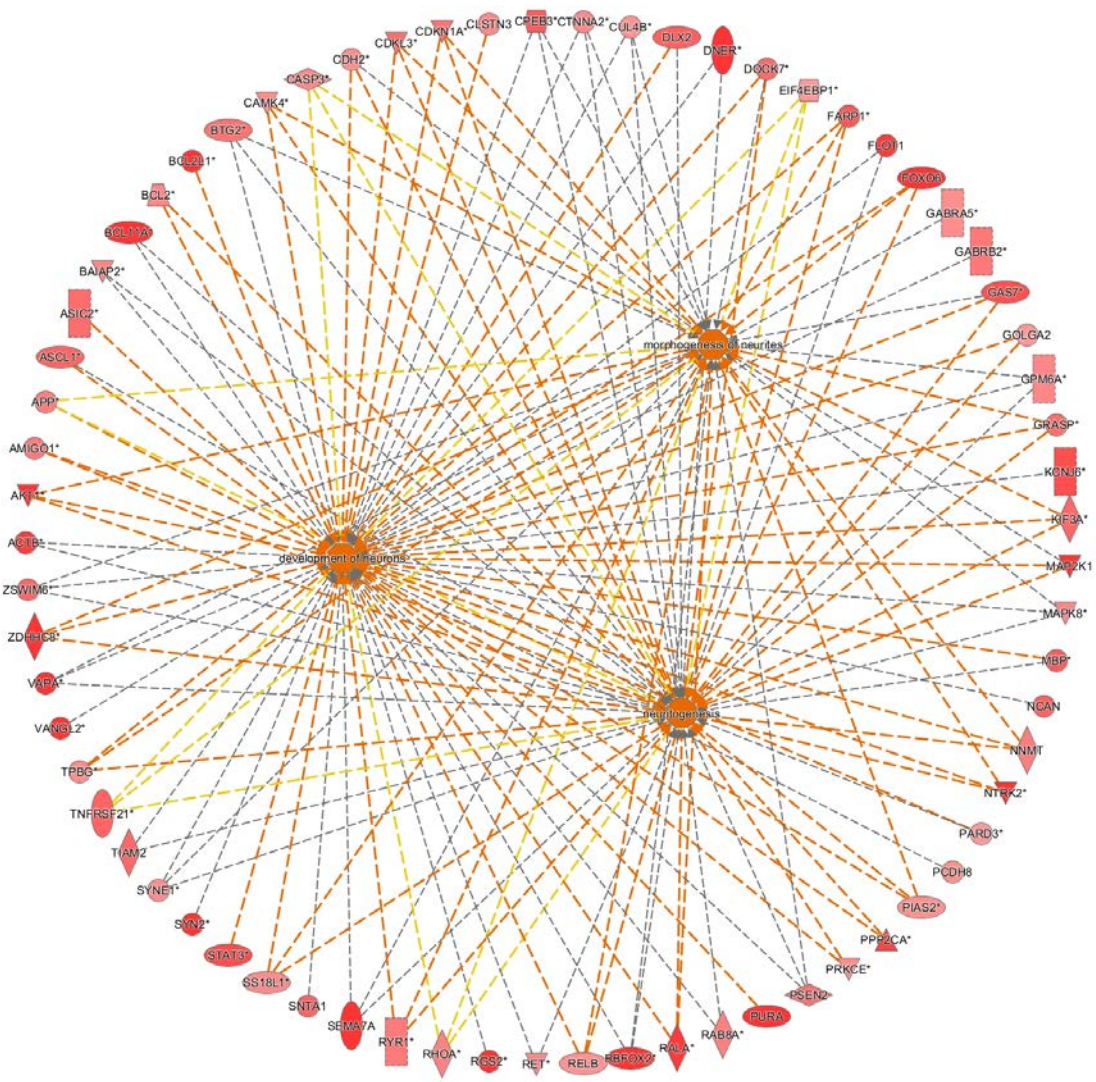
development of neurons
morphogenesis of neurites
neuritogenesis
CDKN1A*
CLSTN3
CPEB3*
CTNNA2*
CUL4B*
DLX2
DNER*
DOCK7*
EIF4EBP1*
FARP1*
FLOT1
FOXO6
GABRA5*
GABRB2*
GAS7*
GOLGA2
GPM6A*
GRASP*
KCNJ6*
KIF3A*
MAP2K1
MAPK8*
MBP*
NCAN
NNMT
NTRK2*
PARD3*
PCDH8
PIAS2*
PPP2CA*
PRKCE*
PSEN2*
PURA
RAB8A*
RALA*
RBFOX2*
RELB
RET*
RGS2*
RHOA*
RYR1*
SEMA7A
SNTA1
SS18L1*
STAT3*
SYN2*
SYNE1*
TIAM2
TNFRSF21*
TPBG*
VANGL2*
VAPA*
ZDHHC8*
ZSWIM6*
ACTB*
AKT1*
AMIGO1*
APP*
ASCL1*
ASIC2*
BAIAP2*
BCL11A*
BCL2*
BCL2L1*
BTG2*
CAMK4*
CASP3*
CDH2*
CDKL3*

Figure 21: An Interaction Web of Genes Involved in the Development of Neurons, Morphogenesis of Neurites and Neuritogenesis. Genes that miR-16 highly targets are shown in dark red, with lighter variations indicating lower targeting potential.

Table 8 is a list of molecules that are most highly abundant in the array. This could represent targets of miR-16 that are most highly abundant in the neuronal cultures, or targets that miR-16 has the highest binding affinity for, or potentially targets containing multiple binding sites for miR-16. The most prominent targets include KANSL1, CRYBB2, PRIMA1 and MAP2K1. KANSL1 is of interest as it has been previously implicated in neurodegeneration, and is related to tau expression (Zollino et al. 2012). CRYBB2 is important in neurodegeneration in the retina of the eye and has been implicated in hippocampal function (Sun et al. 2013). PRIMA1 is important for coordinating acetylcholine receptor subunits in neurons, is important for neuronal outgrowth and is upregulated by MAPK/ERK signaling (Xie et al. 2009). MAP2K1 (MEK) is an important member of the MAPK/ERK pathway (Thomas & Huganir 2004).

A number of genes that have been previously implicated in neurodegenerative disease are more highly represented in miR-16 Ago2-IP than control, including TRPM4 (~5-fold) that is closely related to TRPM2, a voltage-independent cation channel that is important in driving calcium into cells in response to NMDA application (Xie et al. 2010). Interestingly, a number of disease-associated SNPs have been identified in the genes for MAPT (tau) (2.201-fold) and KANSL1 (8098.070-fold) (Wang et al. 2016; Jun et al. 2016). APOE (another important Alzheimer's disease gene) (Akram et al. 2012) is overrepresented 1.922-fold. As well, BACE1 (-2.76-fold) and BACE2 (4.682-fold), APP (5.165-fold), PRNP (-2.188-fold), TP53 (-13.158-fold), BCL2 (4.759-fold) and DICER (2.443-fold) were found to be differentially targeted using the microarray data. In particular MAPK/ERK genes were differentially targeted by miR-16 including BDNF

(-2.101-fold), NTRK1 (1.762 fold), NTRK2 (TrkB) (9.879 fold) and RAF1 (c-Raf) (3.265-fold).

Table 8: Top Molecules Predicted to be Highly Targeted by MiR-16 as Determined by IPA.

Top Analysis-Ready Molecules	Exp. Value
KANSL1	8098.070
CRYBB2	1688.062
PRIMA1	532.320
MAP2K1	502.720
SLC22A1	70.898
TRAPPC12	68.562
TXLNB	38.277
TCP1	30.554
CHD9	29.795
ZFP91	24.411

4.5 Validation of miR-16 Targets at the Protein Level

In accordance with the hypothesis, the microarray investigation into biologically relevant targets of miR-16 in neurons revealed a number of genes, which have large influence on neuronal function and phenotype. In particular, the results of the Ago2-IP microarray indicate that miR-16 binds, sequesters and restricts the expression of many genes that are involved in the MEK/ERK pathway. The direct involvement of the MAPK/ERK pathway components shown to be targeted by miR-16 in this primary culture system (TrkB, MEK and c-Raf) is outlined in Figure 22.

MiR-16 is a putative regulator of the MAPK/ERK pathway, which has been implicated in regulation of neuronal tau phosphorylation as well as neurite growth and development (Hébert, Sergeant, and Buée 2012). Overexpression of miR-16 has been shown to inhibit the MAPK/ERK pathway in an osteosarcoma cell line via directly targeting the 3’UTR of both KRAS and Raf1 (Chen et al. 2013).

Components of this pathway have previously been found to be downregulated in AD, supporting the relevance of these results for many neurodegenerative diseases (Hallock & Thomas 2012). In particular, MAP2K1 a target that was 502.720 fold overrepresented in the miR-16 Ago2-IP relative to scramble was knocked down in AD (Hallock & Thomas 2012). An analysis of patients with varying stages of AD showed there to be an increase in the number of dysregulated MAPK/ERK pathway components with increasing disease severity (Hallock & Thomas 2012).

The MAPK/ERK pathway is also important for cellular proliferation and development as well as the regulation of transcription (Hallock & Thomas 2012), this agrees with the large scale in the IPA analysis, as there is a significant decrease in cellular development and growth, indicating that this may be an important part of miR-16 targeting.

Another gene that was more prevalent in the miR-16 Ago2-IP than control was NTRK2 which was increased by 9.879. This gene encodes TrkB, a neurotrophin receptor that is specifically stimulated by BDNF (Figure 22) (Huang & Reichardt 2001). Both BDNF and TrkB are highly expressed in pyramidal neurons (Cellerino et al. 1996) Neurotrophins, like BDNF, have been shown to induce cytoskeletal rearrangement (Huang & Reichardt 2001). BDNF is often a neuronal marker of plasticity since it is involved in proliferation, growth and remodeling and synapse formation (Zhao et al. 2012). BDNF stimulates cellular pathways to alter neurite morphology, increase neurite number and increase complexity of dendrites likely thorough regulation of cytoskeletal dynamics (McAllister 2001; Gorski et al. 2003; Baker et al. 1998; McAllister et al. 1995; Horch et al. 1999).

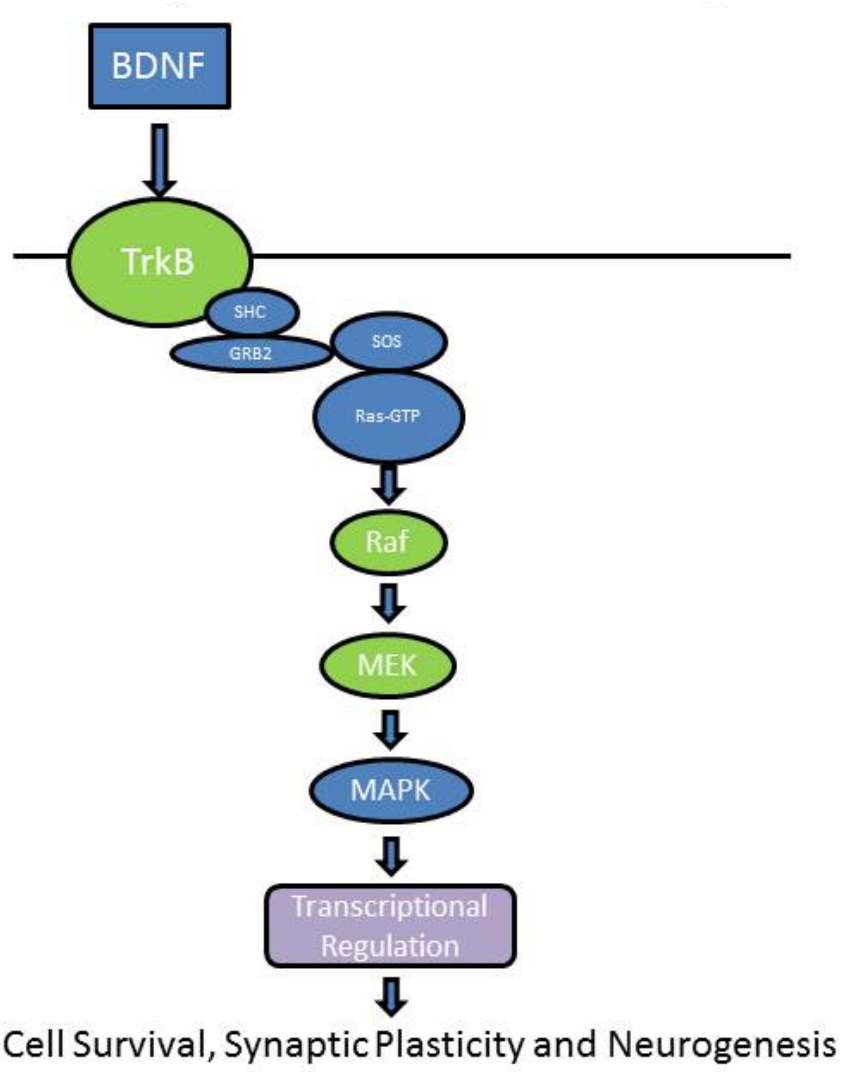
BDNF
TrkB
SHC
GRB2
SOS
Ras-GTP
Raf
MEK
MAPK
Transcriptional Regulation
Cell Survival, Synaptic Plasticity and Neurogenesis

Figure 22: MAPK/ERK Pathway in Neurons. The genes encoding TrkB, Raf and MEK were shown to be targeted by miR-16 in the microarray analysis. The resulting proteins are represented in green in this diagram.

4.5.1 Stimulation of MAPK/ERK Pathway

In order to assess the role of miR-16 in the MAPK/ERK pathway primary cells were treated with miR-16 or miR-Scr in combination with either PBS or BDNF. BDNF was used to stimulate the MAPK/ERK pathway as it was more likely to see changes in protein levels after pathway stimulation when translation of pathway components is likely to be induced. Purified recombinant human BDNF was used. A Blast search showed there to be a 97% protein sequence identity between human and mouse indicating considerable homology and that it is likely to stimulate primary neurons isolated from mice. In support of this methodology, it has been successfully used in murine cell cultures in a number of publications (Hermel et al. 2004; Liu et al. 2014).

Varying amounts of BDNF were added to the cells to elicit an upregulation in stimulation of the pathway, as visualized by increased MEK protein level (Figure 23). There was a dose-responsive effect of the activation of the pathway, with 25ng/mL and 50ng/mL both eliciting a potent effect on MEK expression. For this reason, 25ng/mL was used as the dosage of BDNF for the rest of the experiments. Protein was collected 24 hours after PBS/BDNF treatment and western blots were performed for different components of the MAPK/ERK pathway.

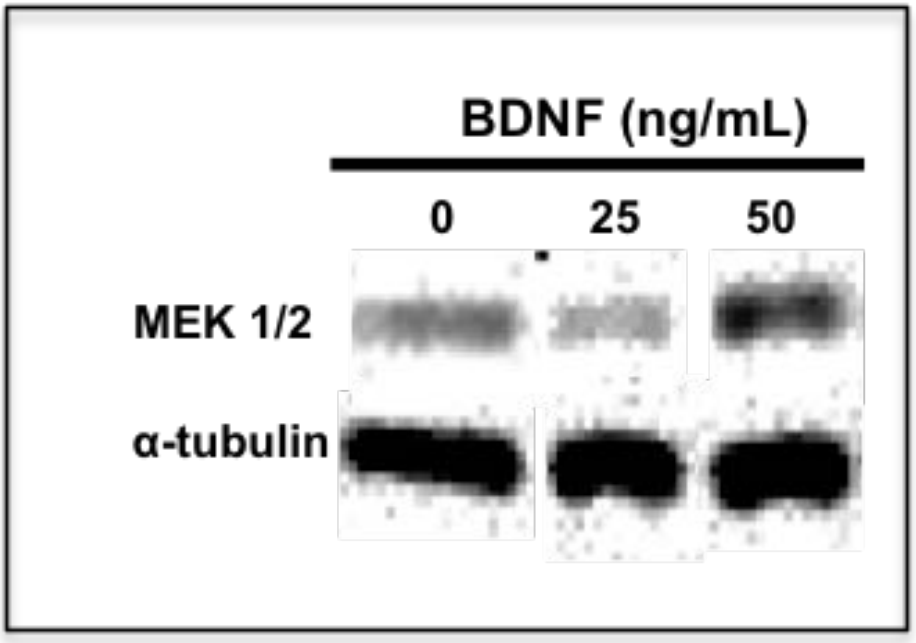
BDNF (ng/mL)
0
25
50
MEK 1/2
α-tubulin

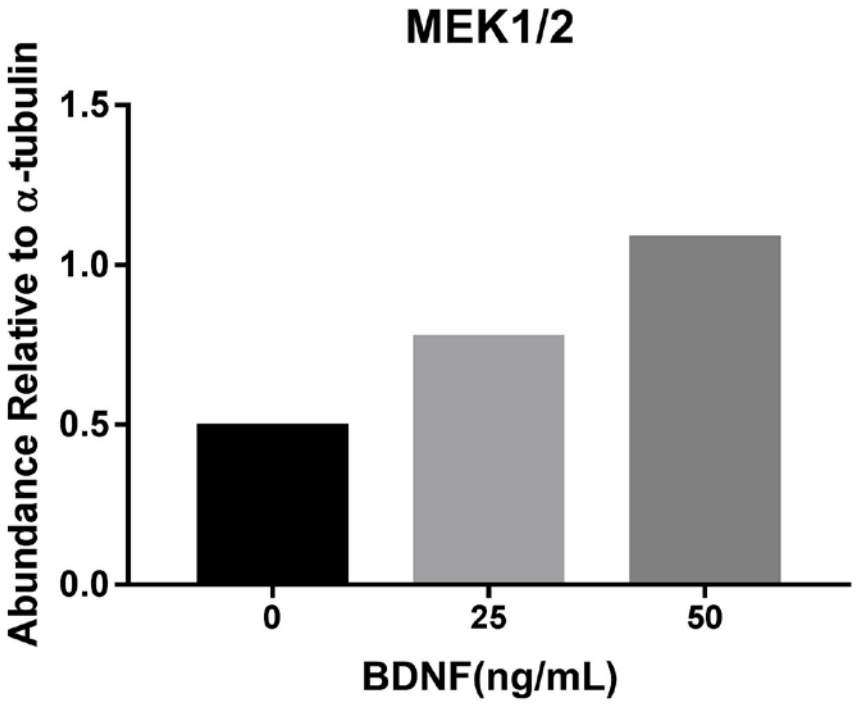
MEK1/2
Abundance Relative to α-tubulin
1.5
1.0
0.5
0.0
0
25
50
BDNF(ng/mL)

Figure 23: Stimulation of Primary Hippocampal Neurons with Increasing Levels of BDNF Resulted in a Dose-Response Relationship. After treating cultures with 0, 25ng/mL or 50ng/mL BDNF in 1X PBS protein was collected and a western blot was performed (top) and quantified by densitometry (bottom). Alpha-tubulin was used as a loading control.

4.5.2 Effect of miR-16 Upregulation on BDNF Activation of the MAPK/ERK Pathway

The levels of different components of the MAPK/ERK pathway were next looked at using western blots. These components include MEK1/2, TrkB, p44/42 MAPK (ERK1/2), c-Raf, β-actin, p-c-Raf(Ser338), p-MEK1/2 (Ser217/221), p-ERK1/2 (Thr202/Tyr204), p-p90RSK (Ser380) and p-MSK1 (Thr581).

On average, in PBS treated wells there was no decrease in protein level of the components with miR-16 addition relative to control. However, when BDNF was added to the cells, there was a relative decrease in protein level of many of the components of the MAPK/ERK in the miR-16 treated cells when compared to BDNF treatment alone. These components include c-Raf, ERK, p-MSK1, p-p90RSK and MEK (Figure 24). Interestingly, in many of these blots there was decreased protein level in the miR-Scr treated wells to levels even lower than the miR-16 treated wells. Also of interest is that although TrkB protein levels were decreased with PBS + miR-16, relative to control, they were in fact increased with BDNF + miR-16. There also appeared to be limited increased TrkB expression with BDNF addition alone.

In regards to the phosphorylated members of the MAPK/ERK pathway, there were some interesting findings as well. For instance, although the phosphorylated transcription factors that represent the “end-point” of the cascade were decreased in protein level with miR-16 and BDNF addition (p-MSK1 and p-p90RSK (Figure 24)) there was increased phosphorylation of p-MEK, p-ERK and p-c-Raf direct components of the pathway.

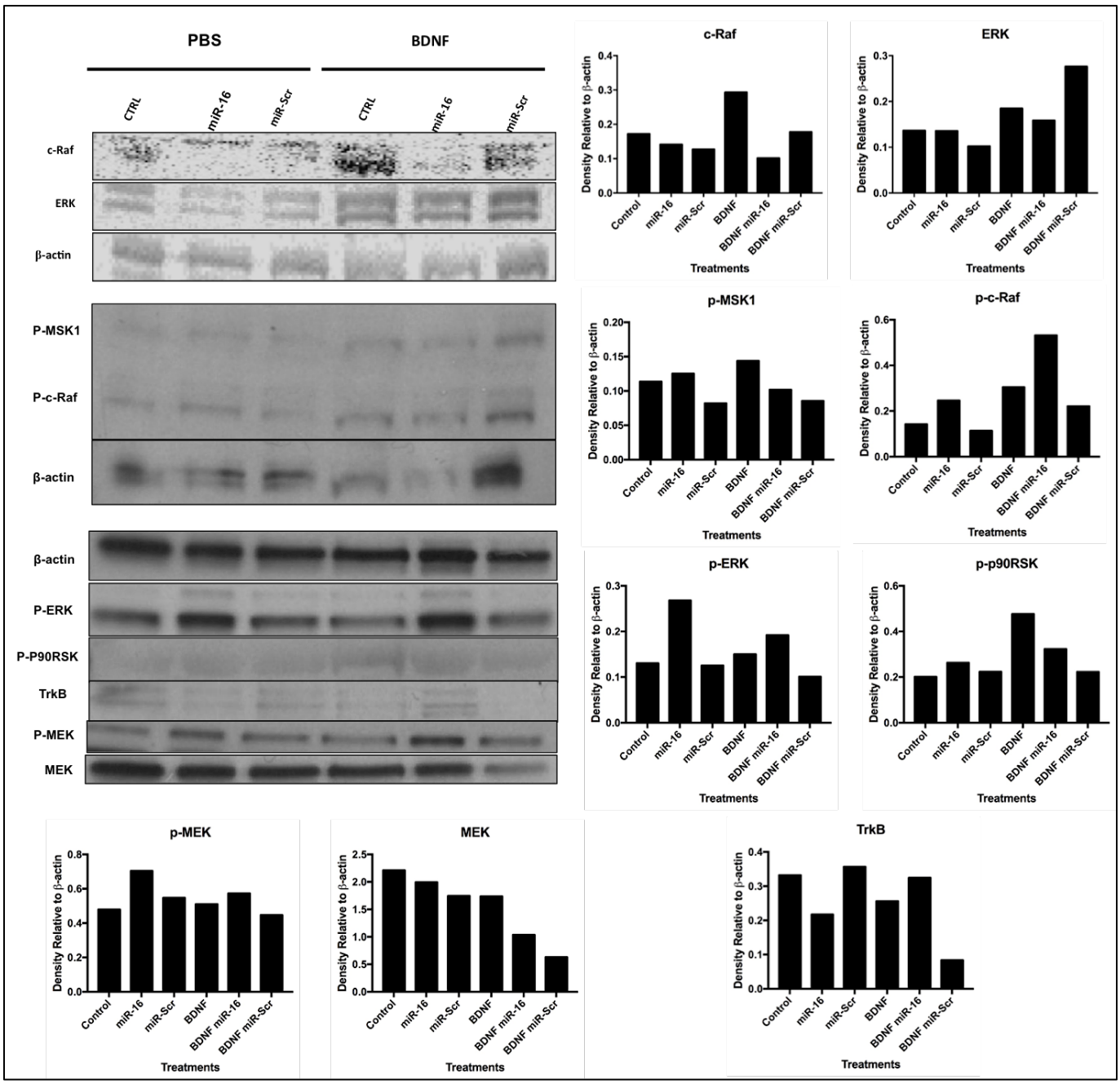
PBS
BDNF
CTRL
miR-16
miR-Scr
CTRL
miR-16
miR-Scr
c-Raf
ERK
β-actin
P-MSK1
P-c-Raf
β-actin
β-actin
P-ERK
P-P90RSK
TrkB
P-MEK
MEK
c-Raf
ERK
p-MSK1
p-c-Raf
p-ERK
p-p90RSK
p-MEK
MEK
TrkB
Density Relative to β-actin
Control
miR-16
miR-Scr
BDNF
BDNF miR-16
BDNF miR-Scr
Treatments

Figure 24: MiR-16 and MiR-Scr Treated Cells Treated with BDNF or PBS were Analyzed for Expression of Multiple Members of the MAPK/ERK Pathway via Western Blot. Cells were treated with 25ng/mL BDNF or PBS for 24 hours prior to protein collection. Three separate blots were used, with β-actin used as a normalizing control for all of them. Densitometry was performed for all blots.

Next, the effect of miR-16 absence on the MAPK/ERK pathway was assessed using miRZIP-16 and miRZIP-Scr in combination with PBS or BDNF treatment. These effects were less obvious on this blot, likely due to redundant regulation of the pathway by other miRNAs. However, in the MEK blot, there does appear to be no difference between miRZIP-16 and miRZIP-Scr treated wells, perhaps indicating that the decrease in expression caused by miR-16 has been prevented by miRZIP-16 (Figure 25). Interestingly, there does appear to be a decrease in MEK level upon addition with the BDNF in combination with the miRZIPs. Moving on to p-MEK, there is a distinct difference compared to the miR-16 treated western blot, in that p-MEK decreases with BDNF addition in combination with miRZIP-16. This is interesting, as increased miR-16 levels in the previous blot (Figure 24) showed increased phosphorylation of MEK in combination with BDNF. There is also an increase in p-p90RSK with BDNF + miRZIP-16 treatment which is opposite to the decrease in phosphorylation that is seen with BDNF + miR16 treatment in the previous figure. The protein levels of TrkB are also opposite of those seen in Figure 24, with miRZIP-16 eliciting high expression of TrkB with PBS and that expression subsequently dropping with addition of BDNF + miRZIP-16.

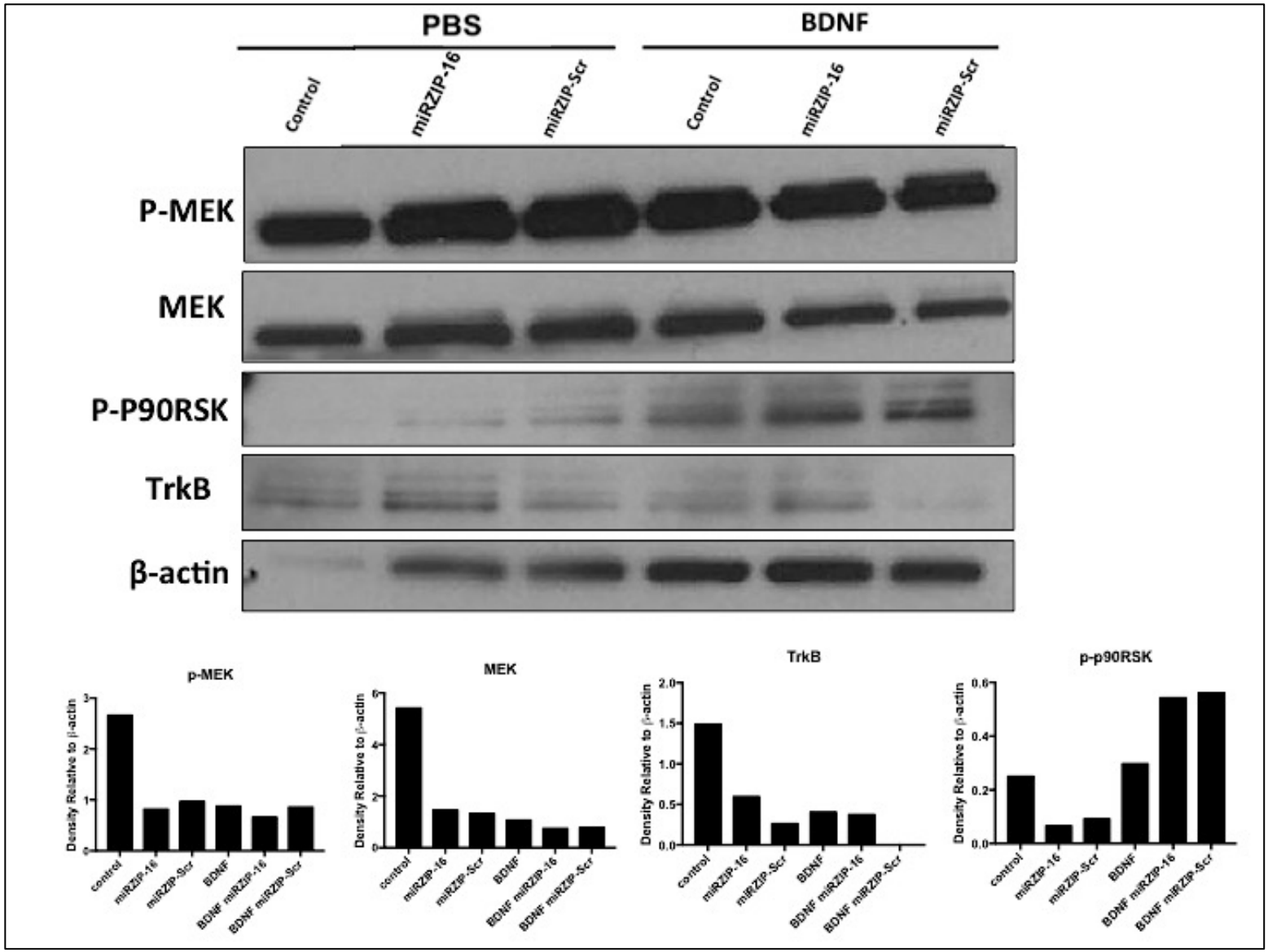
PBS
BDNF
Control
miRZIP-16
miRZIP-Scr
Control
miRZIP-16
miRZIP-Scr
P-MEK
MEK
P-P90RSK
TrkB
β-actin
p-MEK
MEK
TrkB
p-p90RSK
Density Relative to β-actin
control
miRZIP-16
miRZIP-Scr
BDNF
BDNF miRZIP-16
BDNF miRZIP-Scr

Figure 25: MiRZIP-16 and MiRZIP-Scr Treated Cells with PBS or BDNF treatment were Analyzed for Changes in MAPK/ERK Pathway Protein Levels. Cells were treated with 25ng/mL BDNF or PBS for 24 hours prior to protein collection. β-actin was used as a normalizing control. Densitometry was performed for all wells.

Changes in miR-16 expression were assessed after BDNF treatment to ensure that there were no aberrant changes in expression unrelated to the pseudoviral edition. Realtime PCR was used to assess these levels, relative to U6 at both 30 minutes and 24 hours post BDNF addition. There is a trend toward miR-16 being decreased in BDNF treated cells vs. controls, but it is not significant (Figure 26).

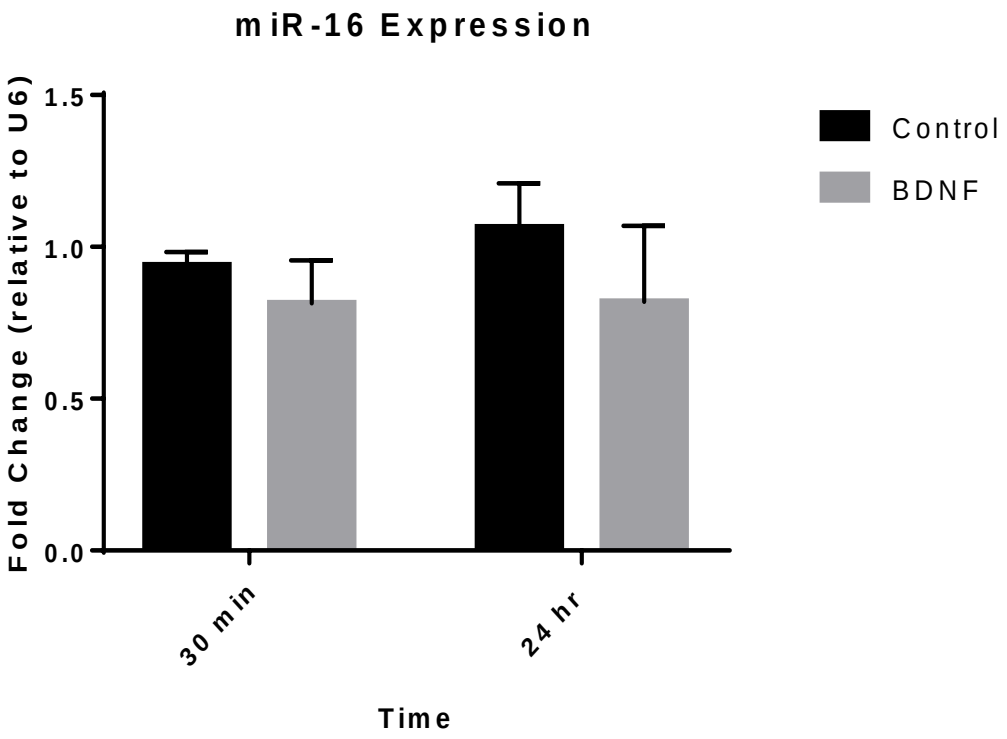
miR-16 Expression
Fold Change (relative to U6)
1.5
1.0
0.5
0.0
30 min
24 hr
Time
Control
BDNF

Figure 26: Fold Change in MiR-16 Expression Relative to U6 upon Treatment with BDNF. Cells were treated with 25ng/mL BDNF or PBS for 24 hours prior to protein collection. N = 3, t-tests revealed no significant difference at any time point between control and BDNF treated cells.

4.6 The Effects of miR-16 Altered Expression on Neuronal Morphology

It is important to look at neuronal morphology, as the ability of neurons to transmit and receive information is directly dependent on their dendritic and axonal morphology (Langhammer et al. 2010). Neuronal morphology is a complex subject, with multiple parameters that are important to look at to get a true picture of neuronal health. Traditionally, these parameters are assayed individually, necessitating hours of manpower with a high probability of human error and bias. For this reason, the development of automated processes to determine these parameters has occurred in order to streamline the process.

SynD is the result of these endeavors; the software automatically analyzes dendrite and synapse characteristics in immunofluorescence images with minimal user input. This program is superior to others in that it is specific for neurons, and automatically can detect soma, dendrites and synapses (Figure 27). Synapse number can be detected using synapse specific antibodies such as PSD95. This program allows detection of dendritic length, synapse number, soma area and dendritic branching via Sholl analysis.

Sholl analysis is an important method to quantify neuronal morphology. This method involves the drawing of concentric circles of increasing radius outward from the geometric center of the soma to the end of the longest neurite. The number of neurites that intersect each circle is then counted, and the complexity of dendritic arborization can be determined.

These experiments endevour to increase understanding of the function of miR-16 in neuronal morphology and dendritic remodeling. Cells were treated with the lentiviral

vectors at 8 DIV and were subsequently fixed and immunostained for MAP2 from 4 days to 28 days post viral inoculation. The cells were treated at 8 DIV to assess the effect of manipulation of miR-16 expression on neurite outgrowth and synapse formation over time, as these characteristics typically begin to be established by 12 DIV (van Spronsen et al. 2013). Intricate single-cell analyses were performed on these cells, with measurements taken to determine neurite length, cell body area and number of branch-points via Sholl analysis.

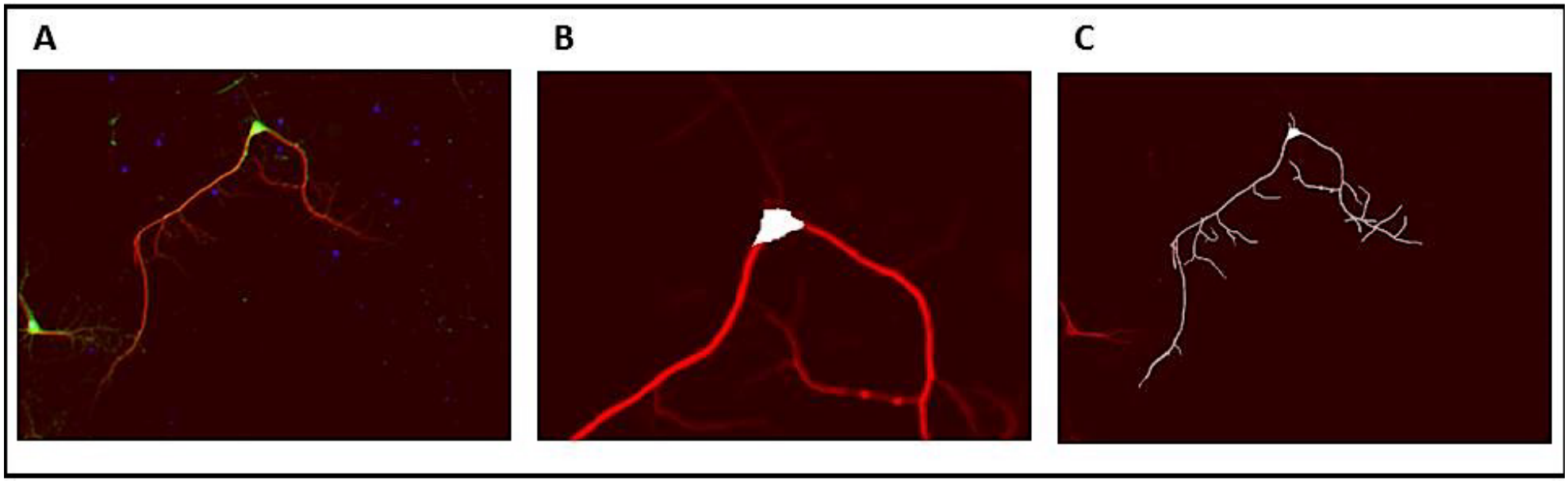
A
B
C

Figure 27: Images of a Neuron Analyzed with SynD Morphological Analysis Software. A: Original image. B: Soma detection. C: Neurite detection.

4.6.1 Effect of miR-16 on Neurite Length

Neurite length is an important indicator of neuronal fitness, with increased length indicating capacity to have more synaptic connections at greater distances, with greater networking capabilities (Brewer et al. 2008). The changes in neurite length overtime in culture for both miR-16 and miR-Scr treated cells are shown in Figure 28. At both 28 DIV and 36 DIV there was a significant decrease in dendritic length of miR-16 treated cells compared to miR-Scr treated cells. There were no significant differences found at any point between miR-Scr and control (no viral treatment) cells (not shown). Indicating that miR-16 treated cells have shorter neurite length on average compared to miR-Scr or control treated cells (not shown). There were significant differences in dendritic length throughout time for both the miR-16 treated and miR-Scr treated groups (p-value <0.0001 for both groups).

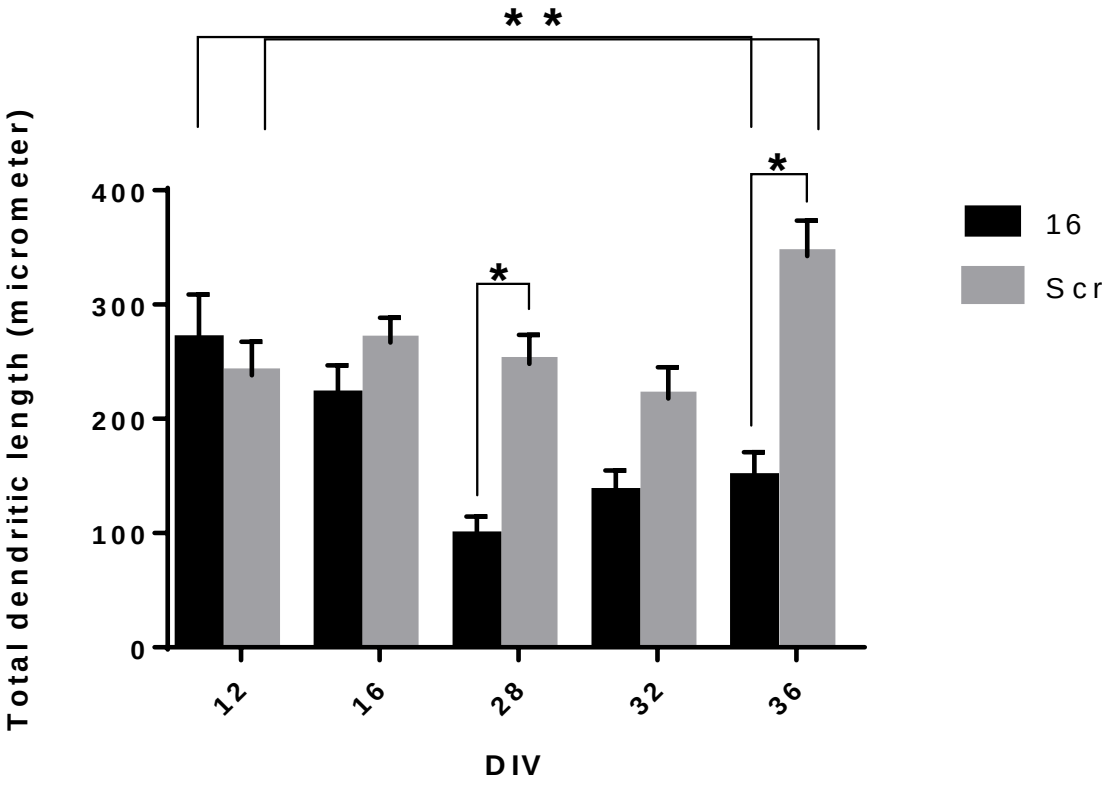
* *
*
*
Total dendritic length (micrometer)
400
300
200
100
0
12
16
28
32
36
DIV
16
Scr

Figure 28: Total Dendritic Length of Primary Hippocampal Cells Treated with Either MiR-16 or MiR-Scr at 8 DIV. Length was measured in micrometers. One sample t-tests were performed using the Holm-Sidak method to find significance. Each treatment was analyzed individually without assuming a constant standard deviation α=0.05. * indicates a p-value <0.005. ** indicates a p-value <0.0005. N = 2-3 representing individual coverslips with cells from different primary cell collections. 15 cells were analyzed per coverslip. Graph shows SEM.

4.6.2 Effect of miR-16 on Cell Body Size

Neuronal cell body size is reduced in the hippocampus of patients with AD and vascular dementia by between 10 and 20% compared to healthy controls (Gemmell et al. 2012). In agreement, studies have shown that cell body size has a positive correlation with cognitive function (Gemmell et al. 2012). The effect of miR-16 overexpression on cell body size was assessed in this thesis, as a change in the size may therefore indicate a change in neuronal health and viability. However, there were no significant changes in soma area found between the treatments throughout time (Figure 29). There were also no significant differences found at any point between miR-Scr and control (no viral treatment) cells (not shown). There were however, significant differences in soma area throughout time within miR-16 treated and miR-Scr treated groups (p-value <0.0001 for both groups). This suggests that the cells became less healthy overtime irrespective of miRNA treatment, simply due to aging within the culture.

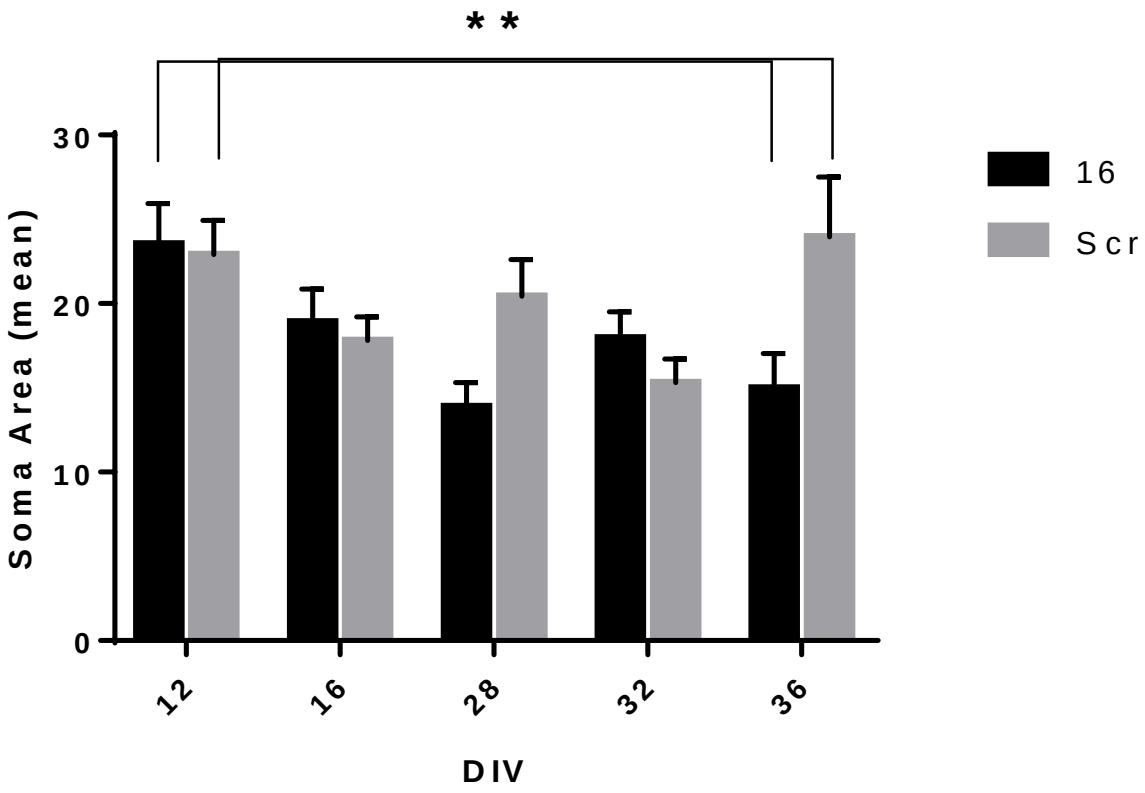
* *
30
20
10
0
Soma Area (mean)
12
16
28
32
36
DIV
16
Scr

Figure 29: Mean Soma Area of Primary Hippocampal Cells Treated with Either MiR-16 or MiR-Scr at DIV 8. One sample t-tests were performed using the Holm-Sidak method to find significance. Each treatment was analyzed individually without assuming a constant standard deviation $\alpha=0.05$. * indicates a p-value <0.005. ** indicates a p-value <0.0005. N= 2-3 representing individual coverslips with cells from different primary cell collections. 15 cells were analyzed per coverslip. Graph shows SEM.

4.6.3 Effect of miR-16 on Branching of Neurites

Sholl analysis has revealed that there were significant differences in the number of neurites/branch points intersected at 28 DIV (Figure 30). Distances between 14 and 34 mu from the soma had p-values <0.0005 while 36 mu had a p-value <0.008. No significant differences were found for any other day between miR-16 and miR-Scr treated primary hippocampal cells. It should also be noted that there was a progressive decrease in the maximum number of neurites intersected over time in both groups, likely indicating cellular aging, with miR-16 appearing to exacerbate the response. There were no significant differences found at any point between miR-Scr and control (no viral treatment) cells (not shown).

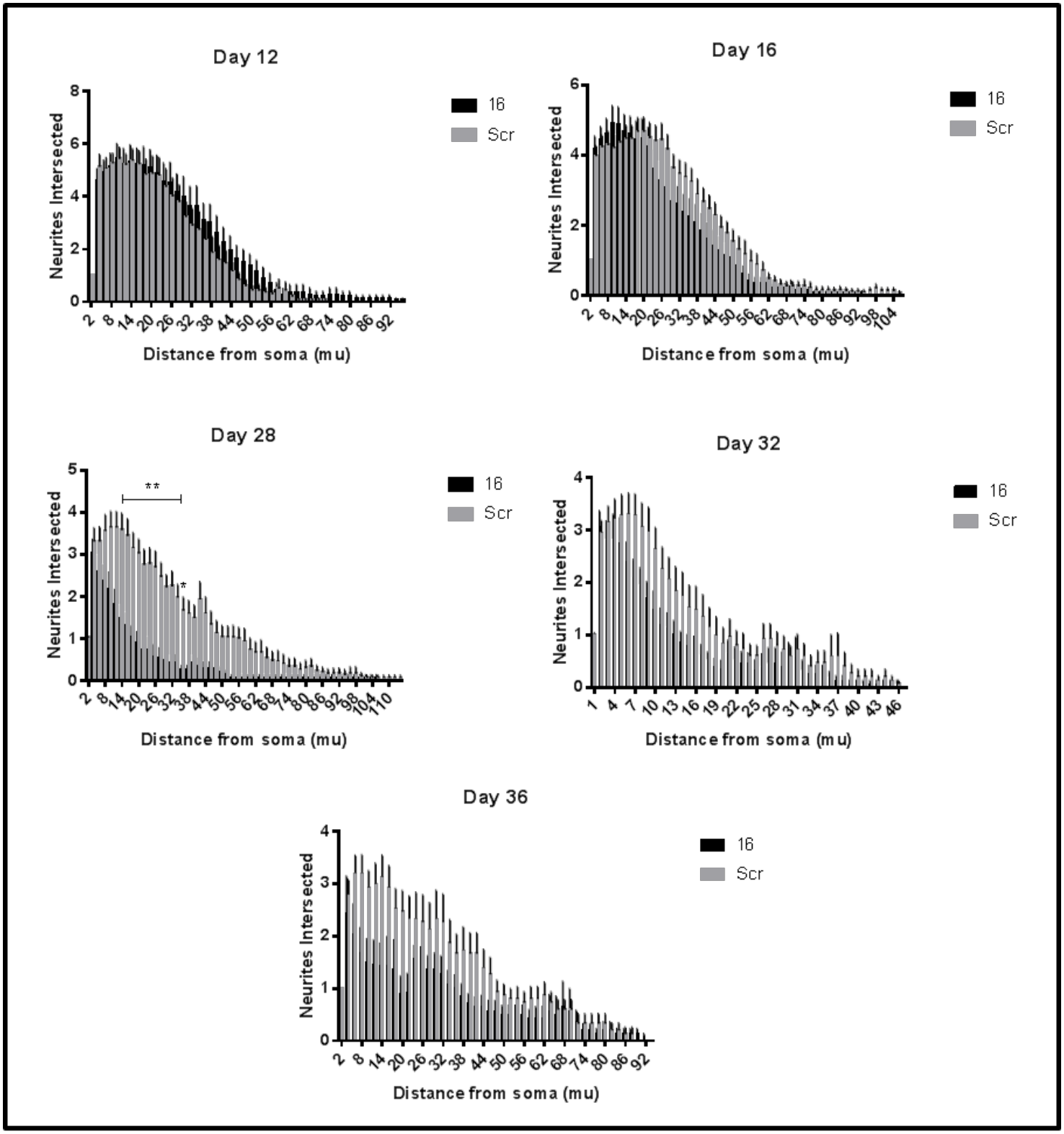
Day 12
Neurites Intersected
Distance from soma (mu)
16
Scr
Day 16
Neurites Intersected
Distance from soma (mu)
16
Scr
Day 28
**
*
Neurites Intersected
Distance from soma (mu)
16
Scr
Day 32
Neurites Intersected
Distance from soma (mu)
16
Scr
Day 36
Neurites Intersected
Distance from soma (mu)
16
Scr

Figure 30: Sholl Analysis of Primary Hippocampal Neurons Treated with Either MiR-16 or MiR-Scr at DIV 8. One sample t-tests were performed using the Holm-Sidak method to find significance. Each treatment was analyzed individually without assuming a constant standard deviation $\alpha=0.05$. * indicates a p-value <0.005. ** indicates a p-value <0.0005. N= 2-3 representing individual coverslips with cells from different primary cell collections. 15 cells were analyzed per coverslip. Graphs show SEM.

4.6.4 Effect of miR-16 on Dendritic Restructuring

Alpha-tubulin is an important molecule involved in dendritic restructuring (Kollins et al. 2009). In order to assess the impact of miR-16 overexpression on this process western blots were performed to determine changes in α-tubulin level (Figure 31). MiR-16 did not have any substantial effect on α-tubulin levels in unstimulated cells. However, BDNF significantly increased α-tubulin protein levels in primary hippocampal cells. Furthermore, in BDNF stimulated cells with miR-16, α-tubulin was reduced compared to BDNF treatment alone. This supports data collected in previous sections that suggested a negative effect by miR-16 on dendritic remodeling and outgrowth. In agreement with these findings, TargetScan revealed that miR-16 has a binding site in the 3'UTR of TUBA1A (not shown), the gene encoding α1a-tubulin, the form of α-tubulin highly expressed in post-mitotic neurons (Yokoi et al. 2015). Interestingly, this was the only subtype of either α- or β-tubulin that was predicted by TargetScan to be targeted by miR-16, however it was not present in the microarray data.

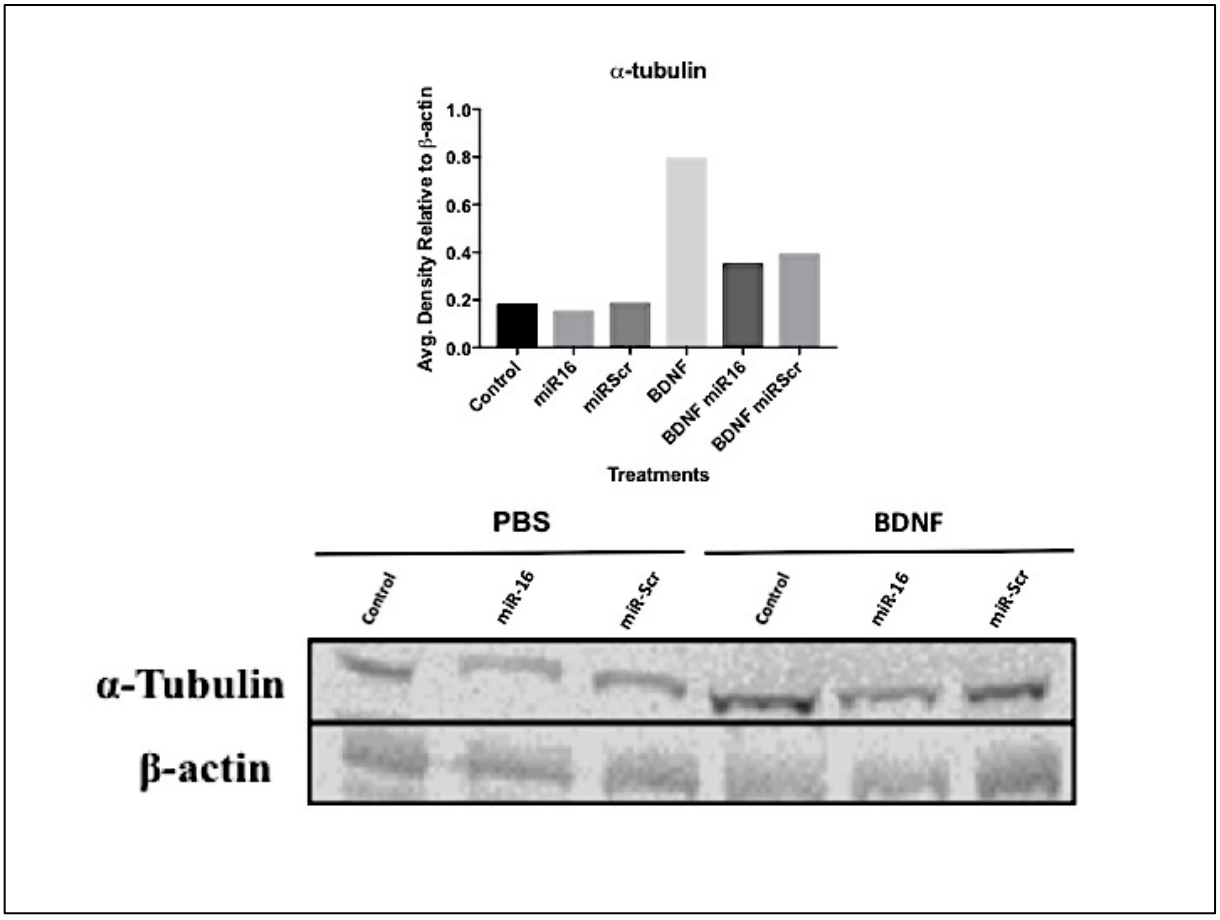
α-tubulin
Avg. Density Relative to β-actin
1.0
0.8
0.6
0.4
0.2
0.0
Control
miR16
miRScr
BDNF
BDNF miR16
BDNF miRScr
Treatments
PBS
BDNF
Control
miR-16
miR-Scr
Control
miR-16
miR-Scr
α-Tubulin
β-actin

Figure 31: Changes in α-tubulin Levels After BDNF addition in MiR-16 and MiR-Scr Treated Cultures. Cells were treated with 25ng/mL BDNF or PBS for 24 hours prior to protein collection. Densitometry was performed relative to β-actin.

4.6.5 Effects of miR-16 expression on Neurodegeneration

A simple way to assess neurodegeneration is by looking at a natural form of neurodegeneration, cell death due to aging. This can be assessed in a culture dish by counting the number of cells/well over time. In this experiment, the aim was to determine if miR-16 had an effect on the life of the culture, by either increasing or decreasing cell viability over time. Of particular interest was whether the decrease in the maximal number of neurites intersected overtime found in Section 4.6.3 was indeed due to an increased cellular aging (and presumably earlier death) of the miR-16 treated cells compared to miR-Scr. The results of this study indicated that although there was a significant change in cell number over time, indicating an increase in cell death, there was no significant change between treatments at any time point (Figure 32). However, there was a trend at Day 36 towards an increased number of viable neurons in miR-16 cultures vs. miR-Scr cultures, which could be suggestive of neuroprotection. Regardless, as assessed in this manner, miR-16 appears to have no significant effect on the life of hippocampal neurons in culture ie) it is not neuroprotective, nor promoting neurodegeneration. Further analysis is required to assess the putative neuroprotective property of miR-16 further.

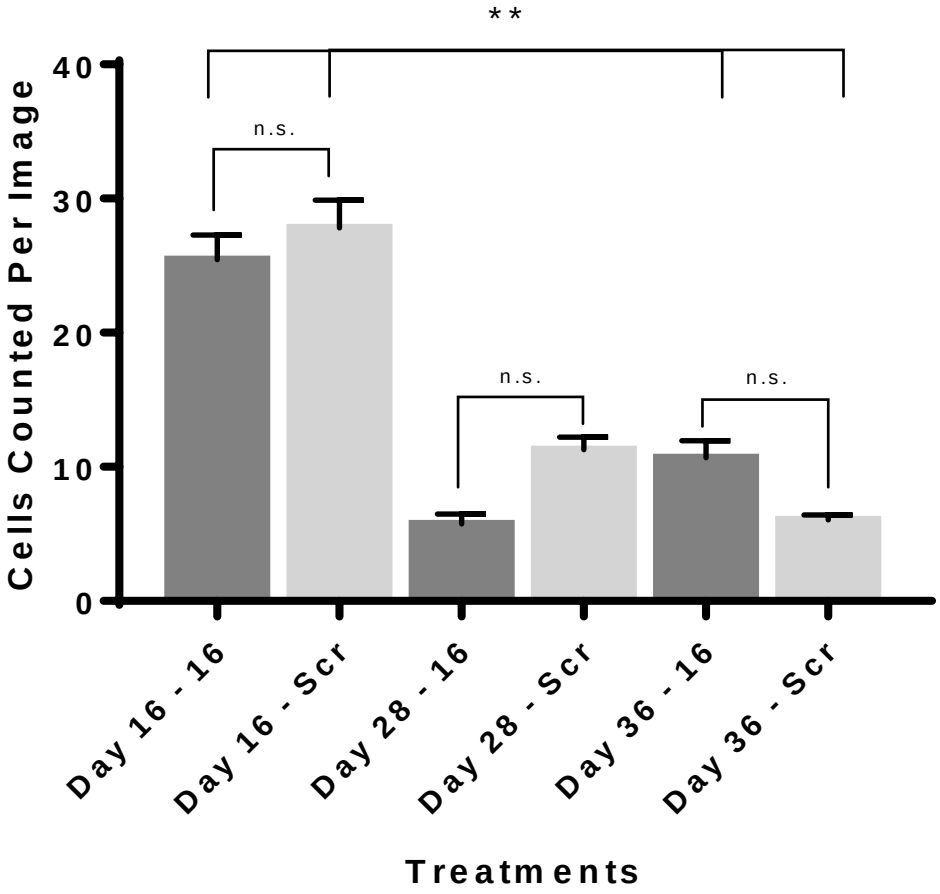
**
n.s.
n.s.
n.s.
40
30
20
10
0
Cells Counted Per Image
Day 16 - 16
Day 16 - Scr
Day 28 - 16
Day 28 - Scr
Day 36 - 16
Day 36 - Scr
Treatments

Figure 32: The Effect of MiR-16 on Neurodegeneration Due to Normal Culture Stress Over Time. Hippocampal primary cells were treated at 8 DIV with either miR-16 or miR-Scr lentivector and cells were fixed at the indicated time points. Cells were counted using ImageJ Cell Counter plugin using images taken at 10x magnification from Scanner files using Panoramic Viewer. A 2way ANOVA using Tukey's multiple comparisons test was performed with $\alpha = 0.05$. n.s.= not significant. **= p-value <0.0001. Data is plotted as SEM of 3 biological replicates.

Chapter 5: Discussion

5.1 Importance/Relevance of Study to Human Health

With the average life expectancy increasing, the prevalence of dementia is expected to increase as well. However, some studies have shown conflicting results, with age-specific incidence (ie. risk of developing dementia at any particular age) declining in high-income countries (Prince et al. 2016; Satizabal et al. 2016). This is thought to be due to an increase in proper treatment of cardiovascular conditions (and consequently an increase in overall cardiovascular health) as well as increased education, as there was a significant decrease in dementia risk found in people with a high school diploma compared to those without (Satizabal et al. 2016). However, this may not be indicative of global trends as the study was primarily people of European ancestry (Satizabal et al. 2016). For instance, there is an increasing prevalence of dementia in East Asia, correlating with worsening cardiovascular risks (Prince et al. 2016). Other studies have been unable to find conclusive evidence suggesting that dementia risk doesn't increase with age (Prince et al. 2016). Regardless of which finding is considered, trends can change very quickly and such multifaceted diseases may have factors that haven't been taken into account in these studies, making the risk of dementia difficult to predict (Satizabal et al. 2016).

Additionally, even with decreasing incidences there can still be increasing prevalence of the disease as the population of at-risk people is growing (Satizabal et al. 2016). Prevalence depends on incidence and duration of illness. It is a measure of the proportion of the population affected at one time, so with a larger at-risk population comes an increased prevalence (Prince et al. 2016). The current statistics indicate that by the year

2050, 13.8 million Americans will have AD with a new case expected to develop ever 33 seconds (Alzheimers Association 2015). Of note, the estimated payments for people with dementia in hospice, health-care or long-term care aged more than 65 years old is $236 billion US dollars (Alzheimers Association 2015). Therefore, dementia is an important issue both clinically and economically and understanding these illnesses is key to preventing and treating them.

Neurodegeneration is a key component of dementias as well as numerous related neurodegenerative diseases. This thesis aimed to assist in increasing the understanding of these diseases by shedding some light on the molecular aspect of neurodegeneration, specifically by elucidating the function of one particular disease related miRNA, miR-16-5p, in neurons. Studies of this nature are important to further our knowledge of disease processes. Information on tissue-specific miRNA function can be directly used to better human health by creating pharmaceuticals such as miRNA mimics or anti-miRs to change the disease-state gene expression profile of the cells to a healthy cell profile. In addition, advances have been made in delivering these therapies specifically to cells of interest in order to facilitate tissue-specific expression. Additionally, cell-type specific promoters can facilitate tissue-specific therapeutic expression, targeting the miRNA-based therapeutic to the region of interest. This substantially minimizes the potential for off-target effects, which are the greatest caveat of miRNA-based therapeutics. There are also a number of delivery methods that have the potential to enable miRNA delivery to the brain, bypassing the blood brain barrier (Campbell & Booth 2015). Overall, the potential for miRNA-based therapeutics is high and investigations like those conducted in this thesis are extremely relevant to the future of medicine.

Overall, the results of this study can be summarized as follows:

1 MiR-16 directly targets many mRNA involved in cellular remodeling including components of the MAPK/ERK pathway

2 MiR-16 overexpression results in a downregulation of a number of components of the MAPK/ERK pathway at the protein level upon stimulation with BDNF

3 MiR-16 overexpression results in decreased length of neurites and decreased arborization

These findings suggest that miR-16 plays an important role in regulating the MAPK/ERK pathway in hippocampal neurons, with inhibition of this pathway by miR-16 likely leading to decreased neuritic growth. This may in fact be a neuroprotective response, as decreasing neurite outgrowth may allow the neuron to save energy and resources to promote survival. The finite details of the study will be discussed in the following sections.

5.2 Manipulating miR-16 Expression in a Primary Culture System

In regards to the hippocampal cell culture, at all time points tested the cultures were more than 70% neuronal. This indicates that these cultures were a suitable model of a hippocampal system. Additionally, this was an effective model to manipulate miR-16 expression in as baseline miR-16 expression was accurately defined within the culture. In addition, the fact that miR-16 changed so drastically in the prion mouse model but very little in the primary hippocampal neurons suggests that this finding during prion disease is likely extremely relevant.

The use of a pseudo-lentiviral vector to manipulate miR-16 expression within the primary hippocampal cells was advantageous as the pseudo-lentivirus directly integrates the miR-16 coding region into the neuronal genome, allowing expression of the miRNA through the normal miRNA-processing pathway. For this reason, there is strong support that changes in gene and protein expression determined in this thesis are due to miR-16 overexpression and are not simply an artifact of extreme overexpression disturbing normal cellular processes.

For all pseudo-lentiviral vectors used in this study, 4μL of virus or 20μL (the same equivalent amount of virus/cell number) was used to transduce cells. This amount of virus only resulted in ~60% transduction (Figure 8). However, the reason that virus that wasn't 100% efficient was used was so that GFP-expressing cells could be visually separated from one another for single-cell analysis (Koshimizu et al. 2013). In addition, other publications have verified that the use of 60% transduction is sufficiently

efficacious (Royo et al. 2006; Dehay et al. 2012). However, use of lentivirus in this way does not necessarily result in high expression of the lentivirally-encoded transcript. For example, one study found that correlations between precursor transcipts for miRNA and the mature miRNA product were not strong, ie) it doesn't matter how much precursor you have expressed, you won't necessarily get more product (Wang et al. 2014). For this reason, the miR-16 expression levels were analyzed as described in Section 4.2.3. The results indicated that 4μL of miR-16 resulted in approximately 5-fold upregulation of miR-16 expression and 4μL of miRZIP-16 resulted in decreased expression of miR-16 to approximately 0.7-fold relative to baseline expression. This indicated that the lentiviral vectors were sufficiently able to change the expression of miR-16 within their respective cultures.

Sequencing revealed that miR-Scr & miRZIP-Scr encoded plant miRNA. This was important to note, as a BLAST search revealed that there were no binding sites for either miRNA within the murine genome, indicating that there should be no off-target effects in the cell culture model. However, given that miRNAs bind by incomplete base pairings it is still possible that there may be a physiological effect of overexpression of the control miRNA. There appear to be some anomalous findings in regards to miR-Scr in the western blots in Figures 24 & 25 with protein levels of investigated targets often being lower in the miR-Scr treated cells than the miR-16 treated cells, with both treatments resulting in much lower protein level than the untreated cells. In future studies, it may be beneficial to use an empty vector rather than miR-Scr as a control.

5.3 IPA-predicted mRNA Targets of miR-16

It should be noted that genes and pathways implicated in cancer were not enriched in the IPA output from the microarray data as had been notable in many other published studies on miR-16-5p. This is likely indicative or the use of primary hippocampal neurons, which enables the study of cell-type specific gene regulation. This is noteworthy, as it indicates that miR-16 has a clearly defined role in neuronal cells that is distinct from its role in dividing cells. In other words, there is an extreme difference in target profile between cell types. This has been shown in other studies that manipulated miR-16 in neuronal cells as well (Parsi et al. 2015). For this reason, we did not investigate changes in miR-15a levels in our study, because although there is strong correlation between miR-15a expression and miR-16 expression in cancer there has been no such information in neurodegenerative disease. Additionally, this finding is therapeutically relevant as it suggests that manipulating miR-16 expression in the brain would not increase the risk of developing cancer, as important cancer-related targets of miR-16 (Bcl-2, Mc11, Ccnd1 and Wnt3a) are not highly regulated by miR-16 in the brain (Parsi et al. 2015). This is likely a result of the fact that abundance of target transcripts varies greatly between tissues, simply changing the target profile due to availability.

Overall, a number of interesting findings came from the IPA microarray analysis. For instance, miR-16 was predicted to regulate targets associated with neurological disease and psychological disorders (181 and 95 targets each, respectively) (Table 5). This is extremely relevant as it is well documented that miR-16 is both implicated in AD (neurological disease) and depression (psychological disorder) (Liu et al. 2012; Song et

al. 2015). Also of interest, the top molecular and cellular functions that miR-16 inhibits are cellular development (182 genes), cellular growth and proliferation (245 genes) and cellular morphology (170 genes) (Table 6). These findings were directly in line with the results of the morphological analysis of neuronal primary cells treated with miR-16, as miR-16 treatment resulted in decreased neurite length (Figure 28) and branching (Figure 30). Finally, IPA predicted that miR-16 inhibits tissue development and is generally pro-survival (Table 7). Together these findings are supportive of the suggestion that miR-16 is neuroprotective.

Growth of neurites is associated with activation of mitogen-activated protein kinase (MAPK) and extracellular signal-regulated kinases -1 and -2 (ERK1 and ERK2) (MAPK/ERK pathway) (Thomas & Huganir 2004; Stokin et al. 2005). Components of the MAPK/ERK pathway are highly stabilized within hippocampal dendrites (Wu, Deisseroth, and Tsien 2001). This pathway is important for cellular proliferation and differentiation, which are essential for synaptic plasticity (Thomas & Huganir 2004). The MAPK/ERK pathway, was revealed to be regulated by miR-16 via the microarray analysis. In particular miR-16 was shown to target TrkB (9.879-fold), c-Raf (3.265-fold) and MAP2k1 (502.720- fold). New dendritic spines are created in hippocampal cultures following depolarization due to sustained ERK activation allowing for long-lasting structural alterations (Wu, Deisseroth, and Tsien 2001). The role of this pathway in neurons is highlighted in Figure 33.

Interestingly, stimulation of this receptor (TrkB) by BDNF has been shown to result in increased nitric oxide production and neurodegeneration (Colombo et al. 2012). In

particular, NO production promoted by this pathway in astrocytes has been shown to cause morphological changes and death of surrounding neurons, which only becomes worse due to NO production within the neurons (Colombo et al. 2012). This suggests that miR-16 is downregulating TrkB expression in a neuroprotective function. Future studies should look at measuring NO production within this cell culture system upon stimulation with BDNF. It is thought that environmental factors can regulate BDNF expression in the hippocampus and that these factors likely work though miRNA (Bai et al. 2012). In TrkB mutant mice, CA1 LTP is reduced, and lack of TrkB in excitatory pyramidal neurons results in deficits in memory acquisition (Minichiello et al. 1999). Without stimulus, TrkB is mostly present in cytoplasmic vesicles (Meyer-Franke et al. 1998). Evidence suggests that decreased BDNF in hippocampus leads to decreased proliferation of neurons and consequently depression (Zhao et al. 2012).

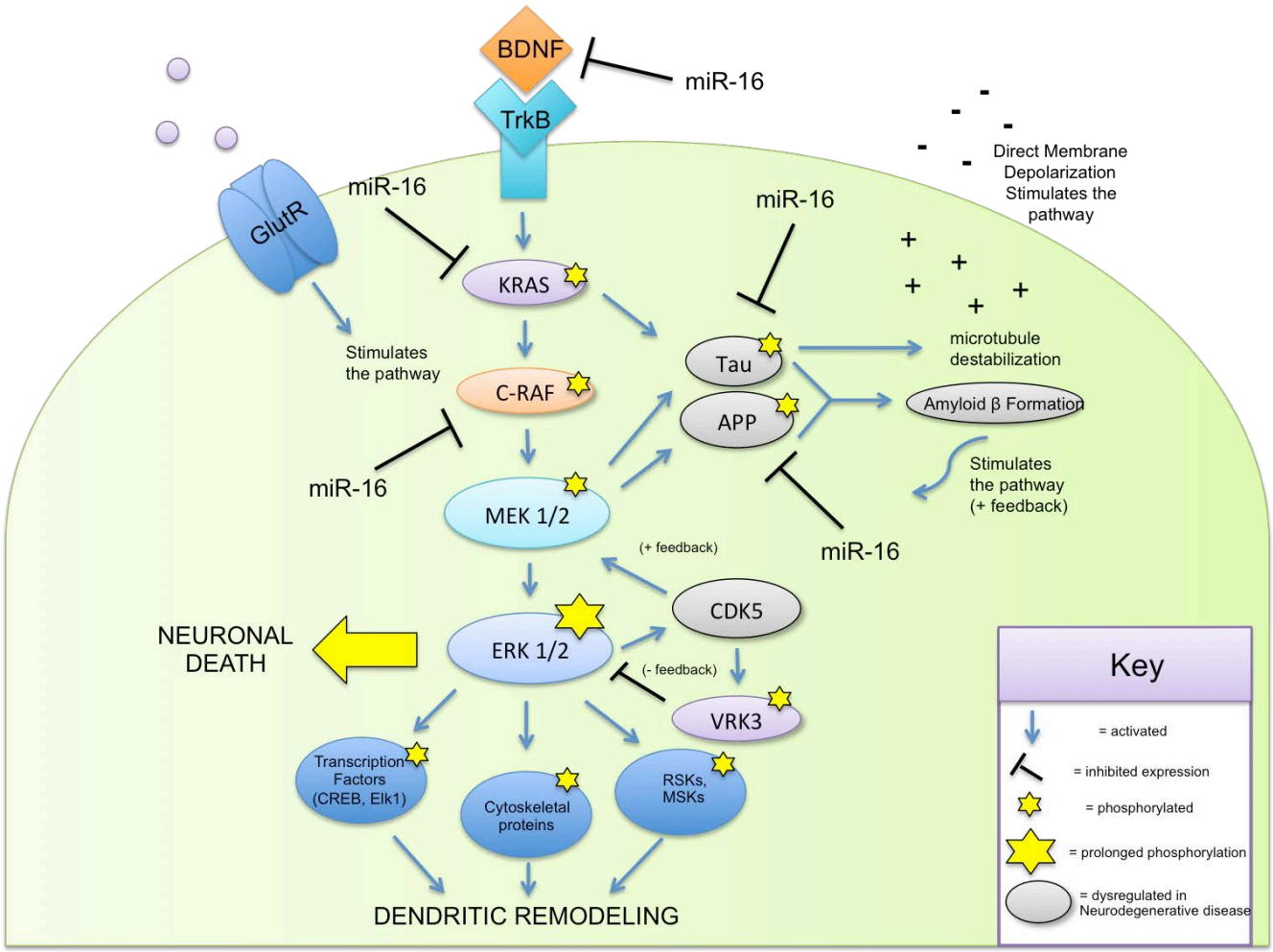
BDNF
miR-16
TrkB
Direct Membrane Depolarization Stimulates the pathway
GlutR
miR-16
miR-16
KRAS
Stimulates the pathway
C-RAF
Tau
APP
microtubule destabilization
Amyloid β Formation
Stimulates the pathway (+ feedback)
miR-16
miR-16
MEK 1/2
(+ feedback)
CDK5
NEURONAL DEATH
ERK 1/2
(- feedback)
VRK3
Transcription Factors (CREB, Elk1)
Cytoskeletal proteins
RSKs, MSKs
DENDRITIC REMODELING
Key
= activated
= inhibited expression
= phosphorylated
= prolonged phosphorylation
= dysregulated in Neurodegenerative disease

Figure 33: The Interwoven Role of the MAPK/ERK pathway in Dendritic Remodeling and Neuronal Death.

Stimulus of TrkB with BDNF promotes an increase in Ras-GTP (active) over Ras-GDP (inactive) (Thomas and Huganir 2004). Ras-GTP activates the protein kinase Raf, which phosphorylates and activates MAPK/ERK kinase (MEK). MEK can then phosphorylate and activate the serine/threonine kinases ERK1 and ERK2 (p44 & p42 MAPK). ERK1 and ERK2 then target transcription factors, cytoskeletal proteins, regulatory enzymes and kinases such as ribosomal protein S6 kinases (RSKs) and RSK-related mitogen-&stress activated kinases (MSKs) within the cytoplasm and the nucleus (Thomas & Huganir 2004; Huang and Reichardt 2001). Substrates probably reside throughout the neuron as p-ERK immunoreactivity develops rapidly throughout dendritic and somatic regions after LTP-inducing stimuli with nuclear translocation occurring, suggesting a role in activity dependent manipulation of gene expression (Davis et al. 2000). Transcription factors are direct targets of ERK, including Elk1 and cAMP regulated enhancer binding protein (CREB) which are phosphorylated following LTP (Davis et al. 2000; Stokin et al. 2005). CREB regulates pro-survival genes in the neuron, knockout in mice results in neurodegeneration in the hippocampus (Mantamadiotis et al. 2002). Additionally, CREB1 was predicted to be a target of miR-16 in this array (Table 4), and previous studies have confirmed that BDNF is a target of miR-16 (Sun et al. 2013). Altogether this indicates that miR-16 is inhibiting the MAPK/ERK pathway on multiple fronts.

ERKs, upstream regulators and some targets are expressed and increased in mature neurons, contrary to their originally thought role of being involved only in proliferation and differentiation (Thomas & Huganir 2004). In addition to BDNF, ERKs can be activated with glutamate via excitatory glutamatergic receptors (important for learning

and memory) in pathways that are either Raf1-dependent or Raf1-independent (Kurino et al. 1995). They can also be activated via direct membrane depolarization in a Ras-dependent manner (Rosen et al. 1994).

The MAPK/ERK pathway has been shown to be important in learning, synaptic plasticity and long-term potentiation in the hippocampus (Hallock & Thomas 2012). ERK is important for long-term memory in spatial learning and fear conditioning (Thomas & Huganir 2004). Interestingly, MAPK has been shown to increase phosphorylation of APP and tau resulting in increased Aβ production and formation of neurofibrillary tangles (Rapoport & Ferreira 2000). Additionally, Aβ has been shown to stimulate the MAPK pathway in neurons, and selective inhibition of this pathway has protected neurons from Aβ induced neurite degeneration (Rapoport & Ferreira 2000).

ERK1/2 usually functions in a pro-survival role, but when it's activated for a prolonged time via oxidative stress it results in neuronal death (Stanciu & Defranco 2002). This occurs via negative feedback inhibition, as stress activates ERK, which activates cyclin-dependent kinase 5 (CDK5) enabling it to phosphorylate vaccinia-related kinase 3 (VRK3) which decreases ERK activation (Song et al. 2016). CDK5 also directly targets MEK1 (Song et al. 2016). Changes and dysregulation of CDK5 have been implicated in the pathogenesis of AD and ALS (Dhavan & Tsai 2001). CDK5 is important for cytoskeletal changes in the neurons with major influences on axonal guidance and synaptic function (Dhavan & Tsai 2001).

Inhibition of MAPK pathway has been shown to protect neurons in culture from oxidative stress induced cell death (Satoh et al. 2000). Inhibition of the ERK network has

been accomplished previously in models of neurodegenerative disease resulting in alleviation of clinical signs of Parkinson's-like disease in mice (Tan et al. 2013). Interestingly, and contrary to other findings, MAPK/ERK pathway has been identified as a key downregulated pathway in AD via a Core bioinformatic analysis of the literature (Hallock & Thomas 2012). But it has been shown that there is increased phosphorylated ERK in brains of AD patients (Ferrer et al. 2001). The MEK/ERK pathway has been implicated in phosphorylation of tau via activation by Ras, which is also found to be activated in AD compared to controls (Ferrer et al. 2001). As well MAPK/ERK pathways, synaptic long-term potentiation and calcium signaling are all dysregulated during prion disease (Sorensen et al. 2008). In one study it was found that prion infection caused a hyperactivation of the MEK/ERK pathway in a scrapie-infected hypothalamic cell line (GT1-1) (Didonna & Legname 2010).

5.4 Western Blot Analysis of the MAPK/ERK Pathway

An interesting aspect of this project was the differences in protein expression of MAPK/ERK pathway components treated with miR-16 or miR-Scr (or the miRZIP equivalents) in combination with PBS or BDNF. Many members of the MAPK/ERK pathway did not have appreciable differences in expression between miR-16 and untreated cells when treated with PBS. Thus, cells were treated with BDNF to stimulate the pathway in order to see more potent changes at the protein level. However, a few prominent differences were noticed between miR-16 (or miRZIP-16) treated cells with PBS vs. BDNF. For instance, TrkB protein level was significantly reduced with miR-16 expression + PBS relative to control, which was anticipated based on the results of the array (Figure 24). However, when BDNF was applied in combination with miR-16, TrkB expression increased (Figure 24). MiRZIP-16 + PBS also showed increased TrkB relative to miRZIP-Scr + PBS, as expected. The results of these analyses suggest that TrkB is increased in expression by BDNF expression (likely because it is a specific receptor for BDNF), and that effect is not completely abolished by the addition of miR-16 to the culture. Additionally, miRZIP-Scr appeared to have a very inhibitory effect on TrkB expression, suggesting that TrkB may be deregulated by viral addition to the cell.

Due to findings such as these, it was important to ensure that BDNF addition was not decreasing the expression of miR-16 within the culture. Interestingly, 24 hours after BDNF addition there was no significant difference in the RNA levels of miR-16, but there was a trend towards decreased miR-16 expression (Figure 26). However, even with some potential decrease in miR-16 expression in the miR-16 overexpressing cells there

was still substantial decreases in MEK, ERK, c-Raf, p-MSK1 and p-p90RSK protein levels in the miR-16 + BDNF treated cells relative to BDNF alone or miR-Scr + BDNF (Figure 24).

Interestingly, there were increased levels of p-ERK, p-MEK and p-c-Raf with miR-16 addition (+PBS or BDNF) compared to control or miR-Scr. This was not expected, as it was anticipated that miR-16 would have a dampening role on activation of the pathway. However, this phosphorylation indicated that the pathway was still functional, and the decrease in expression of the corresponding unphosphorylated variants of these proteins indicates that the inhibition of protein synthesis due to miR-16 addition did occur. It is therefore speculated that the ability of this pathway to still be activated is due to the persistence of proteins that were synthesized before miR-16 addition. Perhaps western blots conducted at a later point post-lentiviral inoculation would reveal diminished activation of this pathway. Only one of these proteins was analyzed on a miRZIP-16/Scr western blot, MEK. Interestingly, miRZIP-16 + BDNF resulted in decreased MEK protein level as well as decreased p-MEK (Figure 25).

It should be kept in mind that cultures *in vitro* are not always able to perform as cells *in vivo* do, due to inherent differences in environment and presence of appropriates stressors (van Rooij, Purcell, and Levin 2012). It is also possible that the pathway would be better stimulated by other treatments as, ERKs can be activated with glutamate via excitatory glutamatergic receptors or direct membrane depolarization (Kurino et al. 1995; Rosen et al. 1994). Nonetheless, these studies focused on stimulation with BDNF as it was known that one target of miR-16 detected via the microarray was TrkB which is a receptor for

BDNF and because BDNF has been shown to stimulate the pathway in neuronal cultures previously (Ying et al. 2002). It would be interesting to try different treatments to assess the pathway response as well as to explore the use of an inhibitor of MEK such as PD98059 or U0126, in order to test that miR-16 has the same effect on cell phenotype as inhibition of the MEK/ERK pathway. Interestingly, it has been shown that exposure to inhibitors of MEK increase the growth of dendrites (Kim et al., 2004). This is the opposite of what is suggested by the results of this thesis and in fact, it has been purposed that the activation of this pathway could both positively and negatively affect axonal growth in certain situations (Kim et al., 2004).

It should be noted that this study was limited to examining the "classical" MAPK/ERK pathway. However, other variants of the pathway do exist, such as the parallel cascade that results in phosphorylation of p38 MAPK which regulates different forms of synaptic plasticity (Thomas & Huganir 2004). It is possible that miR-16 is dampening this pathway in order to promote preferential activation of other pathways implicated in neuronal survival. Further investigation into pathways involved in promoting neuronal survival should be investigated in the future.

5.5 The Impact of miR-16 on Neuronal Phenotype

Traditionally analysis of neuronal morphology was manually performed in a very labour intensive fashion. Automated neuronal analysis helps to cut down on human bias and time (Schmitz et al. 2011; Langhammer et al. 2010). Additionally, automation enables novice observers to conduct neuronal morphological analysis at an expert level (Schmitz et al. 2011).

In keeping with the knowledge that MAPK/ERK is activated when dendritic remodeling occurs, it is not surprising that there was decreased neuritic growth and remodeling in this experimental system. In particular there was significantly decreased neurite length in miR-16 treated cells vs. miR-Scr treated cells at 28 and 36 DIV (Figure 28). There was also a significantly decreased number of branch-points in miR-16 treated cells at 28 DIV vs. miR-Scr treated cells (Figure 30). Clearly, 28 DIV was a significant turning point for the effect of miR-16 on neuronal phenotype. However, at all times from 12 DIV onward in the Sholl analysis there was a trend of decreased number of intersected neurites in the miR-16 treated cells compared to miR-Scr. Also, there is a general trend towards a decreased number of intersections in both treatment groups with increasing DIV. It appears that miR-16 is thus decreasing the length and branching of the neurites, prematurely and exacerbating the effect of cellular aging. It is possible that this is a neuroprotective mechanism, to reduce energy usage and prolong cellular life. In order to address this possibility, the viability of the cells was assessed via an aging assay. The results of this endeavour however, did not show significantly prolonged neuronal survival with miR-16 treatment relative to miR-Scr. However, there was a trend towards miR-16

increasing neuronal survival at the final investigated time point. Therefore, in future studies it would be important to look at neuronal survival vs. untreated cells in culture. In addition, a TUNNEL assay should be performed for ultimate significance.

There was no significant difference in somal area between miR-16 or miR-Scr treated cells at any time point. There was however, a significant decrease in cell size over time, reflective of the aging cellular population. It is possible though, that changes due to treatment type could have been apparent if the three distinct subclasses of neurons within the hippocampus (pyramidal, bipolar and stellate) were analyzed individually (Mattson & Kater 1989). This is something that would be beneficial to explore in future experiments.

In regards to neuronal health, it is known that molecules such as CDK5 are important for stopping the MAPK/ERK pathway activation, which not only prevents neurite development, but also prevents the mechanisms of cell death from activating. It is hypothesized that miR-16 is working in this way, to prevent the overactivation of this pathway during the onset of neurodegenerative disease, to stave off neuronal death and thus the progression of the disease. It is in agreement with this hypothesis that CDK5 is not highly targeted by miR-16 within the microarray (only 1.259 fold upregulated) and no conserved binding sites were found in TargetScan (not shown). For this reason, it is suspected that miR-16 is working in tandem with CDK5 to disrupt MAPK/ERK signalling and prolong neuronal life. Future studies would be imperative to assess the regulation of CDK5 in this cell culture system, along with some “pro-neurite and axon outgrowth” genes such as CORONIN1b, RAB13 and GAP43, to confirm the morphological findings (Tedeschi et Di Giovanni 2009).

One of the cellular processes downregulated preclinically in a prion disease mouse model was cytoskeletal organization (Majer et al. 2012). A number of microtubule-associated proteins have been implicated in the onset of neurodegeneration, including tau, parkin and α-tubulin. Tau is a microtubule associated protein, that promotes microtubule assembly and stability (Dubey, Ratnakaran, and Koushika 2015). Tau is known to be phosphorylated at ~80 sites, and phosphorylation is important for tau's ability to bind microtubules and hyperphosphorylation causes detachment from microtubules which leads to formation of insoluble aggregates typical of AD (Hébert, Sergeant, and Buée 2012). Parkin is an E3 ubiquitin ligase that is implicated in PD. It binds to α- and β-tubulin heterodimers and stabilizes the microtubules (Dubey, Ratnakaran, and Koushika 2015). α-tubulin is a major component of microtubules. Deficiencies in α-tubulin in neurons lead to abnormal neuronal morphology and development (Yokoi et al. 2015).

Interestingly, miR-16 was shown to have an effect on the α-tubulin levels of cells treated with BDNF (Figure 31). It was predicted via TargetScan to target the most common gene encoding α-tubulin in neurons, TUBA1A, and that was the only transcript of either α- or β-tubulin that miR-16 targeted (not shown). Interestingly, tubulin deficiencies have been implicated in neurodegenerative disease in the past, in ALS (Smith et al. 2014). In addition, TargetScan identified that the key miRNA targeting TUBB2A and TUBB2B (two highly abundant forms of β-tubulin found in the brain) (Cushion et al. 2014) was miR-29a, a miRNA that has been highly implicated in dendritic spine development and neurodegenerative disease previously (Majer & Booth 2014). This indicates that the regulation of tubulin subtypes may be important to the progression of neurodegeneration.

Also worth noting, is that the protein levels in the APP/BCL-2 blot were probably subject to loading discrepancies that simply couldn't be seen due to the influence of miR-16 on α -tubulin (the loading control in that blot). This blot was performed before the effect of miR-16 on α –tubulin was discovered. Nonetheless, this blot was still able to show that miR-16 effectively decreases both APP and BCL-2 protein levels compared to miR-Scr treatment.

With the cumulative information in this thesis, it is clear that miR-16 targets members of the MAPK/ERK pathway, decreases neurite length and branching and decreases α-tubulin levels. BDNF stimulates the MAPK/ERK pathway, increases neurite length and branching and increases α-tubulin levels. When BDNF was added in conjunction with miR-16, there was a decrease in the activation of this pathway. It is also likely that the dendritic remodeling process is controlled through this pathway. For this reason, morphological analyses should be repeated with BDNF addition, which will likely result in a more substantial effect of miR-16 downregulating the dendritic remodeling process. Further research needs to be done to fully understand why regulating this process is advantageous to neuronal health and whether it is truly acting in a neuroprotective capacity.

5.6 Future Directions

A number of analyses could still be done to further verify the findings of this thesis. For instance, repeat western blots would be beneficial to solidify the findings. In addition, this study was done entirely *in vitro* and moving to an *in vivo* model system would be beneficial to further the biological relevance of our findings within the murine hippocampus. However, it is essential to perform studies of this nature in the *in vitro* setting first, as animal models are costly and it is inhumane to work directly in animals without knowing the implication of the agent on mortality. With this thesis implicating miR-16 overexpression with decreased dendritic growth and inhibition of the MAPK/ERK pathway, likely involved in a neuroprotective response, with no increase in neuronal death vs. Scr control, the logical next step is to move into a mouse model. Ultimately, targeted infection of the mouse hippocampus with miR-16 containing vector would be the goal, with co-expression of a fluorescent protein to monitor miR-16 expression within that region. This could be accomplished using the IVIS-SpectrumCt Pre-clinical In Vivo Imaging System. Subsequent studies on the effect of overexpressed miR-16 within the hippocampus on the progression of prion disease in the RML scrapie mouse model would ultimately allow understanding of the miR-16's role within the murine hippocampus in both healthy and prion-infected mice. In addition, histological sections, RNA and protein could be collected at time points of interest, to look at aggregation of PrP^{Sc}, presence of markers of neuronal survival, neuronal morphology and the regulation of the MAPK/ERK pathway throughout disease progression.

A couple of interesting points to note for future studies are as follows. First, studies on miRNA associated with synaptoneurosomes in prion-infected mice did not detect miR-16 dysregulation within these bodies preclinically or clinically during infection (Boese et al. 2016). This finding suggests that miR-16 is not as important for synaptic regulation as other miRNA and is not being transmitted to other cells to modulate gene expression. Also of significant note, miR-16 has often been used as a housekeeping gene or "steady state miRNA" in studies looking at changes in miRNA expression (Rinnerthaler et al. 2016). This is important to note as this may be inappropriate in cell types such as neuronal cells or cancer cells, as miR-16 fluctuations have been reported in many disease processes as reviewed in the Section 1.6. This brings up a potential caveat of therapeutic development, as although miR-16 may stave off neurodegeneration, it could potentially cause depression (Song et al. 2015).

In addition, it would be interesting to compare the data generated from the microarray in this study to that generated by Majer et al. in their study of the gene regulation during prion disease in the CA1 region of the hippocampus (Majer et al. 2012). Since miR-16-5p was only one of the numerous miRNA dysregulated in this study it is unlikely that there will be a highly similar profile between the two arrays, but it would be interesting to determine the potential magnitude of miR-16's role in prion-infected cells in this way.

Additionally, there were other pathways represented in the array that would be of interest to study further including mitochondrial dysfunction, synaptic long-term potentiation and amyloid processing (Outlined in Figures 17-19). Some of the established targets of miR-16 present within these pathways include α-synuclein, Aβ, APP, BACE2, BCL2 and

MAP2K1. Western blots to detect the presence of pathway-specific products would be beneficial to confirm the regulation of these processes by miR-16 in hippocampal neurons.

Finally, it is important to note that studies of this nature produce miRNA candidates as targets for neurodegenerative disease therapeutics, but the ability of miRNAs to target specific genes in specific tissues is quite variable. A large amount of research must go into understanding the intricacies of miRNA functions. For this reason, the study of miRNA in disease is challenging but allows for considerable knowledge to be gained for therapeutic discovery.

Chapter 6: Conclusion

The hypothesis of this thesis was that hippocampal miR-16-5p targets mRNA involved in the dendritic remodeling and morphological changes that are central to the early neurodegeneration in prion disease. The outcome of this study supports the hypothesis, implicating miR-16-5p as a direct regulator of the MAPK/ERK pathway and an inhibitor of neuronal growth and differentiation in a pro-survival capacity. Therefore, miR-16 represents a valuable target for therapeutic development for neurodegenerative diseases including prion disease.

References

Absalon, S., D. M. Kochanek, V. Raghavan, and A. M. Krichevsky. 2013. “MiR-26b, Upregulated in Alzheimer’s Disease, Activates Cell Cycle Entry, Tau-Phosphorylation, and Apoptosis in Postmitotic Neurons.” *Journal of Neuroscience* 33 (37): 14645–59. doi:10.1523/JNEUROSCI.1327-13.2013.

Aguzzi, Adriano, and Lawrence Rajendran. 2009. “The Transcellular Spread of Cytosolic Amyloids, Prions, and Prionoids.” *Neuron* 64 (6). Elsevier Inc.: 783–90. doi:10.1016/j.neuron.2009.12.016.

Akram, Afia, James Schmeidler, Pavel Katsel, Patrick R Hof, and Vahram Haroutunian. 2012. “Association of ApoE and LRP mRNA Levels with Dementia and AD Neuropathology.” *Neurobiology of Aging* 33 (3): 1–14. doi:10.1016/j.neurobiolaging.2011.04.010.Association.

Alzheimers Association, Alzheimer. 2015. “2015 Alzheimer’s Disease Facts and Figures.” *Alzheimer’s and Dementia* 11 (3). Elsevier Inc.: 332–84. doi:10.1016/j.jalz.2015.02.003.

Arendt, T., H. G. Zvegintseva, and T. A. Leontovich. 1986. “Dendritic Changes in the Basal Nucleus of Meynert and in the Diagonal Band Nucleus in Alzheimer’s Disease - A Quantitative Golgi Investigation.” *Neuroscience* 19 (4): 1265–78. doi:10.1016/0306-4522(86)90141-7.

Bai, Mei, Xiongzhao Zhu, Yi Zhang, Sheng Zhang, Li Zhang, Liang Xue, Jinyao Yi, Shuqiao Yao, and Xiuwu Zhang. 2012. “Abnormal Hippocampal BDNF and miR-16 Expression Is Associated with Depression-Like Behaviors Induced by Stress during Early Life.” *PLoS ONE* 7 (10): 1–8. doi:10.1371/journal.pone.0046921.

Baker, R. E., P. A. Dijkhuizen, J. Van Pelt, and J. Verhaagen. 1998. “Growth of Pyramidal, but Not Non-Pyramidal, Dendrites in Long-Term Organotypic Explants of Neonatal Rat Neocortex Chronically Exposed to Neurotrophin-3.” *European Journal of Neuroscience* 10 (3): 1037–44. doi:10.1046/j.1460-9568.1998.00118.x.

Bandi, Nora, Samuel Zbinden, Mathias Gugger, Marlene Arnold, Verena Kocher, Lara Hasan, Andreas Kappeler, Thomas Brunner, and Erik Vassella. 2009. “miR-15a and miR-16 Are Implicated in Cell Cycle Regulation in a Rb-Dependent Manner and Are Frequently Deleted or down-Regulated in Non-Small Cell Lung Cancer.” *Cancer Research* 69 (13): 5553–59. doi:10.1158/0008-5472.CAN-08-4277.

Baudry, Anne, Sophie Mouillet-Richard, Benoît Schneider, Jean-Marie Launay, and Odile Kellermann. 2010. “MiR-16 Targets the Serotonin Transporter: A New Facet for Adaptive Responses to Antidepressants.” *Science* 329: 1537–41.

Beaudoin, Gerard M J, Seung-Hye Lee, Dipika Singh, Yang Yuan, Yu-Gie Ng, Louis F Reichardt, and Jyothi Arikkath. 2012. “Culturing Pyramidal Neurons from the Early Postnatal Mouse Hippocampus and Cortex.” *Nature Protocols* 7 (9). Nature Publishing Group: 1741–54. doi:10.1038/nprot.2012.099.

Boese, Amrit S., Reuben Saba, Kristyn Campbell, Anna Majer, Sarah Medina, Lynn Burton, Timothy F. Booth, et al. 2016. “MicroRNA Abundance Is Altered in Synaptoneurosomes during Prion Disease.” *Molecular and Cellular Neuroscience* 71. Elsevier B.V.: 13–24.

doi:10.1016/j.mcn.2015.12.001.

Boese, Amrit S, Anna Majer, Reuben Saba, and Stephanie a Booth. 2013. “Small RNA Drugs for Prion Disease: A New Frontier.” *Expert Opinion on Drug Discovery* 8 (10): 1265–84. doi:10.1517/17460441.2013.818976.

Bonci, Désirée, Valeria Coppola, Maria Musumeci, Antonio Addario, Raffaella Giuffrida, Lorenzo Memeo, Leonardo D’Urso, et al. 2008. “The miR-15a-miR-16-1 Cluster Controls Prostate Cancer by Targeting Multiple Oncogenic Activities.” *Nature Medicine* 14 (11): 1271–77. doi:10.1038/nm.1880.

Brewer, Gregory J., Torrie T. Jones, Michael D. Boehler, and Bruce C. Wheeler. 2008. “NbActiv4 Medium Improvement to Neurobasal/B27 Increases Neuron Synapse Densities and Network Spike Rates on Multielectrode Arrays.” *J Neurosci Methods* 170 (2): 181–87. doi:10.1016/j.pestbp.2011.02.012.Investigations.

Brodaty, Henry, Claudia Woolf, Stacy Andersen, Nir Barzilai, Carol Brayne, Karen Siu-lan Cheung, Maria M Corrada, et al. 2016. “ICC-Dementia (International Centenarian Consortium - Dementia): An International Consortium to Determine the Prevalence and Incidence of Dementia in Centenarians across Diverse Ethnoracial and Sociocultural Groups.” *BMC Neurology*. BMC Neurology, 1–10. doi:10.1186/s12883-016-0569-4.

Burgos, Kasandra, Ivana Malenica, Raghu Metpally, Amanda Courtright, Benjamin Rakela, Thomas Beach, Holly Shill, et al. 2014. “Profiles of Extracellular miRNA in Cerebrospinal Fluid and Serum from Patients with Alzheimer’s and Parkinson’s Diseases Correlate with Disease Status and Features of Pathology.” *PLoS ONE* 9 (5). doi:10.1371/journal.pone.0094839.

Calin, George Adrian, Calin Dan Dumitru, Masayoshi Shimizu, Roberta Bichi, Simona Zupo, Evan Noch, Hansjuerg Aldler, et al. 2002. “Frequent Deletions and down-Regulation of Micro- RNA Genes miR15 and miR16 at 13q14 in Chronic Lymphocytic Leukemia.” *Proceedings of the National Academy of Sciences of the United States of America* 99 (24): 15524–29. doi:10.1073/pnas.242606799.

Campbell, Kristyn, and Stephanie a Booth. 2015. “MicroRNA in Neurodegenerative Drug Discovery: The Way Forward?” *Expert Opinion on Drug Discovery* 10 (1). Informa UK, Ltd.: 9–16. doi:10.1517/17460441.2015.981254.

Cellerino, A., L. Maffei, and L. Domenici. 1996. “The Distribution of Brain-Derived Neurotrophic Factor and Its Receptor trkB in Parvalbumin-Containing Neurons of the Rat Visual Cortex.” *European Journal of Neuroscience* 8 (6): 1190–97. doi:10.1111/j.1460-9568.1996.tb01287.x.

Chandler, R.L. 1961. “Encephalopathy in Mice Produced By Inoculation With Scrapie Brain Material.” *The Lancet* 278 (7194): 152. doi:10.1016/S0140-6736(61)92671-X.

Chen, Lei, Qing Wang, Guo Dong Wang, Hua Song Wang, Yong Huang, Xi Ming Liu, and Xian Hua Cai. 2013. “MiR-16 Inhibits Cell Proliferation by Targeting IGF1R and the Raf1-MEK1/2-ERK1/2 Pathway in Osteosarcoma.” *FEBS Letters* 587 (9). Federation of European Biochemical Societies: 1366–72. doi:10.1016/j.febslet.2013.03.007.

Cheng, Pei-Hsun, Chia-Ling Li, Yu-Fan Chang, Shaw-Jeng Tsai, Yen-Yu Lai, Anthony W S

Chan, Chuan-Mu Chen, and Shang-Hsun Yang. 2013. “miR-196a Ameliorates Phenotypes of Huntington Disease in Cell, Transgenic Mouse, and Induced Pluripotent Stem Cell Models.” *American Journal of Human Genetics* 93 (2). The American Society of Human Genetics: 306–12. doi:10.1016/j.ajhg.2013.05.025.

Choi, Dennis W. 1988. “Glutamate Neurotoxicity and Diseases of the Nervous System.” *Neuron* 1 (8): 623–34. doi:10.1016/0896-6273(88)90162-6.

Cimmino, Amelia, George Adrian Calin, Muller Fabbri, Marilena V Iorio, Manuela Ferracin, Masayoshi Shimizu, Sylwia E Wojcik, et al. 2005. “miR-15 and miR-16 Induce Apoptosis by Targeting BCL2.” *Proc Natl Acad Sci U S A* 102 (39): 13944–49. doi:10.1073/pnas.0506654102.

Clavaguera, Florence, Tristan Bolmont, R Anthony Crowther, Dorothee Abramowski, Stephan Frank, Alphonse Probst, Graham Fraser, et al. 2009. “Transmission and Spreading of Tauopathy in Transgenic Mouse Brain.” *Nature Publishing Group* 11 (7). Nature Publishing Group: 909–13. doi:10.1038/ncb1901.

Clinton, J, C Forsyth, M Claire Royston, and GW Roberts. 1993. “Synaptic Degeneration Is the Primary Neuropathological Feature in Prion Disease: A Preliminary Study.” *NeuroReport*. doi:10.1097/00001756-199301000-00017.

Collinge, John. 1999. “Variant Creutzfeldt-Jakob Disease.” *The Lancet* 354: 317–23.

Collinge, John, Jerome Whitfi, Edward Mckintosh, John Beck, Simon Mead, Dafydd J Thomas, and Michael P Alpers. 2006. “Kuru in the 21st Century — an Acquired Human Prion Disease with Very Long Incubation Periods.” *Lancet* 367: 2068–74.

Cunningham, C., R. Deacon, H. Wells, D. Boche, S. Waters, C. Picanco Diniz, H. Scott, J. N P Rawlins, and V. H. Perry. 2003. “Synaptic Changes Characterize Early Behavioural Signs in the ME7 Model of Murine Prion Disease.” *European Journal of Neuroscience* 17 (10): 2147–55. doi:10.1046/j.1460-9568.2003.02662.x.

Cushion, Thomas D., Alex R. Paciorkowski, Daniela T. Pilz, Jonathan G L Mullins, Laurie E. Seltzer, Robert W. Marion, Emily Tuttle, et al. 2014. “De Novo Mutations in the Beta-Tubulin Gene TUBB2A Cause Simplified Gyral Patterning and Infantile-Onset Epilepsy.” *American Journal of Human Genetics* 94 (4). The American Society of Human Genetics: 634–41. doi:10.1016/j.ajhg.2014.03.009.

Davis, S, P Vanhoutte, C Pages, J Caboche, and S Laroche. 2000. “The MAPK/ERK Cascade Targets Both Elk-1 and cAMP Response Element-Binding Protein to Control Long-Term Potentiation-Dependent Gene Expression in the Dentate Gyrus in Vivo.” *The Journal of Neuroscience : The Official Journal of the Society for Neuroscience* 20 (12): 4563–72. doi:20/12/4563 [pii].

Davis, Tigwa H, Trinna L Cuellar, Selina M Koch, Allison J Barker, Brian D Harfe, Michael T McManus, and Erik M Ullian. 2008. “Conditional Loss of Dicer Disrupts Cellular and Tissue Morphogenesis in the Cortex and Hippocampus.” *The Journal of Neuroscience : The Official Journal of the Society for Neuroscience* 28 (17): 4322–30. doi:10.1523/JNEUROSCI.4815-07.2008.

Dehay, Benjamin, Deniz Dalkara, Sandra Dovero, Qin Li, and Erwan Bezard. 2012. “Systemic

scAAV9 Variant Mediates Brain Transduction in Newborn Rhesus Macaques." *Scientific Reports* 2 (253): 1–3. doi:10.1038/srep00253.

Desplats, Paula, He-Jin Lee, Eun-Jin Bae, Christina Patrick, Edward Rockenstein, Leslie Crews, Brian Spencer, Eliezer Masliah, and Seung-Jae Lee. 2009. "Inclusion Formation and Neuronal Cell Death through Neuron-to-Neuron Transmission of Alpha-Synuclein." *Proceedings of the National Academy of Sciences of the United States of America* 106 (31): 13010–15. doi:10.1073/pnas.0903691106.

Dhavan, R, and L H Tsai. 2001. "A Decade of CDK5." *Nature Reviews. Molecular Cell Biology* 2 (10): 749–59. doi:10.1038/35096019.

Didonna, Alessandro, and Giuseppe Legname. 2010. "Aberrant ERK 1/2 Complex Activation and Localization in Scrapie-Infected GT1-1 Cells." *Molecular Neurodegeneration* 5: 29. doi:10.1186/1750-1326-5-29.

Diringer, H, H Gelderblom, H Hilmert, M Ozel, and C Edelbluth. 1983. "Scrapie Infectivity, Fibrils and Low Molecular Weight Protein." *Nature* 306 (1): 476–78.

Dorval, Véronique, Wim Mandemakers, Francis Jolivette, Laetitia Coudert, Rachid Mazroui, Bart De Strooper, and Sébastien S. Hébert. 2014. "Gene and microRNA Transcriptome Analysis of Parkinson's Related LRRK2 Mouse Models." *PLoS ONE* 9 (1): 1–10. doi:10.1371/journal.pone.0085510.

Dubey, Jyoti, Neena Ratnakaran, and Sandhya P. Koushika. 2015. "Neurodegeneration and Microtubule Dynamics: Death by a Thousand Cuts." *Frontiers in Cellular Neuroscience* 9 (September): 343. doi:10.3389/fncel.2015.00343.

Dwivedi, Shailendra Kumar Dhar, Soumyajit Banerjee Mustafi, Lingegowda S. Mangala, Dahai Jiang, Sunila Pradeep, Cristian Rodriguez-Aguayo, Hui Ling, et al. 2016. "Therapeutic Evaluation of microRNA-15a and microRNA-16 in Ovarian Cancer." *Oncotarget* 7 (12): 15093–104. doi:10.18632/oncotarget.7618.

Eberwine, J, K Miyashiro, J E Kacharmina, and C Job. 2001. "Local Translation of Classes of mRNAs That Are Targeted to Neuronal Dendrites." *Proceedings of the National Academy of Sciences of the United States of America* 98 (13): 7080–85. doi:10.1073/pnas.121146698.

Eisele, Yvonne S, Tristan Bolmont, Mathias Heikenwalder, Franziska Langer, Laura H Jacobson, Zheng-xin Yan, Klaus Roth, et al. 2009. "Induction of Cerebral Beta-Amyloidosis : Intracerebral versus Systemic Abeta Inoculation." *Proc Natl Acad Sci U S A* 106 (31): 12926–31.

Fan, Meiyun, Raisa Krutilina, Jing Sun, Aarti Sethuraman, Chuan He Yang, Zhao Hui Wu, Junming Yue, and Lawrence M. Pfeffer. 2013. "Comprehensive Analysis of MicroRNA (miRNA) Targets in Breast Cancer Cells." *Journal of Biological Chemistry* 288 (38): 27480–93. doi:10.1074/jbc.M113.491803.

Ferrer, I, R Blanco, M Carmona, R Ribera, E Goutan, B Puig, M J Rey, a Cardozo, F Viñals, and T Ribalta. 2001. "Phosphorylated Map Kinase (ERK1, ERK2) Expression Is Associated with Early Tau Deposition in Neurones and Glial Cells, but Not with Increased Nuclear DNA Vulnerability and Cell Death, in Alzheimer Disease, Pick's Disease, Progressive Supranuclear Palsy an." *Brain Pathology (Zurich, Switzerland)* 11 (2): 144–58.

doi:10.1111/j.1750-3639.2001.tb00387.x.

Friedman, Robin C., Kyle Kai-How Farh, Christopher B. Burge, and David P. Bartel. 2009. "Most Mammalian mRNAs Are Conserved Targets of microRNAs." *Genome Research* 19: 92–105. http://www-ncbi-nlm-nih-gov.ezproxy.cscscience.ca/pmc/articles/PMC2612969/pdf/92.pdf.

Gajdusek, DC, CJ Gibbs, and MP Alpers. 1966. "Experimental Transmission of a Kuru-like Syndrome to Chimpanzees." *Nature* 209: 794–96.

Gemmell, Elizabeth, Helen Bosomworth, Louise Allan, Roslyn Hall, Ahmad Khundakar, Arthur E. Oakley, Vincent Deramecourt, Tuomo M. Polvikoski, John T. O'Brien, and Raj N. Kalaria. 2012. "Hippocampal Neuronal Atrophy and Cognitive Function in Delayed Poststroke and Aging-Related Dementias." *Stroke* 43 (3): 808–14. doi:10.1161/STROKEAHA.111.636498.

Gibbs, Author C J, D C Gajdusek, D M Asher, M P Alpers, Elizabeth Beck, and W B Matthews. 1968. "Creutzfeldt-Jakob Disease (Spongiform Encephalopathy): Transmission to the Chimpanzee." *Science* 161 (3839): 388–89.

Ginsberg, Stephen D., Melissa J. Alldred, and Shaoli Che. 2012. "Gene Expression Levels Assessed by CA1 Pyramidal Neuron and Regional Hippocampal Dissections in Alzheimer's Disease." *Neurobiology of Disease* 45 (1): 99–107. doi:10.1016/j.nbd.2011.07.013.

Goff, Loyal A., Jonathan Davila, Mavis R. Swerdel, Jennifer C. Moore, Rick I. Cohen, Hao Wu, Yi E. Sun, and Ronald P. Hart. 2009. "Ago2 Immunoprecipitation Identifies Predicted MicroRNAs in Human Embryonic Stem Cells and Neural Precursors." *PLoS ONE* 4 (9). doi:10.1371/journal.pone.0007192.

Gorski, Jessica a, Steven R Zeiler, Susan Tamowski, and Kevin R Jones. 2003. "Brain-Derived Neurotrophic Factor Is Required for the Maintenance of Cortical Dendrites." *The Journal of Neuroscience* 23 (17): 6856–65. doi:10.3410/f.1004415.195300.

Götz, Jürgen, Lars M. Ittner, and Stefan Kins. 2006. "Do Axonal Defects in Tau and Amyloid Precursor Protein Transgenic Animals Model Axonopathy in Alzheimer's Disease?" *Journal of Neurochemistry* 98 (4): 993–1006. doi:10.1111/j.1471-4159.2006.03955.x.

Guentchev, M, T Voigtlander, C Haberler, M H Groschup, and H Budka. 2000. "Evidence for Oxidative Stress in Experimental Prion Disease." *Neurobiol Dis* 7 (4): 270–73. doi:10.1006/nbdi.2000.0290.

Gui, Yaxing, Hai Liu, Lishan Zhang, Wen Lv, and Xingyue Hu. 2015. "Altered microRNA Profiles in Cerebrospinal Fluid Exosome in Parkinson Disease and Alzheimer Disease." *Oncotarget* 6 (35): 37043–53. doi:10.18632/oncotarget.6158.

Gurtan, Allan M., and Phillip A. Sharp. 2013. "The Role of miRNAs in Regulating Gene Expression Networks." *Journal of Molecular Biology* 425 (19). Elsevier Ltd: 3582–3600. doi:10.1016/j.jmb.2013.03.007.

Haber, M., Lei Zhou, and Keith K. Murai. 2006. "Cooperative Astrocyte and Dendritic Spine Dynamics at Hippocampal Excitatory Synapses." *Journal of Neuroscience* 26 (35): 8881–91. doi:10.1523/JNEUROSCI.1302-06.2006.

Hallock, Peter, and Michael A Thomas. 2012. “Integrating the Alzheimer’s Disease Proteome and Transcriptome: A Comprehensive Network Model of a Complex Disease.” *Omics : A Journal of Integrative Biology* 16 (1–2): 37–49. doi:10.1089/omi.2011.0054.

He, Lin, and Gregory J. Hannon. 2004. “MicroRNAs: Small RNAs with a Big Role in Gene Regulation.” *Nature Reviews Genetics*. http://www.nature.com.ezproxy.cscscience.ca/nrg/journal/v5/n7/pdf/nrg1379.pdf.

Hébert, Sébastien S., Nicolas Sergeant, and Luc Buée. 2012. “MicroRNAs and the Regulation of Tau Metabolism.” *International Journal of Alzheimer’s Disease* 2012. doi:10.1155/2012/406561.

Hébert, Sébastien S, Katrien Horré, Laura Nicolaï, Aikaterini S Papadopoulou, Wim Mandemakers, Asli N Silahtaroglu, Sakari Kauppinen, André Delacourte, and Bart De Strooper. 2008. “Loss of microRNA Cluster miR-29a/b-1 in Sporadic Alzheimer’s Disease Correlates with Increased BACE1/beta-Secretase Expression.” *Proceedings of the National Academy of Sciences of the United States of America* 105 (17): 6415–20. doi:10.1073/pnas.0710263105.

Hermel, E, J Gafni, S S Propp, B R Leavitt, C L Wellington, J E Young, A S Hackam, et al. 2004. “Specific Caspase Interactions and Amplification Are Involved in Selective Neuronal Vulnerability in Huntington’ S Disease.” *Cell Death and Differentiation* 11: 424–38. doi:10.1038/sj.cdd.4401358.

Horch, Hadley Wilson, Alex Krüttgen, Stuart D. Portbury, and Lawrence C. Katz. 1999. “Destabilization of Cortical Dendrites and Spines by BDNF.” *Neuron* 23 (2): 353–64. doi:10.1016/S0896-6273(00)80785-0.

Huang, E J, and L F Reichardt. 2001. “Neurotrophins: Roles in Neuronal Development and Function.” *Annual Review of Neuroscience* 24: 677–736. doi:10.1146/annurev.neuro.24.1.677.

Huang, Yu-Wen, Claudia R Ruiz, Elizabeth C H Eyler, Kathie Lin, and Mollie K Meffert. 2012. “Dual Regulation of miRNA Biogenesis Generates Target Specificity in Neurotrophin-Induced Protein Synthesis.” *Cell* 148 (5). Elsevier Inc.: 933–46. doi:10.1016/j.cell.2012.01.036.

Hullinger, Thomas G., Rusty L. Montgomery, Anita G. Seto, Brent A. Dickinson, Hillary M. Semus, Joshua M. Lynch, Christina M. Dalby, et al. 2012. “Inhibition of miR-15 Protects against Cardiac Ischemic Injury.” *Circulation Research* 110 (1): 71–81. doi:10.1161/CIRCRESAHA.111.244442.

Ishikura, Nako, Jared L. Clever, Essia Bouzamondo-Bernstein, Erik Samayoa, Stanley B. Prusiner, Eric J. Huang, and Stephen J. DeArmond. 2005. “Notch-1 Activation and Dendritic Atrophy in Prion Disease.” *Proceedings of the National Academy of Sciences of the United States of America* 102 (3): 886–91. doi:10.1073/pnas.0408612101.

Janssen, Harry L a, Hendrik W Reesink, Eric J Lawitz, Stefan Zeuzem, Maribel Rodriguez-Torres, Keyur Patel, Adriaan J van der Meer, et al. 2013. “Treatment of HCV Infection by Targeting microRNA.” *The New England Journal of Medicine* 368 (18): 1685–94. doi:10.1056/NEJMoa1209026.

Jeffrey, M, W G Halliday, J Bell, a R Johnston, N K MacLeod, C Ingham, a R Sayers, D a Brown, and J R Fraser. 2000. “Synapse Loss Associated with Abnormal PrP Precedes Neuronal Degeneration in the Scrapie-Infected Murine Hippocampus.” *Neuropathology and Applied Neurobiology* 26 (1): 41–54. http://www.ncbi.nlm.nih.gov/pubmed/10736066.

Jucker, Mathias. 2010. “The Benefits and Limitations of Animal Models for Translational Research in Neurodegenerative Diseases.” *Nature Medicine* 16 (11). Nature Publishing Group: 1210–14. doi:10.1038/nm.2224.

Jun, G, C A Ibrahim-verbaas, M Vronskaya, J-c Lambert, J Chung, A C Naj, B W Kunkle, et al. 2016. “A Novel Alzheimer Disease Locus Located near the Gene Encoding Tau Protein.” *Molecular Psychiatry* 21: 108–17. doi:10.1038/mp.2015.23.

Kao, Steven C. 2015. “A Significant Metabolic and Radiological Response after a Novel Targeted MicroRNA-Based Treatment Approach in Malignant Pleural Mesothelioma.” *American Journal of Respiratory and Critical Care Medicine* 191 (12): 1467–69.

Kaplan, Barry B, Anthony E Gioio, Mi Hillefors, and Armaz Aschrafi. 2009. “Axonal Protein Synthesis and the Regulation of Local Mitochondrial Function.” *Results and Problems in Cell Differentiation* 48: 225–42. doi:10.1007/400.

Kessels, Helmut W, Louis N Nguyen, Sadegh Nabavi, and Roberto Malinow. 2010. “The Prion Protein as a Receptor for Amyloid-Beta.” *Nature* 466 (7308): E3-4-5. doi:10.1038/nature09217.

Kim, John, Anna Krichevsky, Yonatan Grad, Gabriel D Hayes, Kenneth S Kosik, George M Church, and Gary Ruvkun. 2004. “Identification of Many microRNAs That Copurify with Polyribosomes in Mammalian Neurons.” *Proceedings of the National Academy of Sciences of the United States of America* 101 (1): 360–65. doi:10.1073/pnas.2333854100.

Klausberger, Thomas, and Peter Somogyi. 2008. “Neuronal Diversity and Temporal Dynamics : The Unity of Hippocampal Circuit Operations.” *Science* 321: 53–58.

Klingeborn, Mikael, Brent Race, Kimberly D Meade-white, Rebecca Rosenke, James F Striebel, and Bruce Chesebro. 2011. “Crucial Role for Prion Protein Membrane Anchoring in the Neuroinvasion and Neural Spread of Prion Infection .” *Journal of Virology* 85 (4): 1484–94. doi:10.1128/JVI.02167-10.

Kocerha, Jannet, Yan Xu, Melinda S Prucha, Dongming Zhao, and Anthony W S Chan. 2014. “microRNA-128a Dysregulation in Transgenic Huntington’s Disease Monkeys.” *Molecular Brain* 7 (1): 46. doi:10.1186/1756-6606-7-46.

Kollins, Katherine, Robert Bell, Matthew Butts, and Ginger Withers. 2009. “Dendrites Differ from Axons in Patterns of Microtubule Stability and Polymerization during Development.” *Neural Development* 4 (1): 26. doi:10.1186/1749-8104-4-26.

Koshimizu, Yoshinori, Fumino Fujiyama, Kouichi C Nakamura, Takahiro Furuta, and Takeshi Kaneko. 2013. “Quantitative Analysis of Axon Bouton Distribution of Subthalamic Nucleus Neurons in the Rat by Single Neuron Visualization With a Viral Vector.” *The Journal of Comparative Neurology* 521: 2125–46. doi:10.1002/cne.23277.

Kozomara, Ana, and Sam Griffiths-Jones. 2014. “MiRBase: Annotating High Confidence

microRNAs Using Deep Sequencing Data." *Nucleic Acids Research* 42 (D1): 68–73. doi:10.1093/nar/gkt1181.

Krell, Jonathan, Justin Stebbing, Claudia Carissimi, Aleksandra F. Dabrowska, Alexander De Giorgio, Adam E. Frampton, Victoria Harding, et al. 2016. "TP53 Regulates miRNA Association with AGO2 to Remodel the miRNA-mRNA Interaction Network." *Genome Research* 26 (3): 331–41. doi:10.1101/gr.191759.115.

Kumar, P, S Bhattacharyya, K W Peters, M L Glover, a Sen, R T Cox, S Kundu, et al. 2015. "miR-16 Rescues F508del-CFTR Function in Native Cystic Fibrosis Epithelial Cells." *Gene Therapy* 22 (February). Nature Publishing Group: 1–9. doi:10.1038/gt.2015.56.

Kumar, Pavan, Zoltan Dezso, Crystal MacKenzie, Judy Oestreicher, Sergei Agoulnik, Michael Byrne, Francois Bernier, Mamoru Yanagimachi, Ken Aoshima, and Yoshiya Oda. 2013. "Circulating miRNA Biomarkers for Alzheimer's Disease." *PloS One* 8 (7): e69807. doi:10.1371/journal.pone.0069807.

Kurino, M, K Fukunaga, Y Ushio, and E Miyamoto. 1995. "Activation of Mitogen-Activated Protein Kinase in Cultured Rat Hippocampal Neurons by Stimulation of Glutamate Receptors." *J Neurochem* 65 (3): 1282–89. http://www.ncbi.nlm.nih.gov/entrez/query.fcgi?cmd=Retrieve&db=PubMed&dopt=Citation&list_uids=7643105.

Langhammer, Christopher, Michelle Previtera, Eric Sweet, Simranjeet S Sran, Maxine Chen, and Bonnie L Firestein. 2010. "Automated Sholl Analysis of Digitized Neuronal Morphology at Multiple Scales: Whole-Cell Sholl Analysis vs. Sholl Analysis of Arbor Sub-Regions." *Cytometry A.* 77 (12): 1160–68. doi:10.1038/nbt.3121.ChIP-nexus.

Lau, Pierre, Koen Bossers, Rekin's Janky, Evgenia Salta, Carlo Sala Frigerio, Shahar Barbash, Roy Rothman, et al. 2013. "Alteration of the microRNA Network during the Progression of Alzheimer's Disease." *EMBO Molecular Medicine* 5 (10): 1613–34. doi:10.1002/emmm.201201974.

Launay, J M, S Mouillet-Richard, A Baudry, M Pietri, and O Kellermann. 2011. "Raphe-Mediated Signals Control the Hippocampal Response to SRI Antidepressants via miR-16." *Translational Psychiatry* 1 (e56). Nature Publishing Group: 1–8. doi:10.1038/tp.2011.54.

Laurén, Juha, David a Gimbel, Haakon B Nygaard, John W Gilbert, and Stephen M Strittmatter. 2009. "Cellular Prion Protein Mediates Impairment of Synaptic Plasticity by Amyloid-Beta Oligomers." *Nature* 457 (7233): 1128–32. doi:10.1038/nature07761.

Lee, Junghee, Yu Jin Hwang, Ki Yoon Kim, Neil W. Kowall, and Hoon Ryu. 2013. "Epigenetic Mechanisms of Neurodegeneration in Huntington's Disease." *Neurotherapeutics* 10 (4): 664–76. doi:10.1007/s13311-013-0206-5.

Lewis, David A, Leisa A Glantz, Joseph N Pierri, and Robert A Sweet. 2003. "Altered Cortical Glutamate Neurotransmission in Schizophrenia." *New York Academy of Sciences* 1003: 102–12.

Lezina, L, N Purmessur, AV Antonov, T Ivanova, E Karpova, K Krishan, M Ivan, et al. 2013. "miR-16 and miR-26a Target Checkpoint Kinases Wee1 and Chk1 in Response to p53 Activation by Genotoxic Stress." *Cell Death and Disease* 4 (e953): 1–10.

http://www.nature.com/cddis/journal/v4/n12/pdf/cddis2013483a.pdf.

Lin, Michael T, and M.Flint F Beal. 2006. “Mitochondrial Dysfunction and Oxidative Stress in Neurodegenerative Diseases.” *Nature* 443 (7113): 787–95. doi:nature05292 [pii]\r10.1038/nature05292.

Linsley, Peter S, Janell Schelter, Julja Burchard, Miho Kibukawa, Melissa M Martin, Steven R Bartz, Jason M Johnson, et al. 2007. “Transcripts Targeted by the microRNA-16 Family Cooperatively Regulate Cell Cycle Progression.” *Molecular and Cellular Biology* 27 (6): 2240–52. doi:10.1128/MCB.02005-06.

Lippi, Giordano, Joern R. Steinert, Emma L. Marczylo, Sabina D’Oro, Roberto Fiore, Ian D. Forsythe, Gerhard Schratt, Michele Zoli, Pierluigi Nicotera, and Kenneth W. Young. 2011. “Targeting of the Arpc3 Actin Nucleation Factor by miR-29a/b Regulates Dendritic Spine Morphology.” *Journal of Cell Biology* 194 (6): 889–904. doi:10.1083/jcb.201103006.

Liu, G, H Anisman, J Bobyn, and S Hayley. 2014. “Interaction Between Nonviral Reprogrammed Fibroblast Stem Cells and Trophic Factors for Brain Repair.” *Mol Neurobiol* 50: 673–84. doi:10.1007/s12035-014-8680-2.

Liu, Qin, Hanjiang Fu, Fang Sun, Haoming Zhang, Yi Tie, Jie Zhu, Ruiyun Xing, Zhixian Sun, and Xiaofei Zheng. 2008. “miR-16 Family Induces Cell Cycle Arrest by Regulating Multiple Cell Cycle Genes.” *Nucleic Acids Research* 36 (16): 5391–5404. doi:10.1093/nar/gkn522.

Liu, Wei, Chang Liu, Jingxi Zhu, Pengcheng Shu, Bin Yin, Yanhua Gong, Boqin Qiang, Jiangang Yuan, and Xiaozhong Peng. 2012. “MicroRNA-16 Targets Amyloid Precursor Protein to Potentially Modulate Alzheimer’s-Associated Pathogenesis in SAMP8 Mice.” *Neurobiology of Aging* 33 (3). Elsevier Inc.: 522–34. doi:10.1016/j.neurobiolaging.2010.04.034.

Majer, Anna, and Stephanie A Booth. 2014. “Microdissection and Transcriptional Profiling.” *Prion* 8 (1): 67–74. doi:10.4161/pri.27729.

Majer, Anna, Sarah J Medina, Yulian Niu, Bernard Abrenica, Kathy J Manguiat, Kathy L Frost, Clark S Philipson, Debra L Sorensen, and Stephanie A Booth. 2012. “Early Mechanisms of Pathobiology Are Revealed by Transcriptional Temporal Dynamics in Hippocampal CA1 Neurons of Prion Infected Mice.” *PLoS Pathogens* 8 (11): e1003002. doi:10.1371/journal.ppat.1003002.

Mallucci, G., A. Dickinson, J. Linehan, P. Klöhn, S. Brandner, and J. Collinge. 2003. “Depleting Neuronal PrP in Prion Infection Prevents Disease and Reverses S.” *Science* 302 (5646): 871–74. doi:10.1126/science.1090187.

Mallucci, Giovanna R., Melanie D. White, Michael Farmer, Andrew Dickinson, Husna Khatun, Andrew D. Powell, Sebastian Brandner, John G R Jefferys, and John Collinge. 2007. “Targeting Cellular Prion Protein Reverses Early Cognitive Deficits and Neurophysiological Dysfunction in Prion-Infected Mice.” *Neuron* 53 (3): 325–35. doi:10.1016/j.neuron.2007.01.005.

Mantamadiotis, Theo, Thomas Lemberger, Susanne C Bleckmann, Heidrun Kern, Oliver Kretz, Ana Martin Villalba, François Tronche, et al. 2002. “Disruption of CREB Function in Brain

Leads to Neurodegeneration." *Nature Genetics* 31 (1): 47–54. doi:10.1038/ng882.

Mattson, M P, and S B Kater. 1989. "Development and Selective Neurodegeneration in Cell Cultures from Different Hippocampal Regions." *Brain Research* 490 (1): 110–25. http://www.ncbi.nlm.nih.gov/pubmed/2569350.

McAllister, A. Kimberley. 2001. "Neurotrophins and Neuronal Differentiation in the Central Nervous System." *Cellular and Molecular Life Sciences : CMLS* 58 (8): 1054–60. doi:10.1007/PL00000920.

McAllister, A Kimberley, Donald C Lo, Lawrence C Katz, and North Carolina. 1995. "Neurotrophins Regulate Dendritic Growth in Developing Visual Codex." *Neuron* 15 (Figure 1): 791–803. doi:10.1016/0896-6273(95)90171-X.

Meyer-Franke, Anke, George A. Wilkinson, Alex Kruttgen, Minjie Hu, Elizabeth Munro, Martin G. Hanson, Louis F. Reichardt, and Ben A. Barres. 1998. "Depolarization and cAMP Elevation Rapidly Recruit TrkB to the Plasma Membrane of CNS Neurons." *Neuron* 21 (4): 681–93. doi:10.1016/S0896-6273(00)80586-3.

Meyer-luehmann, Melanie, Janaky Coomaraswamy, Tristan Bolmont, Stephan Kaeser, Claudia Schaefer, Ellen Kilger, Anton Neuenschwander, et al. 2006. "Exogenous Induction of Cerebral B-Amyloidogenesis Is Governed by Agent and Host." *Science* 313: 1781–84.

Minichiello, Liliana, Martin Korte, David Wolfer, Ralf Kühn, Klaus Unsicker, Vincenzo Cestari, Clelia Rossi-Arnaud, Hans Peter Lipp, Tobias Bonhoeffer, and Rüdiger Klein. 1999. "Essential Role for TrkB Receptors in Hippocampus-Mediated Learning." *Neuron* 24 (2): 401–14. doi:10.1016/S0896-6273(00)80853-3.

Monteys, Alex Mas, Ryan M Spengler, Brett D Dufour, Matt S Wilson, Clayton K Oakley, Matt J Sowada, Jodi L McBride, and Beverly L Davidson. 2014. "Single Nucleotide Seed Modification Restores in Vivo Tolerability of a Toxic Artificial miRNA Sequence in the Mouse Brain." *Nucleic Acids Research* 42 (21): 13315–27. doi:10.1093/nar/gku979.

Müller, Mareike, H. Bea Kuiperij, Jurgen A. Claassen, Benno Küsters, and Marcel M. Verbeek. 2014. "MicroRNAs in Alzheimer's Disease: Differential Expression in Hippocampus and Cell-Free Cerebrospinal Fluid." *Neurobiology of Aging* 35 (1). Elsevier Ltd: 152–58. doi:10.1016/j.neurobiolaging.2013.07.005.

Natera-Naranjo, Orlangie, Armaz Aschrafi, Anthony E Gioio, and Barry B Kaplan. 2010. "Identification and Quantitative Analyses of microRNAs Located in the Distal Axons of Sympathetic Neurons." *RNA (New York, N.Y.)* 16 (8): 1516–29. doi:10.1261/rna.1833310.

Nelson, Peter T, D O N a Baldwin, Wigard P Kloosterman, Sakari Kauppinen, Ronald H a Plasterk, and Zissimos Mourelatos. 2006. "RAKE and LNA-ISH Reveal microRNA Expression and Localization in RAKE and LNA-ISH Reveal microRNA Expression and Localization in Archival Human Brain." *Rna* 12: 187–91. doi:10.1261/rna.2258506.Expression.

Nolan, Katie, Mollie R Mitchem, Eva M Jimenez-Mateos, David C Henshall, Caoimhín G Concannon, and Jochen H M Prehn. 2014. "Increased Expression of MicroRNA-29a in ALS Mice: Functional Analysis of Its Inhibition." *Journal of Molecular Neuroscience : MN* 53 (2): 231–41. doi:10.1007/s12031-014-0290-y.

Norrby, E. 2011. “Prions and Protein-Folding Diseases.” *Journal of Internal Medicine* 270: 1–14. doi:10.1111/j.1365-2796.2011.02387.x.

Nunomura, A, G Perry, G Aliev, K Hirai, A Takeda, E K Balraj, P K Jones, et al. 2001. “Oxidative Damage Is the Earliest Event in Alzheimer Disease.” *Journal of Neuropathology and Experimental Neurology* 60 (8): 759–67. doi:10.1093/jnen/60.8.759.

Panegyres, Peter K, and Elizabeth Armari. 2013. “Therapies for Human Prion Diseases.” *Am J Neurodegener Dis* 2 (3): 176–86.

Parsi, Sepideh, Pascal Y Smith, Claudia Goupil, Véronique Dorval, and Sébastien S Hébert. 2015. “Preclinical Evaluation of miR-15/107 Family Members as Multifactorial Drug Targets for Alzheimer’s Disease.” *Molecular Therapy—Nucleic Acids* 4 (10): e256. doi:10.1038/mtna.2015.33.

Prince, Martin, Gemma-Claire Ali, Maëlenn Guerchet, A. Matthew Prina, Emiliano Albanese, Yu-Tzu Wu, M Prince, et al. 2016. “Recent Global Trends in the Prevalence and Incidence of Dementia, and Survival with Dementia.” *Alzheimer’s Research & Therapy* 8 (1). Alzheimer’s Research & Therapy: 23. doi:10.1186/s13195-016-0188-8.

Prince, Martin, Renata Bryce, Emiliano Albanese, Anders Wimo, Wagner Ribeiro, and Cleusa P Ferri. 2013. “The Global Prevalence of Dementia: A Systematic Review and Metaanalysis.” *Alzheimer’s & Dementia : The Journal of the Alzheimer’s Association* 9 (1). Elsevier Ltd: 63–75.e2. doi:10.1016/j.jalz.2012.11.007.

Prusiner, Stanley B. 1982. “Novel Proteinaceous Infectious Particles Cause Scrapie.” *Science* 216 (4542): 136–44.

Prusiner, Stanley B., Amanda L. Woerman, Daniel A. Mordes, Joel C. Watts, Ryan Rampersaud, David B. Berry, Smita Patel, et al. 2015. “Evidence for α-Synuclein Prions Causing Multiple System Atrophy in Humans with Parkinsonism.” *Proceedings of the National Academy of Sciences of the United States of America* 112 (38): E5308-17. doi:10.1073/pnas.1514475112.

Rapoport, Mark, and Adriana Ferreira. 2000. “PD98059 Prevents Neurite Degeneration Induced by Fibrillar β-Amyloid in Mature Hippocampal Neurons.” *Journal of Neurochemistry* 74 (1): 125–33. doi:10.1046/j.1471-4159.2000.0740125.x.

Reid, G, M E Pel, M B Kirschner, Y Y Cheng, N Mugridge, J Weiss, M Williams, et al. 2013. “Restoring Expression of miR-16: A Novel Approach to Therapy for Malignant Pleural Mesothelioma.” *Annals of Oncology : Official Journal of the European Society for Medical Oncology / ESMO* 24 (12): 3128–35. doi:10.1093/annonc/mdt412.

Ren, Pei-hsien, Jane E Lauckner, Ioulia Kachirskaia, John E Heuser, Ronald Melki, and Ron R Kopito. 2009. “Cytoplasmic Penetration and Persistent Infection of Mammalian Cells by Polyglutamine Aggregates.” *Nature Cell Biology* 11 (2): 219–25. doi:10.1038/ncb1830.

Rinnerthaler, Gabriel, Hubert Hackl, Simon Peter Gampenrieder, Frank Hamacher, Clemens Hufnagl, Cornelia Hauser-kronberger, Franz Zehentmayr, et al. 2016. “miR-16-5p Is a Stably-Expressed Housekeeping MicroRNA in Breast Cancer Tissues from Primary Tumors and from Metastatic Sites.” *International Journal of Molecular Sciences* 17 (156): 1–12. doi:10.3390/ijms17020156.

Rosen, Laura B., David D. Ginty, Michael J. Weber, and Michael E. Greenberg. 1994. "Membrane Depolarization and Calcium Influx Stimulate MEK and MAP Kinase via Activation of Ras." *Neuron* 12 (6): 1207–21. doi:10.1016/0896-6273(94)90438-3.

Royo, Nicolas C, Luk H Vandenberghe, Julie Johnston, Margaret Maronski, Marc A Dichter, James M Wilson, and Deborah J Watson. 2006. "Specific AAV Serotypes Stably Transduce Hippocampal and Cortical Cultures with High Efficiency and Low Toxicity." *Molecular Therapy* 13: S347.

Sanuki, Rikako, Akishi Onishi, Chieko Koike, Rieko Muramatsu, Satoshi Watanabe, Yuki Muranishi, Shoichi Irie, et al. 2011. "miR-124a Is Required for Hippocampal Axogenesis and Retinal Cone Survival through Lhx2 Suppression." *Nature Neuroscience* 14 (9). Nature Publishing Group: 1125–34. doi:10.1038/nn.2897.

Satizabal, Claudia L, Alexa S Beiser, Vincent Chouraki, Geneviève Chêne, Carole Dufouil, and Sudha Seshadri. 2016. "Incidence of Dementia over Three Decades in the Framingham Heart Study." *New England Journal of Medicine* 374: 523–32. doi:10.1056/NEJMoa1504327.

Satoh, Takumi, Daisaku Nakatsuka, Yasuyoshi Watanabe, Izumi Nagata, Haruhiko Kikuchi, and Shobu Namura. 2000. "Neuroprotection by MAPK/ERK Kinase Inhibition with U0126 against Oxidative Stress in a Mouse Neuronal Cell Line and Rat Primary Cultured Cortical Neurons." *Neuroscience Letters* 288 (2): 163–66. doi:10.1016/S0304-3940(00)01229-5.

Saugstad, Julie A. 2010. "MicroRNAs as Effectors of Brain Function with Roles in Ischemia and Injury, Neuroprotection, and Neurodegeneration." *Journal of Cerebral Blood Flow and Metabolism : Official Journal of the International Society of Cerebral Blood Flow and Metabolism* 30 (9). Nature Publishing Group: 1564–76. doi:10.1038/jcbfm.2010.101.

Schacher, Samuel, and Fang Wu. 2002. "Synapse Formation in the Absence of Cell Bodies Requires Protein Synthesis." *The Journal of Neuroscience : The Official Journal of the Society for Neuroscience* 22 (5): 1831–39. http://www.ncbi.nlm.nih.gov/pubmed/11880512.

Schaefer, Andreas T., Matthew Evan Larkum, Bert Sakmann, and Arnd Roth. 2003. "Coincidence Detection in Pyramidal Neurons Is Tuned by Their Dendritic Branching Pattern." *Journal of Neurophysiology* 89 (6): 3143–54. doi:10.1152/jn.00046.2003.

Schmitz, Sabine K., J. J Johannes Hjorth, Raoul M S Joemai, Rick Wijntjes, Susanne Eijgenraam, Petra de Bruijn, Christina Georgiou, et al. 2011. "Automated Analysis of Neuronal Morphology, Synapse Number and Synaptic Recruitment." *Journal of Neuroscience Methods* 195 (2): 185–93. doi:10.1016/j.jneumeth.2010.12.011.

Schwanhäusser, Björn, Matthias Selbach, Nadine Thierfelder, Nikolaus Rajewsky, Raya Khanin, and Zhuo Fang. 2008. "Widespread Changes in Protein Synthesis Induced by microRNAs." *Nature* 455 (7209): 58–63. doi:10.1038/nature07228.

Sempere, Lorenzo F, Sarah Freemantle, Ian Pitha-Rowe, Eric Moss, Ethan Dmitrovsky, and Victor Ambros. 2004. "Expression Profiling of Mammalian microRNAs Uncovers a Subset of Brain-Expressed microRNAs with Possible Roles in Murine and Human Neuronal Differentiation." *Genome Biology* 5 (3): R13. doi:10.1186/gb-2004-5-3-r13.

Shioya, M., S. Obayashi, H. Tabunoki, K. Arima, Y. Saito, T. Ishida, and J. Satoh. 2010.

"Aberrant microRNA Expression in the Brains of Neurodegenerative Diseases: MiR-29a Decreased in Alzheimer Disease Brains Targets Neurone Navigator 3." *Neuropathology and Applied Neurobiology* 36 (4): 320–30. doi:10.1111/j.1365-2990.2010.01076.x.

Siegel, Gabriele, Reuben Saba, and Gerhard Schratt. 2011. "microRNAs in Neurons: Manifold Regulatory Roles at the Synapse." *Current Opinion in Genetics & Development* 21 (4). Elsevier Ltd: 491–97. doi:10.1016/j.gde.2011.04.008.

Šišková, Zuzana, Anton Page, Vincent O'Connor, and Victor Hugh Perry. 2009. "Degenerating Synaptic Boutons in Prion Disease." *The American Journal of Pathology* 175 (4). American Society for Investigative Pathology: 1610–21. doi:10.2353/ajpath.2009.090372.

Smith, Bradley N., Nicola Ticozzi, Claudia Fallini, Athina Soragia Gkazi, Simon Topp, Kevin P. Kenna, Emma L. Scotter, et al. 2014. "Exome-Wide Rare Variant Analysis Identifies TUBA4A Mutations Associated with Familial ALS." *Neuron* 84 (2): 324–31. doi:10.1038/nbt.3121.ChIP-nexus.

Solforosi, Laura, Michela Milani, Nicasio Mancini, Massimo Clementi, and Roberto Burioni. 2013. "A Closer Look at Prion Strains Characterization and Important Implications." *Prion* 7 (2): 99–108.

Song, Haengjin, Wanil Kim, Jung-Hyun Choi, Sung-Hoon Kim, Dohyun Lee, Choon-Ho Park, Sangjune Kim, Do-Yeon Kim, and Kyong-Tai Kim. 2016. "Stress-Induced Nuclear Translocation of CDK5 Suppresses Neuronal Death by Downregulating ERK Activation via VRK3 Phosphorylation." *Nature Publishing Group*, no. March. Nature Publishing Group: 1–14. doi:10.1038/srep28634.

Song, Ming Fen, Jie Zheng Dong, Yu Wen Wang, Jun He, Xuan Ju, Long Zhang, Yong Hua Zhang, Jian Fei Shi, and Ya Ying Lv. 2015. "CSF miR-16 Is Decreased in Major Depression Patients and Its Neutralization in Rats Induces Depression-like Behaviors via a Serotonin Transmitter System." *Journal of Affective Disorders* 178. Elsevier: 25–31. doi:10.1016/j.jad.2015.02.022.

Sorensen, Garrett, Sarah Medina, Debra Parchaliuk, Clark Phillipson, Catherine Robertson, and Stephanie A Booth. 2008. "Comprehensive Transcriptional Profiling of Prion Infection in Mouse Models Reveals Networks of Responsive Genes." *BMC Genomics* 9: 114. doi:10.1186/1471-2164-9-114.

Stanciu, Madalina, and Donald B. Defranco. 2002. "Prolonged Nuclear Retention of Activated Extracellular Signal-Regulated Protein Kinase Promotes Cell Death Generated by Oxidative Toxicity or Proteasome Inhibition in a Neuronal Cell Line." *Journal of Biological Chemistry* 277 (6): 4010–17. doi:10.1074/jbc.M104479200.

Stokin, Gorazd B, Concepcion Lillo, Tomas L Falzone, Richard G Brusch, Edward Rockenstein, Stephanie L Mount, Rema Raman, et al. 2005. "Axonopathy and Transport Deficits Early in the Pathogenesis of Alzheimer's Disease." *Science* 307 (5713): 1282–88.

Sun, Minxuan, Sabine M. Hölter, Jens Stepan, Lillian Garrett, Just Genius, Elisabeth Kremmer, Martin Hrabě De Angelis, et al. 2013. "Crybb2 Coding for βb2-Crystallin Affects Sensorimotor Gating and Hippocampal Function." *Mammalian Genome* 24 (9–10): 333–48. doi:10.1007/s00335-013-9478-7.

Sun, Yun Xiao, Jian Yang, Ping Yu Wang, You Jie Li, Shu Yang Xie, and Ruo Peng Sun. 2013. "Cisplatin Regulates SH-SY5Y Cell Growth through Downregulation of BDNF via miR-16." *Oncology Reports* 30 (5): 2343–49. doi:10.3892/or.2013.2731.

Takeshita, Fumitaka, Lubna Patrawala, Mitsuhiko Osaki, Ryou-u Takahashi, Yusuke Yamamoto, Nobuyoshi Kosaka, Masaki Kawamata, et al. 2010. "Systemic Delivery of Synthetic microRNA-16 Inhibits the Growth of Metastatic Prostate Tumors via Downregulation of Multiple Cell-Cycle Genes." *Molecular Therapy : The Journal of the American Society of Gene Therapy* 18 (1). Nature Publishing Group: 181–87. doi:10.1038/mt.2009.207.

Tan, Chan Lek, Joshua L Plotkin, Morten T Venø, Melanie von Schimmelmann, Philip Feinberg, Silas Mann, Annie Handler, et al. 2013. "MicroRNA-128 Governs Neuronal Excitability and Motor Behavior in Mice." *Science (New York, N.Y.)* 342 (6163): 1254–58. doi:10.1126/science.1244193.

Thomas, Gareth M, and Richard L Huganir. 2004. "MAPK Cascade Signalling and Synaptic Plasticity." *Nat Rev Neurosci* 5 (3): 173–83. doi:10.1038/nrn1346.

Turchinovich, Andrey, Ludmila Weiz, Anne Langheinz, and Barbara Burwinkel. 2011. "Characterization of Extracellular Circulating microRNA." *Nucleic Acids Research* 39 (16): 7223–33. doi:10.1093/nar/gkr254.

van Rooij, Eva, Angela L Purcell, and Arthur a Levin. 2012. "Developing microRNA Therapeutics." *Circulation Research* 110 (3): 496–507. doi:10.1161/CIRCRESAHA.111.247916.

van Spronsen, Myrrhe, Eljo Y. van Battum, Marijn Kuijpers, Vamshidhar R. Vangoor, M. Liset Rietman, Joris Pothof, Laura F. Gumy, Wilfred F J van IJcken, et al. 2013. "Developmental and Activity-Dependent miRNA Expression Profiling in Primary Hippocampal Neuron Cultures." *PLoS ONE* 8 (10): e74907. doi:10.1371/journal.pone.0074907.

van Spronsen, Myrrhe, Eljo Y van Battum, Marijn Kuijpers, Vamshidhar R Vangoor, M Liset Rietman, Joris Pothof, Laura F Gumy, Wilfred F J van Ijcken, et al. 2013. "Developmental and Activity-Dependent miRNA Expression Profiling in Primary Hippocampal Neuron Cultures." *PloS One* 8 (10): e74907. doi:10.1371/journal.pone.0074907.

Vetter, Philipp, Arnd Roth, and Michael Häusser. 2001. "Propagation of Action Potentials in Dendrites Depends on Dendritic Morphology." *Journal of Neurophysiology* 85 (2): 926–37.

von Engelhardt, Jakob, Irinel Coserea, Verena Pawlak, Elke C. Fuchs, Georg K??hr, Peter H. Seeburg, and Hannah Monyer. 2007. "Excitotoxicity in Vitro by NR2A- and NR2B-Containing NMDA Receptors." *Neuropharmacology* 53 (1): 10–17. doi:10.1016/j.neuropharm.2007.04.015.

Wadsworth, Jonathan D F, and John Collinge. 2011. "Molecular Pathology of Human Prion Disease." *Acta Neuropathol* 121: 69–77. doi:10.1007/s00401-010-0735-5.

Wang, Gang, Yue Huang, Wei Chen, Shuai Chen, Ying Wang, Qin Xiao, Jun Liu, Victor S C Fung, Glenda Halliday, and Shengdi Chen. 2016. "Parkinsonism and Related Disorders Variants in the SNCA Gene Associate with Motor Progression While Variants in the MAPT Gene Associate with the Severity of Parkinson ' S Disease." *Parkinsonism and Related Disorders* 24. Elsevier Ltd: 89–94. doi:10.1016/j.parkreldis.2015.12.018.

Wang, Wang Xia, Robert J. Danaher, Craig S. Miller, Joseph R. Berger, Vega G. Nubia, Bernard S. Wilfred, Janna H. Neltner, Christopher M. Norris, and Peter T. Nelson. 2014. "Expression of miR-15/107 Family microRNAs in Human Tissues and Cultured Rat Brain Cells." *Genomics, Proteomics and Bioinformatics* 12 (1). Beijing Institute of Genomics, Chinese Academy of Sciences and Genetics Society of China: 19–30. doi:10.1016/j.gpb.2013.10.003.

Watts, Joel C, Carlo Condello, Jan Stöhr, Abby Oehler, Joanne Lee, Stephen J DeArmond, Lars Lannfelt, Martin Ingelsson, Kurt Giles, and Stanley B Prusiner. 2014. "Serial Propagation of Distinct Strains of Aβ Prions from Alzheimer's Disease Patients." *Proceedings of the National Academy of Sciences of the United States of America* 111 (28): 10323–28. doi:10.1073/pnas.1408900111.

Wayman, Gary a, Monika Davare, Hideaki Ando, Dale Fortin, Olga Varlamova, Hai-Ying M Cheng, Daniel Marks, et al. 2008. "An Activity-Regulated microRNA Controls Dendritic Plasticity by down-Regulating p250GAP." *Proceedings of the National Academy of Sciences of the United States of America* 105 (26): 9093–98. doi:10.1073/pnas.0803072105.

Winter, Julia, Stephanie Jung, Sarina Keller, Richard I Gregory, and Sven Diederichs. 2009. "Many Roads to Maturity: microRNA Biogenesis Pathways and Their Regulation." *Nature Cell Biology* 11 (3): 228–34. doi:10.1038/ncb0309-228.

Wu, G Y, K Deisseroth, and R W Tsien. 2001. "Spaced Stimuli Stabilize MAPK Pathway Activation and Its Effects on Dendritic Morphology." *Nature Neuroscience* 4 (2): 151–58. doi:10.1038/83976.

Xie, Heidi Q., Roy C Y Choi, K. Wing Leung, Vicky P. Chen, Glanice K Y Chu, and Karl W K Tsim. 2009. "Transcriptional Regulation of Proline-Rich Membrane Anchor (PRiMA) of Globular Form Acetylcholinesterase in Neuron: An Inductive Effect of Neuron Differentiation." *Brain Research* 1265. Elsevier B.V.: 13–23. doi:10.1016/j.brainres.2009.01.065.

Xie, Yu-feng, John F Macdonald, and Michael F Jackson. 2010. "TRPM2 , Calcium and Neurodegenerative Diseases." *Int J Physiol Pathophysiol Pharmacol* 2 (2): 95–103.

Yan, Xin, Hongwei Liang, Ting Deng, Kegan Zhu, Suyang Zhang, Nan Wang, Xueyuan Jiang, et al. 2013. "The Identification of Novel Targets of miR-16 and Characterization of Their Biological Functions in Cancer Cells." *Molecular Cancer* 12 (92): 1–11. http://www.molecular-cancer.com/content/pdf/1476-4598-12-92.pdf.

Ying, Shui-Wang, Marie Futter, Kobi Rosenblum, Mark J Webber, Stephen P Hunt, Timothy V P Bliss, and Clive R Bramham. 2002. "Brain-Derived Neurotrophic Factor Induces Long-Term Potentiation in Intact Adult Hippocampus: Requirement for ERK Activation Coupled to CREB and Upregulation of Arc Synthesis." *The Journal of Neuroscience : The Official Journal of the Society for Neuroscience* 22 (5): 1532–40. doi:22/5/1532 [pii].

Yokoi, Setsuri, Naoko Ishihara, Fuyuki Miya, Makiko Tsutsumi, Itaru Yanagihara, Naoko Fujita, Hiroyuki Yamamoto, et al. 2015. "TUBA1A Mutation Can Cause a Hydranencephaly-like Severe Form of Cortical Dysgenesis." *Scientific Reports* 5. Nature Publishing Group: 15165. doi:10.1038/srep15165.

Zanetti, Filippo, Andrea Carpi, Roberta Menabò, Marco Giorgio, Rainer Schulz, Guro Valen,

Anton Baysa, et al. 2014. “The Cellular Prion Protein Counteracts Cardiac Oxidative Stress.” *Cardiovascular Research* 104 (1): 93–102. doi:10.1093/cvr/cvu194.

Zhang, Zhelin, and Yan Cheng. 2014. “MiR-16-1 Promotes the Aberrant Alpha -Synuclein Accumulation in Parkinson Disease via Targeting Heat Shock Protein 70.” *Scientific World Journal* 2014. doi:10.1155/2014/938348.

Zhao, Yunan, Zhongli Wang, Jianguo Dai, Lin Chen, Yufang Huang, and Zhen Zhan. 2012. “Beneficial Effects of Benzodiazepine Diazepam on Chronic Stress-Induced Impairment of Hippocampal Structural Plasticity and Depression-like Behavior in Mice.” *Behavioural Brain Research* 228 (2). Elsevier B.V.: 339–50. doi:10.1016/j.bbr.2011.12.013.

Zollino, Marcella, Daniela Orteschi, Marina Murdolo, Serena Lattante, Domenica Battaglia, Chiara Stefanini, Eugenio Mercuri, Pietro Chiurazzi, Giovanni Neri, and Giuseppe Marangi. 2012. “Mutations in KANSL1 Cause the 17q21.31 Microdeletion Syndrome Phenotype.” *Nature Genetics* 44 (6). Nature Publishing Group: 636–38. doi:10.1038/ng.2257.

Appendix

1.1 Bioanalyzer Nanochip Results for Endogenous RNA

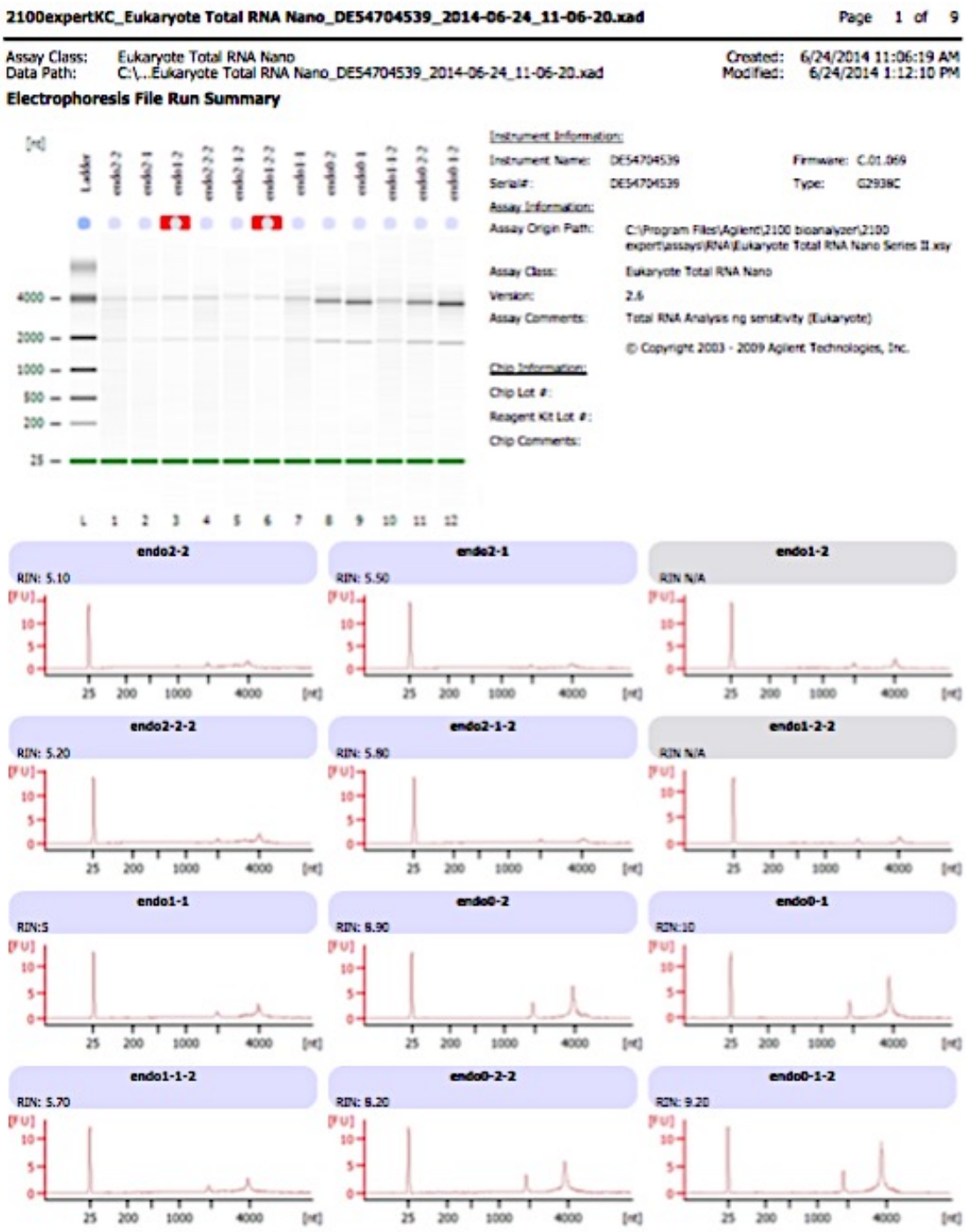

1.2 Vector Sequences Visualized using DNASTAR Lasergene 13 - SeqMan Pro & SeqBuilder and Aligned using NCBI Align Sequences Nucleotide Blast or miRBase Blast Search Directed at Hairpin Sequences.

1.2.1 miR-16

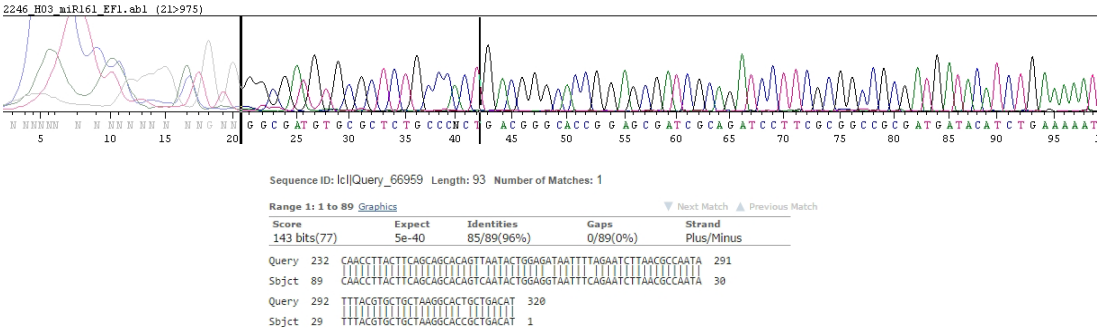

Above image illustrates a Blast alignment using:

Mus musculus microRNA 16-1 (Mir16-1), microRNA NCBI Reference Sequence: NR_029734.1

Appendix 1: miRBase Blast search using miR-16 Plasmid Sequence

Accession	ID	Query start	Query end	Subject start	Subject end	Strand	Score	Evalue	Alignment
MI0028779	efu-mir-16-1	212	334	4	125	-	512	7e-35	Align
MI0006887	oan-mir-16a	217	332	4	119	-	454	5e-30	Align
MI0000070	hsa-mir-16-1	232	320	1	89	-	445	3e-29	Align
MI0002946	age-mir-16	232	320	1	89	-	445	3e-29	Align
MI0002948	ggo-mir-16	232	320	1	89	-	445	3e-29	Align
MI0002950	mne-mir-16	232	320	1	89	-	445	3e-29	Align
MI0002952	sla-mir-16	232	320	1	89	-	445	3e-29	Align
MI0002954	ppa-mir-16	232	320	1	89	-	445	3e-29	Align
MI0002958	mml-mir-16-1	232	320	1	89	-	445	3e-29	Align
MI0002960	ppy-mir-16-1	232	320	1	89	-	445	3e-29	Align
MI0002962	ptr-mir-16-1	232	320	1	89	-	445	3e-29	Align
MI0030646	chi-mir-16a	232	320	1	89	-	436	1e-28	Align
MI0002964	lla-mir-16	232	320	1	89	-	427	8e-28	Align
MI0009753	bta-mir-16a	232	320	1	89	-	427	8e-28	Align
MI0005334	mdo-mir-16-1	231	320	1	90	-	414	1e-26	Align
MI0000565	mmu-mir-16-1	230	322	1	93	-	411	2e-26	Align
MI0020418	cgr-mir-16	234	316	1	83	-	406	5e-26	Align
MI0008212	ssc-mir-16-2	237	315	1	79	-	395	4e-25	Align
MI0008049	cfa-mir-16-1	243	307	1	65	-	325	2e-19	Align
MI0012830	eca-mir-16-2	245	307	1	63	-	315	2e-18	Align
MI0002956	lca-mir-16	248	320	1	74	-	303	2e-17	Align
MI0013811	tgu-mir-16a	230	312	6	86	-	288	3e-16	Align
MI0031368	oha-mir-16a	234	318	1	85	-	272	6e-15	Align

MI0000115	hsa-mir-16-2	241	307	10	76	-	146	2e-04	Align
MI0000566	mmu-mir-16-2	241	307	17	83	-	146	2e-04	Align

1.2.2 miR-Scr

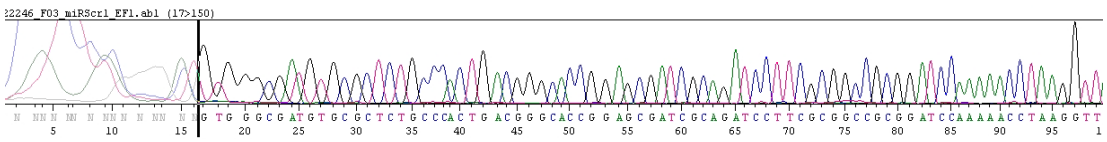

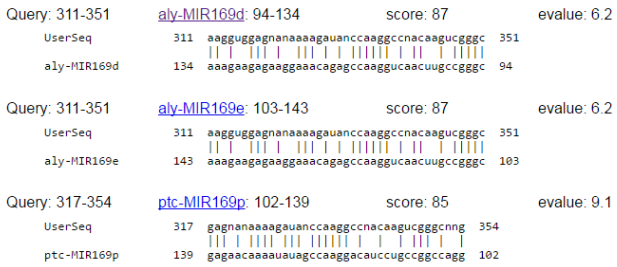

1.2.3 miRZIP-16

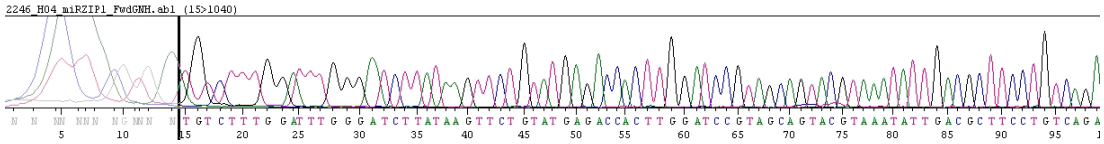

Appendix 2: miRBase Blast search using miR-ZIP16 Plasmid Sequence

Accession	ID	Query start	Query end	Subject start	Subject end	Strand	Score	Evalue	Alignment
MI0007073	hiv1-mir-TAR	157	217	1	61	+	305	1e-17	Align
MI0031369	oha-mir-16b	66	120	14	68	-	158	2e-05	Align
MI0013816	tgu-mir-16b	81	120	11	50	-	137	0.001	Align
MI0019491	ola-mir-16	81	120	23	62	-	128	0.006	Align
MI0031369	oha-mir-16b	62	119	11	68	+	128	0.006	Align
MI0004910	xtr-mir-16b	66	122	12	70	-	123	0.016	Align
MI0000115	hsa-mir-16-2	98	128	2	32	-	119	0.034	Align
MI0000566	mmu-mir-16-2	98	128	9	39	-	119	0.034	Align
MI0001894	dre-mir-16a	81	120	13	52	-	119	0.034	Align
MI0007589	mml-mir-16-2	98	128	2	32	-	119	0.034	Align
MI0008555	ptr-mir-16-2	98	128	1	31	-	119	0.034	Align
MI0017013	pma-mir-16	94	120	10	36	-	117	0.050	Align
MI0026531	ssa-mir-16c	94	120	1	27	-	117	0.050	Align
MI0031061	gma-MIR9762	348	419	45	116	+	117	0.050	Align
MI0000070	hsa-mir-16-1	98	120	14	36	-	115	0.073	Align
MI0000565	mmu-mir-16-1	98	120	16	38	-	115	0.073	Align

1.2.4 miRZIP-Scr

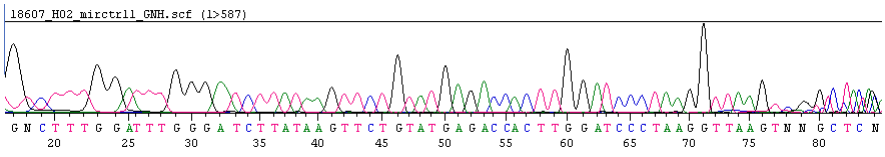

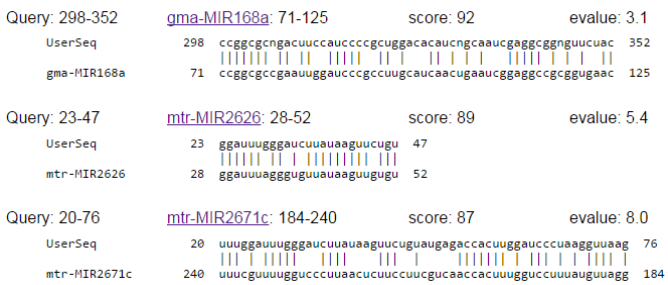

1.3 Bioanalyzer Picochip Results for Argonaute Immunoprecipitation RNA

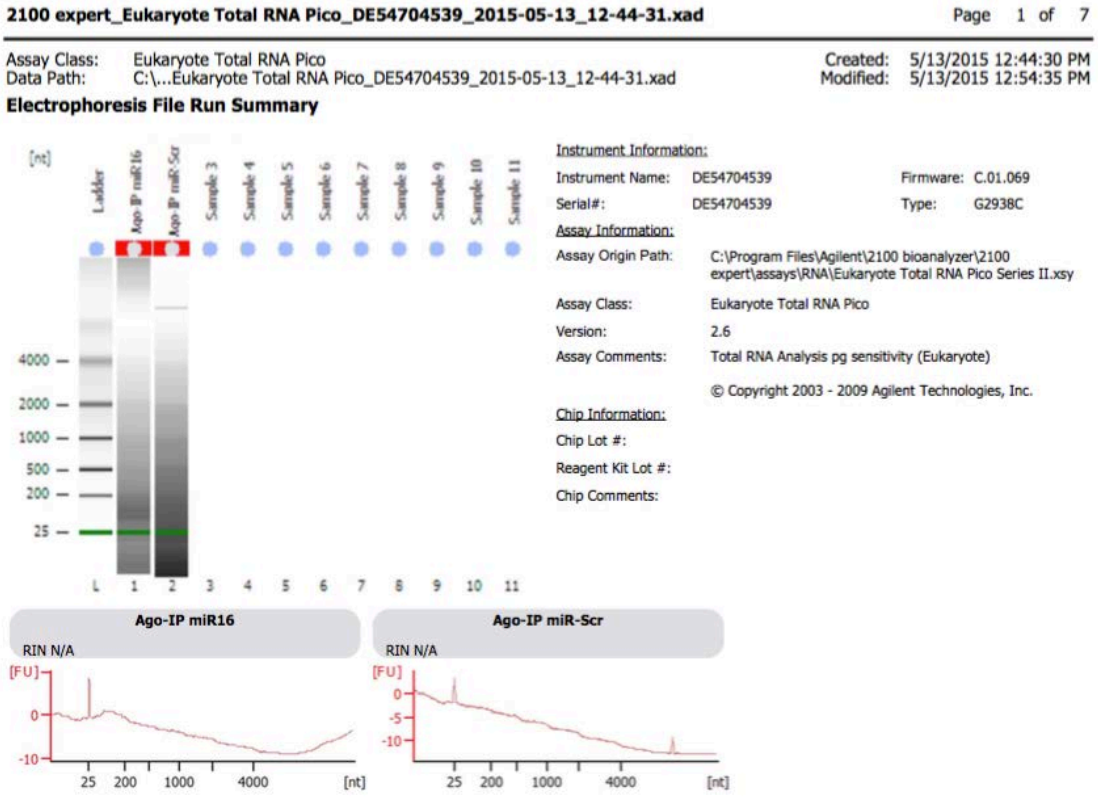

2100 expert_Eukaryote Total RNA Pico_DE54704539_2015-05-13_12-44-31.xad Page 1 of 7

Assay Class: Eukaryote Total RNA Pico
Data Path: C:\...Eukaryote Total RNA Pico_DE54704539_2015-05-13_12-44-31.xad

Created: 5/13/2015 12:44:30 PM
Modified: 5/13/2015 12:54:35 PM

Electrophoresis File Run Summary

[nt] Ladder Ago IP miR16 Ago IP miR Scr Sample 3 Sample 4 Sample 5 Sample 6 Sample 7 Sample 8 Sample 9 Sample 10 Sample 11

4000 2000 1000 500 200 25

L 1 2 3 4 5 6 7 8 9 10 11

Instrument Information:
Instrument Name: DE54704539 Firmware: C.01.069
Serial#: DE54704539 Type: G2938C

Assay Information:
Assay Origin Path: C:\Program Files\Agilent\2100 bioanalyzer\2100 expert\assays\RNA\Eukaryote Total RNA Pico Series II.xsy
Assay Class: Eukaryote Total RNA Pico
Version: 2.6
Assay Comments: Total RNA Analysis pg sensitivity (Eukaryote)

Chip Information:
Chip Lot #:
Reagent Kit Lot #:
Chip Comments:

Ago-IP miR16
RIN N/A
[FU] 0 -10
25 200 1000 4000 [nt]

Ago-IP miR-Scr
RIN N/A
[FU] 0 -5 -10
25 200 1000 4000 [nt]

1.4 Feature Extraction Quality Control Report

Spot Finding of the Four Corners of the Array

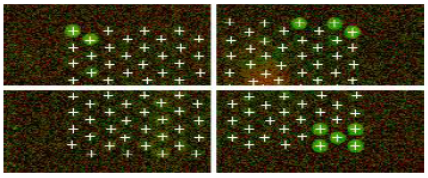

Grid Normal

	Feature		Local Background	
	Red	Green	Red	Green
Non Uniform	19	95	38	62
Population	154	175	671	675

Spatial Distribution of All Outliers on the Array

532 rows x 85 columns

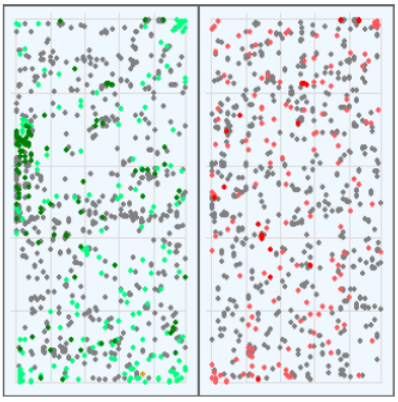

FeatureNonUnif (Red or Green) = 100(0.22%)

GeneNonUnif (Red or Green) = 87 (0.211 %)

- BG NonUniform
- Red FeaturePopulation
- Green FeaturePopulation
- BG Population
- Red Feature NonUniform
- Green Feature NonUniform

Net Signal Statistics

Agilent SpikeIns:

	Red	Green
# Saturated Features	0	0
99% of Sig. Distrib.	76	52
50% of Sig. Distrib.	67	20
1% of Sig. Distrib.	59	10

Non-Control probes:

	Red	Green
# Saturated Features	0	1
99% of Sig. Distrib.	197	965
50% of Sig. Distrib.	67	21
1% of Sig. Distrib.	60	10

Red and Green Background Corrected Signals (Non-Control Inliers)

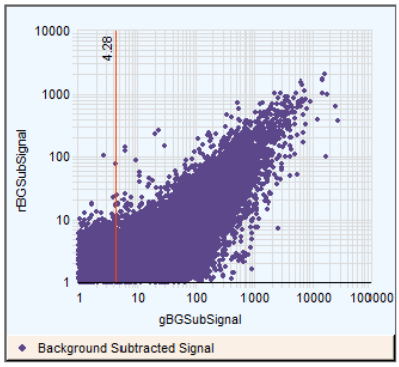

Features (NonCtrl) with BGSubSignals < 0: 20416 (Red); 12387 (Green)